

Membrane emulsification: process principles

Promotor: Prof. Dr. Ir. R.M. Boom
Hoogleraar levensmiddelenproceskunde, Wageningen Universiteit

Co-promotor: Dr. Ir. A. van der Padt
Voormalig universitair docent sectie proceskunde, thans werkzaam bij
Friesland Coberco Dairy Foods, Corporate Research te Deventer

Promotiecommissie: Prof. Dr. M.A. Cohen Stuart
Wageningen Universiteit
Dr. J.J.M. Janssen
Unilever R&D Vlaardingen
Prof. Dr.-Ing. habil. H. Schubert
Universiteit Karlsruhe, Duitsland
Prof. Dr.-Ing. M. Wessling
Universiteit Twente

Anneke Gijsbertsen-Abrahamse

Membrane emulsification: process principles

Proefschrift

Ter verkrijging van de graad van doctor
op gezag van de rector magnificus
van Wageningen Universiteit,
Prof. Dr. Ir. L. Speelman,
in het openbaar te verdedigen
op woensdag 4 juni 2003
des namiddags te vier uur in de Aula.

Anneke Gijsbertsen-Abrahamse

Membrane emulsification: process principles

Thesis Wageningen University, The Netherlands, 2003 – with Dutch summary

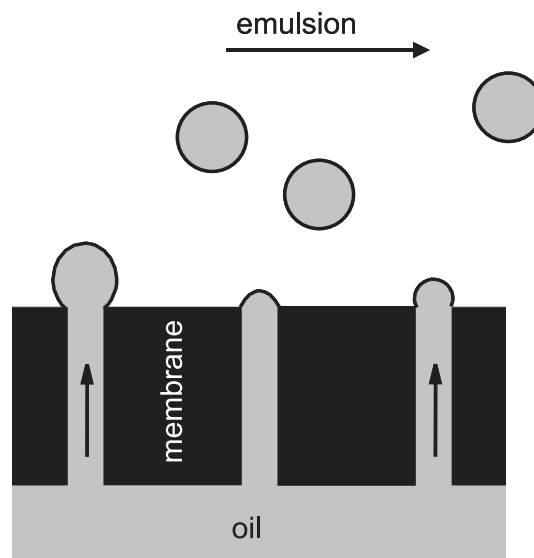
ISBN 90-5808-845-6

Contents of Membrane emulsification: process principles

1.	Introduction	7
2.	Simulation of droplet formation	15
3.	Analysis of droplet formation	29
4.	Effect of membrane morphology on pore activation	47
5.	Estimating pore size distributions of interconnected porous materials with liquid displacement methods	63
6.	Discussion and outlook for industrial application	79
	Summary	97
	Samenvatting	99
	Nawoord	102
	Curriculum vitae	104

1 Introduction

Membrane emulsification is a technique that makes use of a membrane to produce emulsion droplets. The to-be-dispersed phase is pressed through the membrane pores; under certain conditions droplets are formed at the membrane surface. In cross-flow membrane emulsification the droplets are detached by the continuous phase flowing across the membrane surface.



Emulsions

An emulsion is a dispersion of one liquid into another liquid. These liquids do not mix or are mutually only slightly soluble. The dispersed liquid is present in the form of droplets in the continuous phase. Two emulsions found in nature are milk and rubber latex [1]. Emulsions and emulsion production are subjects of extensive research [2]. Emulsions are used in a variety of fields: in foods, pharmaceuticals, cosmetics, paints, in agents for crop protection and in bitumen [1, 3]. For large-scale production of emulsions, rotor-stator systems, colloid mills and high-pressure homogenizers are mostly used [2, 4]. A coarse emulsion, prepared by stirring, is fed to the above mentioned equipment for further emulsification. In a colloid mill, which is a rotor-stator system, the droplets are broken up by shear stresses in the small space between the rotor and the stator. Colloid mills are particularly suitable for producing emulsions with a medium to high viscosity of the continuous phase. Minimum droplet sizes are around 1 μm . A narrow droplet size distribution can be obtained if the energy density (a measure of the energy input per cubic meter) in the space between rotor and stator can be controlled well [4, 5]. In a high-pressure homogenizer, the droplets are broken up in the nozzle by turbulence and cavitation. Pressures up to 100 MPa are used to produce up to 50 m^3 emulsion per hour with droplet sizes down to 0.1 μm [6, 7]. In Figure 1 the droplet size is shown as a function of the energy density for different types of equipment. Energy requirements are high because only a fraction of the energy input is used for droplet break-up. In a high-pressure homogenizer, about 99.8% of the energy supplied is lost and converted into heat. Figure 1 shows that cross-flow membrane emulsification, invented relatively recently by Nakashima *et al.* [8] is a more efficient process, especially for the production of emulsion droplets smaller than 1 μm .

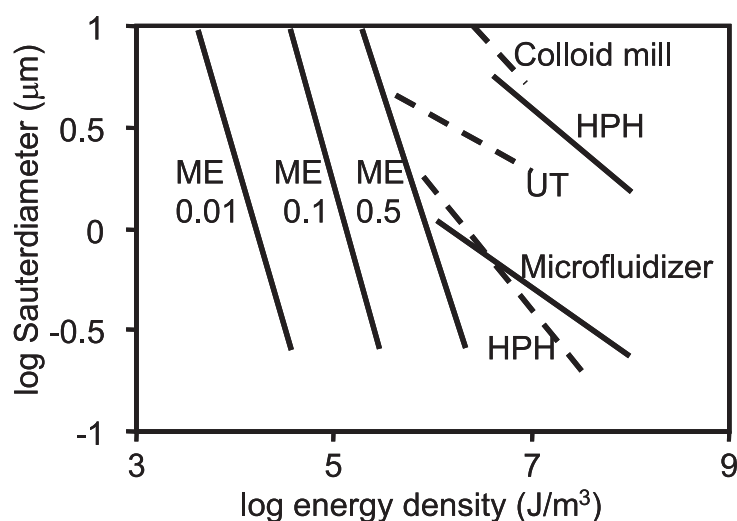


Figure 1: Droplet diameter as a function of the energy density supplied by different types of equipment. ME: cross-flow membrane emulsification, numbers denote the disperse phase fraction; HPH: high-pressure homogenizer; UT: Ultra Turrax. Solid lines reprinted from [9], dashed lines reprinted from [10].

Membrane emulsification

Techniques to produce emulsions using membranes can be divided in two groups: either a coarse pre-mixed emulsion can be pressed through the membrane to reduce the droplet size of the disperse phase, or only the to-be-dispersed phase is pressed through the membrane and forms droplets at the pore openings in the membrane surface, the droplets are detached by the cross-flowing continuous phase. The first technique, which may be called dead-end or pre-mix membrane emulsification, gives a reasonable emulsification flux (about $10 \text{ m}^3 \text{ m}^{-2} \text{ h}^{-1}$ at $15 \cdot 10^5 \text{ Pa}$). In spite of that, up till now only one research group published results on this process [11, 12]. Conversely, the effect of different factors on cross-flow membrane emulsification performance were studied by several groups and reviewed by Joscelyne and Trägårdh. Typically, droplets of $1 - 10 \text{ }\mu\text{m}$ and disperse phase fluxes of $0.01 - 0.1 \text{ m}^3 \text{ m}^{-2} \text{ h}^{-1}$ are obtained [13]. Table 1 shows the importance of the processing parameters on the average droplet size, droplet size distribution and the disperse phase flux, including relevant references to results published in literature.

One of the frequently mentioned advantages of membrane emulsification over other techniques is the lower energy density requirement (mentioned above), which also implies that less shear stress is exerted on the ingredients. Another feature is the monodispersity of the droplets, obtained under certain conditions. Making use of the advantages of the technique,

Table 1: The importance of several parameters on the average droplet size (d_{dr}), width of the droplet size distribution (σ) and the disperse phase flux, based on references or estimated by the authors. The symbols indicate: $\circ\circ\circ$: parameter is very important; $\circ\circ$: important; \circ : not important.

	parameter	d_{dr}	Ref.	σ	Ref.	flux	Ref.
membrane parameters	average pore radius	$\circ\circ\circ$	[14, 15]	\circ		$\circ\circ\circ$	
	shape of the pore opening	$\circ\circ$	[16]	$\circ\circ\circ$	[16]	$\circ\circ$	
	pore length	\circ		\circ		$\circ\circ$	
	wetting	$\circ\circ\circ$	[17]	$\circ\circ$	[17]	\circ	
	porosity	$\circ\circ$		$\circ\circ\circ$	[18, 19]	$\circ\circ\circ$	
	thickness	\circ		\circ		$\circ\circ\circ$	
	proc. cond.	cross-flow velocity	$\circ\circ\circ$	[14, 15, 18, 20]	$\circ\circ\circ$	[9, 18, 21]	\circ
transmembrane pressure		$\circ\circ\circ$	[14, 22, 23]	$\circ\circ$	[19, 22, 24]	$\circ\circ\circ$	[14, 15, 25]
temperature		\circ		\circ		$\circ\circ$	
ingredients prop.	continuous phase viscosity	$\circ\circ$	[9, 26]	\circ		\circ	[9]
	disperse phase viscosity	$\circ\circ$	[9, 26]	\circ		$\circ\circ\circ$	[9]
	emulsifier type	$\circ\circ\circ$	[18, 25]	$\circ\circ$	[25]	$\circ\circ$	[25]

amongst other things, the following applications were studied:

- a low-fat spread was developed and commercialized [27];
- drug-delivery systems: an anti-cancer drug was encapsulated in oil and after injection in the blood was slowly released in the target organ [27, 28];
- porous beads were prepared to be used as packing beads in gel permeation chromatography or as carriers for immobilizing e.g. glucoamylase [22]. The required sizes (several tens of micrometers) and monodispersity are difficult to prepare by conventional techniques;
- microcapsules with metal oxides encapsulated to be used as pigments for cosmetics and paints and as photo-oxidation catalysts e.g. for waste water treatment [29].

Thus, cross-flow membrane emulsification has potential to produce monodisperse emulsions, perhaps even nanosized, and emulsions with shear sensitive components with relatively low energy input. However, a limiting factor for emulsion production on a commercial scale will be a low disperse phase flux [13]. Table 1 clearly shows that the disperse phase flux largely depends on properties of the membrane, yet, these parameters did not gain much attention. Better knowledge of how membrane parameters affect the disperse phase flux would enable the targeted development of membranes, optimal for the process of cross-flow membrane emulsification for a given application. Therefore, the objective of this research is to gain a fundamental understanding of the mechanism of droplet formation at the membrane surface and of the flow of the disperse phase through the membrane as a function of the membrane characteristics.

Outline of the thesis

During this study the focus gradually shifted from a micrometer scale (chapter 2) towards emulsion production scale (chapter 6). Along with the keywords describing the contents of the chapters of this thesis, the scale range is shown in Figure 2. Droplet formation was studied at a microscopic level with computational fluid dynamics (CFD) simulations (chapter 2) and by microscopic experiments of droplet formation at a very thin microsieve[®] with uniform pores (chapter 3). Since these membranes are extremely well defined, they are a good model system for detailed study. Results from both simulations and experiments indicate that to prevent coalescence and steric hindrance of droplets, the membrane porosity should be very low. Steric hindrance resulted in polydisperse emulsions and led to coupling of droplet detachment from neighboring pores. Furthermore, although the pores all had the same diameter, the number of pores at which droplets were formed only increased gradually with increasing transmembrane pressure. This effect was further studied with a scaled-up analogon and could be modeled by taking the resistance of the pores and the resistance of a membrane substructure into account (chapter 4). In chapter 5 this model is compared with a model for flow through an isotropic membrane with interconnected uniform pores and extended to describe flow through a membrane with a pore size distribution of the membrane surface.

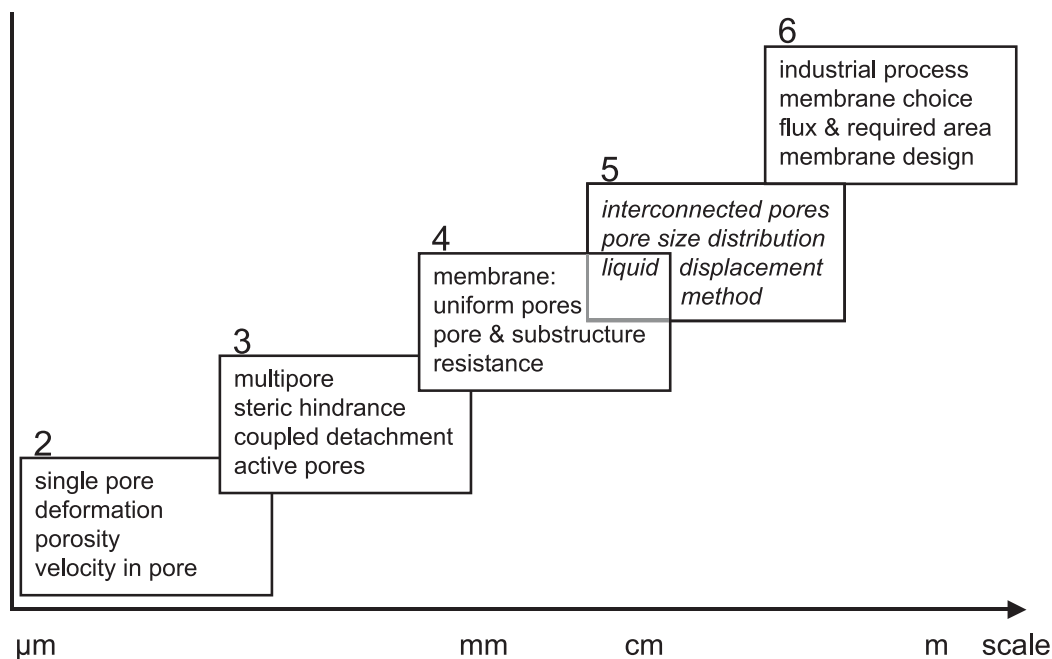


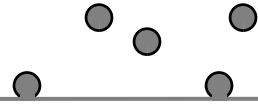
Figure 2: Scheme of the study towards the effect of membrane parameters on disperse phase flux in cross-flow membrane emulsification, described in chapters 2 – 6 of this thesis.

This model is used to show that in most cases the estimation of a membrane pore size distribution by using the liquid displacement method is not correct. Just as in membrane emulsification, pores become active at higher transmembrane pressures than expected. Finally, in chapter 6 the effects of several membrane parameters on membrane emulsification performance are summarized. As an example, the membrane area required for a typical industrial application is estimated for different types of membranes, using the models described in chapters 4 and 5.

Reference list

- 1 W.C. Griffin, Emulsions, in H.F. Mark, D.F. Othmer and C.G. Overberger (Ed.), Kirk-Othmer Encyclopedia of Chemical Technology, Volume 8, John Wiley & Sons, New York, 1979, 900-930.
- 2 P. Walstra, Formation of Emulsions, in P. Becher (Ed.), Encyclopedia of Emulsion Technology, Volume 1 Basic Theory, Marcel Dekker, Inc., New York, 1983, 57-127.
- 3 D.Z. Becher, P. Becher, M.M. Breuer, D. Clausse, S.S. Davis, J. Hadgraft, E.N. Jaynes, N.J. Krog, K. Larsson, V.B. Menon, K.J. Palin, T.H. Riisom and D.T. Wasan, Encyclopedia of Emulsion Technology, Volume 2 Applications, Marcel Dekker, Inc., New York, 1985.
- 4 H. Schubert and H. Armbruster, Principles of Formation and Stability of Emulsions, Int. Chem. Eng., 32 (1992) 14.
- 5 W.S. Arbuckle, Emulsification, in C.W. Hall, A.W. Farrall and A.L. Rippen (Ed.), Encyclopedia of Food Engineering, Avi Publishing Company Inc., Westport, Connecticut, 1986, 286-288.
- 6 H. Reuter, Homogenization, in M.S. Peterson and A.H. Johnson (Ed.), Encyclopedia of Food Science, Avi Publishing Company Inc., Westport, Connecticut, 1978, 374-376.
- 7 J.G. Brennan, Emulsification, Mechanical Procedures, in C.W. Hall, A.W. Farrall and A.L. Rippen (Ed.), Encyclopedia of Food Engineering, Avi Publishing Company Inc., Westport, Connecticut, 1986, 288-291.

- 8 T. Nakashima, M. Shimizu and M. Kukizaki, Membrane Emulsification by Microporous Glass, *Key Eng. Mater.*, 61 & 62 (1991) 513.
- 9 V. Schröder, Herstellen von Öl-in-Wasser-Emulsionen mit Mikroporösen Membranen, PhD thesis, Technische Hochschule Karlsruhe, 1999.
- 10 P. Walstra and P.E.A. Smulders, Emulsion Formation, in B.P. Binks (Ed.), *Modern Aspects of Emulsion Science*, The Royal Society of Chemistry, Cambridge, 1998, 56-99.
- 11 K. Suzuki, I. Shuto and Y. Hagura, Application of Membrane Emulsification Method for Preparing Food Emulsions and Emulsion Characteristics, in *Proceedings of the Developments in Food Engineering, Proceedings of the 6th International Congress on Engineering and Food Part 1*, (1994) 167.
- 12 K. Suzuki, I. Fujiki and Y. Hagura, Preparation of Corn Oil/Water and Water/Corn Oil Emulsions Using PTFE Membranes, *Food Sci. Technol. Int. Tokyo*, 4 (1998) 164.
- 13 S.M. Joscelyne and G. Trägårdh, Membrane Emulsification - a Literature Review, *J. Membrane Sci.*, 169 (2000) 107.
- 14 R. Katoh, Y. Asano, A. Furuya, K. Sotoyama and M. Tomita, Preparation of Food Emulsions Using a Membrane Emulsification System, *J. Membrane Sci.*, 113 (1996) 131.
- 15 S.J. Peng and R.A. Williams, Controlled Production of Emulsions Using a Crossflow Membrane. Part I: Droplet Formation From a Single Pore, *Trans. Inst. Chem. Eng.*, 76 (1998) 894.
- 16 I. Kobayashi, M. Nakajima, K. Chun, Y. Kikuchi and H. Fujita, Silicon Array of Elongated Through-Holes for Monodisperse Emulsion Droplets, *AIChE Journal*, 48 (2002) 1639.
- 17 N.C. Christov, D.N. Ganchev, N.D. Vassileva, N.D. Denkov, K.D. Danov and P.A. Kralchevsky, Capillary Mechanisms in Membrane Emulsification: Oil-in-Water Emulsions Stabilized by Tween 20 and Milk Proteins, *Coll. Surfaces A: Physicochemical Eng. Aspects*, 209 (2002) 83.
- 18 I. Kobayashi, M. Yasuno, S. Iwamoto, A. Shono, K. Satoh and M. Nakajima, Microscopic Observation of Emulsion Droplet Formation From a Polycarbonate Membrane, *Coll. Surfaces A: Physicochemical Eng. Aspects*, 207 (2002) 185.
- 19 Chapter 3, published as: A.J. Abrahamse, R. van Lierop, R.G.M. van der Sman, A. van der Padt and R.M. Boom, Analysis of Droplet Formation and Interactions During Cross-Flow Membrane Emulsification, *J. Membrane Sci.*, 204 (2002) 125.
- 20 V. Schröder and H. Schubert, Production of Emulsions Using Microporous, Ceramic Membranes, *Coll. Surfaces A: Physicochemical Eng. Aspects*, 152 (1999) 103.
- 21 S.M. Joscelyne and G. Trägårdh, Food Emulsions Using Membrane Emulsification: Conditions for Producing Small Droplets, *J. Food Eng.*, 39 (1999) 59.
- 22 N. Yamazaki, H. Yuyama, M. Nagai, G.H. Ma and S. Omi, A Comparison of Membrane Emulsification Obtained Using SPG (Shirasu Porous Glass) and PTFE [Poly(Tetrafluoroethylene)] Membranes, *J. Dispersion Sci. Technol.*, 23 (2002) 279.
- 23 V. Schröder, M. Stang and H. Schubert, Emulgieren mit Mikroporösen Membranen, *Lebensmittel- und Verpackungstechnik*, 43 (1998) 80.
- 24 H. Yuyama, T. Watanabe, G.H. Ma, M. Nagai and S. Omi, Preparation and Analysis of Uniform Emulsion Droplets Using SPG Membrane Emulsification Technique, *Coll. Surfaces A: Physicochemical Eng. Aspects*, 168 (2000) 159.
- 25 V. Schröder, O. Behrend and H. Schubert, Effect of Dynamic Interfacial Tension on the Emulsification Process Using Microporous, Ceramic Membranes, *J. Colloid Interface Sci.*, 202 (1998) 334.
- 26 T. Kawakatsu, G. Trägårdh, Ch. Trägårdh, M. Nakajima, N. Oda and T. Yonemoto, The Effect of the Hydrophobicity of Microchannels and Components in Water and Oil Phases on Droplet Formation in Microchannel Water-in-Oil Emulsification, *Coll. Surfaces A: Physicochemical Eng. Aspects*, 179 (2001) 29.



-
- 27 T. Nakashima, M. Shimizu and M. Kukizaki, Particle Control of Emulsion by Membrane Emulsification and Its Applications, *Adv. Drug Delivery Rev.*, 45 (2000) 47.
 - 28 S. Higashi and T. Setoguchi, Hepatic Arterial Injection Chemotherapy for Hepatocellular Carcinoma With Epirubicin Aqueous Solution As Numerous Vesicles in Iodinated Poppy-Seed Oil Microdroplets: Clinical Application of Water-in-Oil-in-Water Emulsion Prepared Using a Membrane Emulsification System, *Adv. Drug Delivery Rev.*, 45 (2000) 57.
 - 29 A. Supsakulchai, G.H. Ma, M. Nagai and S. Omi, Uniform Titanium Dioxide (TiO₂) Microcapsules Prepared by Glass Membrane Emulsification With Subsequent Solvent Evaporation, *J. Microencapsulation*, 19 (2002) 425.



2 Simulation of droplet formation

Abstract

Membrane emulsification is a process in which a to-be-dispersed phase is pressed through a membrane; the droplets formed are carried away with the continuous phase. To design a suitable membrane setup, more insight into the formation of the droplets at the membrane surface is needed. Therefore, the formation of one droplet from a cylindrical pore was calculated using computational fluid dynamics. From the resulting droplet diameter (33 μm ; pore diameter, 5 μm) and the calculated droplet shape, the maximum membrane porosity was calculated to be 1.5%, to prevent coalescence of droplets growing on neighboring pores. Due to the deformation of the droplet and the formation of the neck, the pressure drop over the pore and the velocity of oil in the pore varied in time. During necking, the velocity in the pore decreased sharply. After detachment of the first droplet, no satellite droplets were formed, but a small oil volume remained attached at the pore, forming a new droplet.

Introduction

Emulsification is an important structure-forming process applied in the food, pharmaceutical and cosmetics industry. A relatively new technique to produce emulsions is membrane emulsification: a process in which a to-be-dispersed phase is pressed through a membrane and droplets formed at the membrane surface are carried away with the continuous phase flowing across the membrane. Compared to other emulsification processes, this technique presents several advantages: low energy consumption, because only small shear stresses are needed to form the droplets; control of droplet size and droplet-size distribution; and easy scalability of the process [1-3]. Thus, with this process, food, cosmetic and pharmaceutical emulsions can be improved and new products can be developed.

Until now, membrane emulsification has been studied with ceramic [2, 4] or glass tubular membranes [5]. Originally these membranes were developed for separation purposes. Therefore, they are not necessarily optimal for emulsification. For example, their high porosity may increase coalescence of growing droplets at the membrane surface, which would enlarge the average droplet size and would render the emulsion more heterodisperse. In a different system, in which the droplet formation was visualized by microscopy, a well-defined emulsion was made [6]. However, scale-up of this research system will not be a trivial task. Altogether, a scalable membrane system, tailor-made for membrane emulsification, will make this process commercially more viable.

To make a better design possible, insight into the process of droplet formation at the membrane surface is required. Recently, the important parameters determining the droplet size were identified by calculating the overall forces that act on the forming droplets [3, 4]. Assuming a rigid, spherical droplet, the droplet size is determined by the cross-flow velocity of the continuous phase, the pore diameter, the transmembrane pressure and the (dynamic) interfacial tension. In the two aforementioned studies the authors recognized that the droplet will be deformed because the acting forces have several directions, but the effect of this deformation on the final droplet size was not taken into account. To design an optimal membrane for emulsification, it is important to know the shape of the droplets during their formation. The shape will determine, for instance, whether droplets coalesce at a given membrane surface. However, this shape cannot be calculated using overall (global) force equations. The shape changes locally due to variations in viscous and inertial forces. For example, the greater the distance from the membrane, the higher is the velocity of the continuous phase. As a result, local forces on the droplet vary in place and time, resulting in a changing droplet shape. Of course, this shape also depends on the values of other parameters such as dynamic interfacial tension and transmembrane pressure.

We calculated the shape of an oil droplet forming at a single cylindrical pore with computational fluid dynamics (CFD). In this article we describe the effect of droplet shape on the maximum porosity of the emulsification membrane and on the oil flux through the pore.

Model Setup

The CFD software package used in this research was CFX 4.2 (AEA Technology, UK), which is a finite-volume code. The droplet formation was modeled as a 3-dimensional, multiphase system with laminar flow. Oil flowed through a cylindrical pore and water through a rectangular flow channel. The physical properties and constants are given in Table 1.

Table 1: Values of the physical properties and constants used in the simulation.

Property	Value
density water	1000 kg m^{-3}
density oil	773 kg m^{-3}
viscosity water	$1 \cdot 10^{-3} \text{ Pa s}$
viscosity oil	$3 \cdot 10^{-3} \text{ Pa s}$
interfacial tension	30 mN m^{-1}
wall contact angle for water	0°
gravitational constant	9.81 m s^{-2}

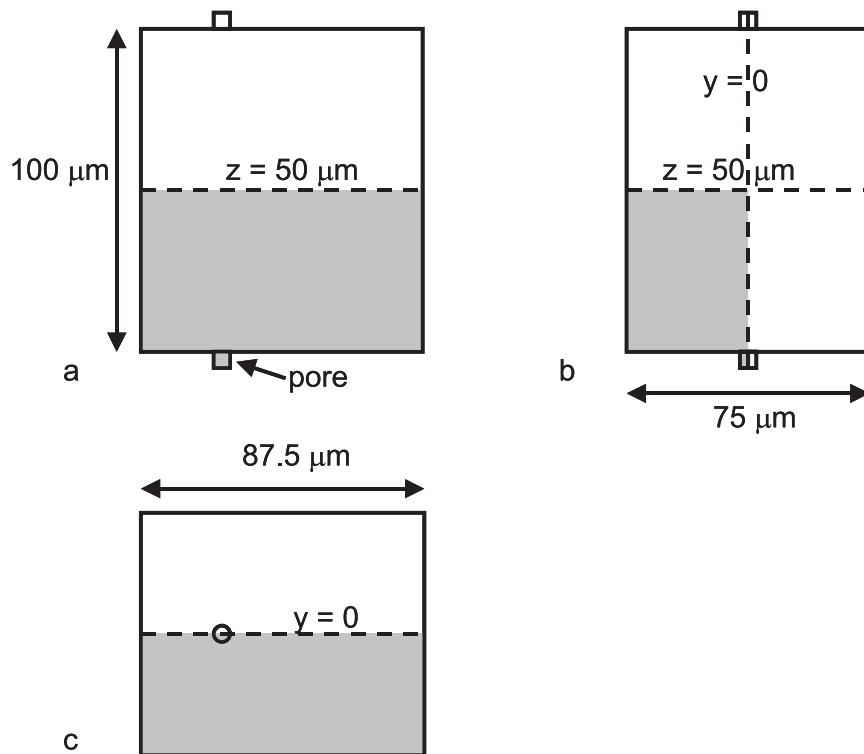


Figure 1: Rectangular flow channel and cylindrical pore. The grey planes depict the modeled geometry; dashed lines represent the symmetry planes. a: front view (x - z plane); b: side view (y - z plane); c: bottom view (x - y plane).

Geometry

The cylindrical pore had a diameter and a length of 5 μm . Only half of the height of the rectangular flow channel was modeled, since the flow is assumed to be symmetrical in the center plane of the channel ($z = 50 \mu\text{m}$; Figure 1a and 1b). The plane $y = 0$ was a symmetry plane as well (Figure 1b and 1c). The part of the flow channel that was modeled had a height of 50 μm (z -direction), a width of 37.5 μm (y -direction), and a length of 87.5 μm (x -direction).

Since it was expected that the velocities of both phases and the pressure change fastest at the

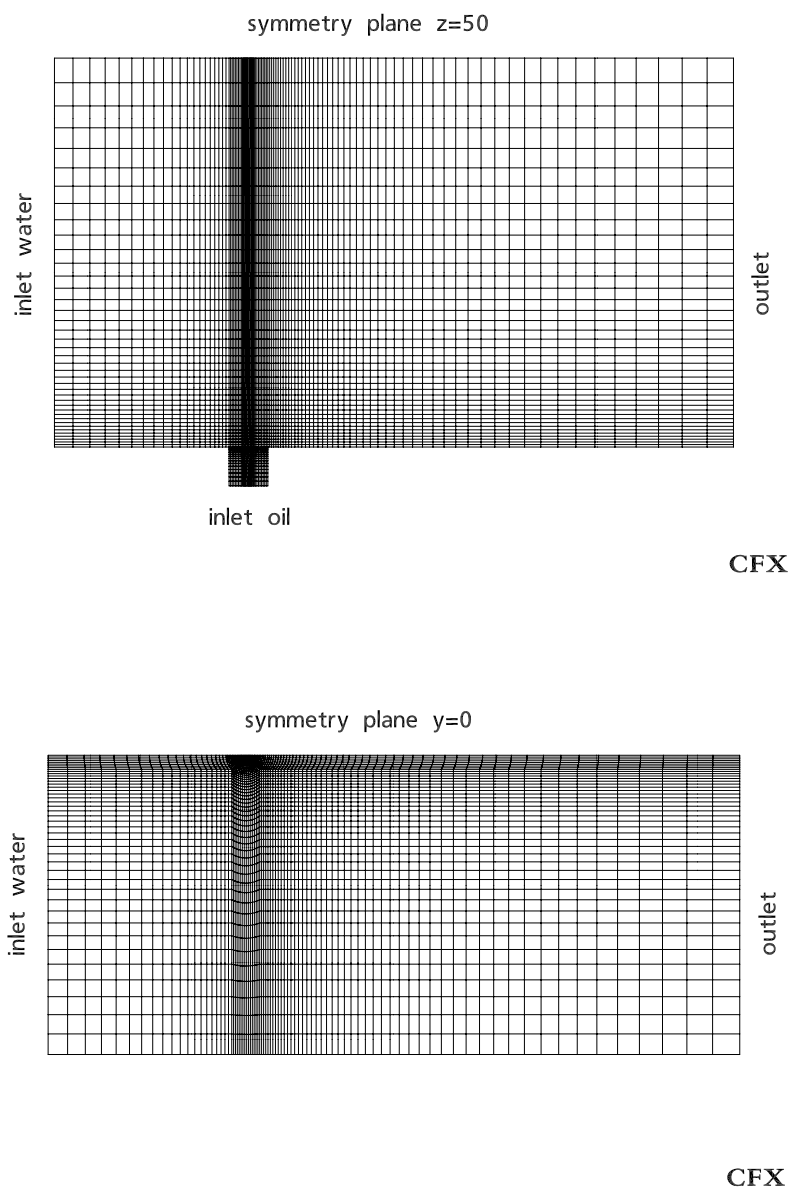
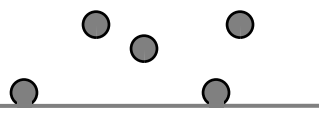


Figure 2: Grid and boundaries of the geometry. top: x - z plane ($y = 0$); bottom: x - y plane ($z = 0$). Compare Figures 1a and 1c.



outflow of the pore into the flow channel, the grid was made finest in that region. The pore was divided into 5520 control volumes, whereas the flow channel contained 156,120 control volumes (Figure 2). The smallest volume cell, which is approximately $1.5 \cdot 10^{-20} \text{ m}^3$, contains about $3 \cdot 10^7$ oil molecules. This number is sufficient to consider the fluid as a continuum, hence the fluid can be described adequately with macroscopic properties such as velocity, pressure, and density.

Boundary conditions

Water flowed through the inlet of the flow channel in the x -direction with an average velocity of 0.5 m/s. A laminar (parabolic) velocity profile at the inlet was generated. At the outlet of the flow channel the pressure was set at $1.0 \cdot 10^5$ Pa. At the inlet of the pore the pressure was set at $1.3 \cdot 10^5$ Pa. The other geometry boundaries were walls, except for the symmetry planes ($y = 0$ and $z = 50 \text{ }\mu\text{m}$). We assumed the no-slip condition to be valid at the walls, which means a local fluid velocity of 0 m/s at the walls.

Initial conditions

The initial conditions were programmed in Fortran. At $t = 0$ s the flow channel was filled with laminary flowing water and the pore was completely filled with oil. At $t = 0$ s the interface between oil and water was flat.

Solver data

The calculation was controlled by the minimum residual value through adaptive time stepping. The values of the parameters are given in Table 2. Unless the parameters are mentioned in this paragraph, the default values of the software package were used.

Table 2: Values of the solver parameters used in the simulation.

Solver parameter	Value
initial time step	$5 \cdot 10^{-7} \text{ s}$
minimum interval between increments	4 time steps
time step multiplying factor ¹	2
time step dividing factor ²	1.5
maximum number of iterations per time step	20
control parameter: minimum residual value	$5 \cdot 10^{-12} \text{ kg/s}$

1. After 4 successfully calculated time steps, the time step is multiplied with this factor. Successfully calculated means that the residual value is lower than the given minimum residual value within less than 20 iterations per time step.
2. The time step is divided by this factor after a failed calculation; this is the case if the residual value is still higher than the minimum residual value after 20 iterations.

It took 2320 time steps to calculate the formation of one oil droplet. This required 16 days of CPU time on a dual Pentium-II workstation (operating system Windows NT) with an internal memory of 2*256 MB.

Calculation of the pressure drop over the pore (Δp_p) and the average oil velocity in the pore ($\bar{v}_{p,oil}$)

At several time steps the pressure and the velocity, calculated by CFD, were extracted from the data files. We took the values calculated in the grid cell in the center of the pore at a distance of 0.51 μm below the pore opening. This distance was chosen to avoid effects from the outflow of oil from the pore into the flow channel on the laminar flow in the pore, which was indeed the case for most time steps.

To calculate the total pressure drop over the pore we subtracted the extracted pressure values from the applied absolute pressure ($1.3 \cdot 10^5$ Pa) and these values were multiplied by the factor 5.00/4.49, to correct for the total length of the pore. The values for the (maximum) oil velocity, extracted from the datafiles, were divided by 2 to calculate the average oil velocity in the pore at several time steps (for laminar flow in a cylindrical pore: $v_{max} = 2 \bar{v}_{p,oil}$).

Calculation of the equivalent Laplace pressure

By calculating the oil flux with the average velocity, we calculated the droplet volume increase and the resulting droplet volume at the different time steps [$V_{dr}(t)$]. From the droplet volume we calculated a corresponding equivalent sphere diameter and from that value an equivalent Laplace pressure (equation 1).

$$\Delta p_{lapl,eq}(t) = \frac{4\gamma}{d_{dr,eq}(t)} = \frac{4\gamma}{[6V_{dr}(t)/\pi]^{1/3}} \quad (1)$$

in which γ is the interfacial tension coefficient (30 mN/m). This equivalent Laplace pressure is an approximation, because with the CFD calculations it was shown that the droplet is not spherical, but has more curvatures. However, the equivalent Laplace pressure agrees quite well (within 20%) with the pressure drop over the interface in the part of the droplet that is almost spherical.

Results and Discussion

Figure 3a-d show the velocity profiles of oil and water and the shape of the droplet at four steps in time. Contour lines connect the control volumes in which the volume fraction of oil is equal. The five lines in Figure 3a span the whole oil volume fraction range from 0 to 1 (0.0, 0.25, 0.5, 0.75, and 1.0). In the other figures only the contour line at a volume fraction of 0.5 is shown. Although the interface is rather broad (about five grid cells), we assume that the

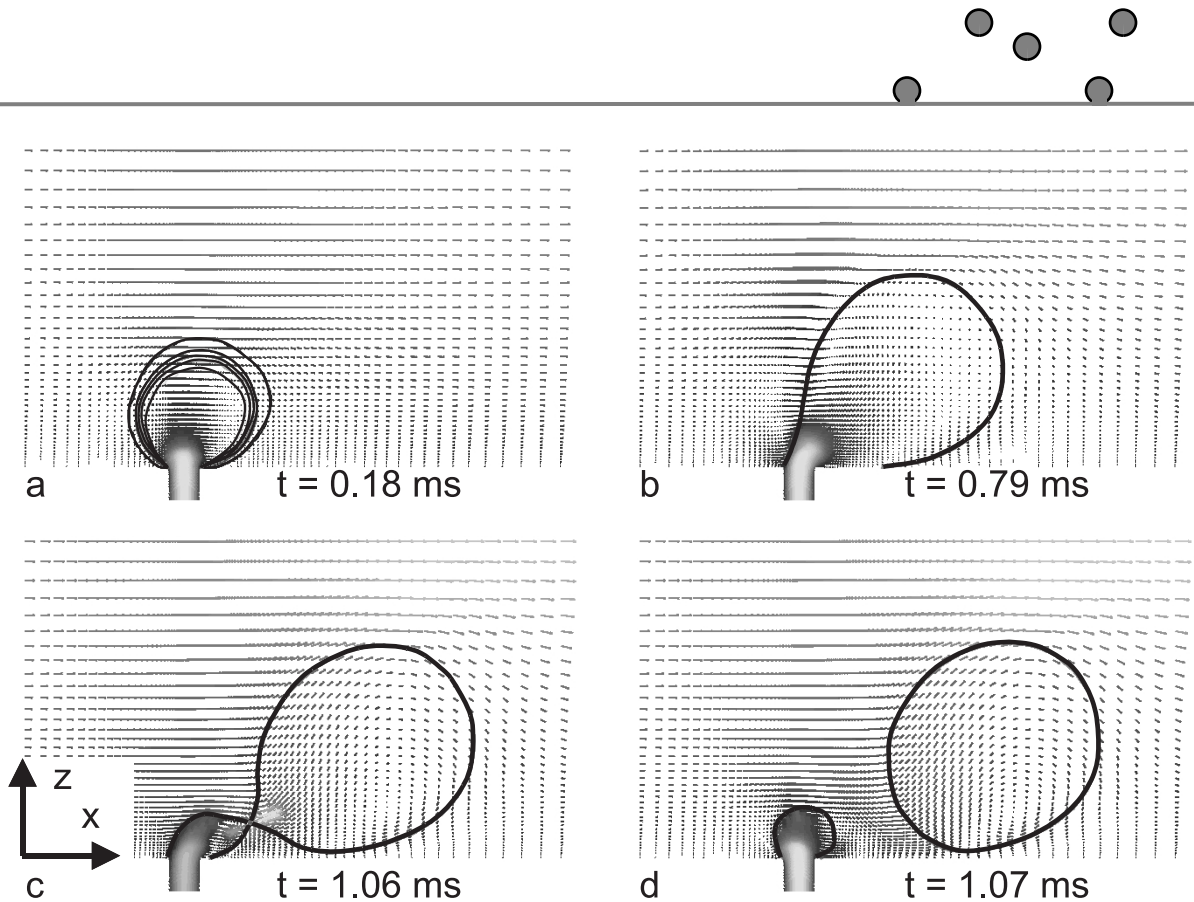


Figure 3 (a-d): Droplet shape (contour lines) and velocities (in m/s, indicated by arrows) of both phases in each grid cell as a function of time, for the plane through the centre of the pore (x - z plane; $y = 0$).

interfacial tension force was calculated correctly. The calculation of this force is based on the continuum surface force (CSF) model developed by Brackbill *et al.* and implemented in CFX 4 by Burt *et al.* [7, 8]. The interfacial tension force is introduced as a body force that is a function of the interfacial tension coefficient and the curvature. The local curvature is described by the normal vector to the free surface. This vector is given by the gradient of the volume fractions. Both groups validated the model against a series of test cases, including free-surface flows and wall effects [7, 8]. Therefore, our assumption of the validity of the interfacial tension force calculations is reasonable.

Porosity of the membrane

The oil droplet diameter was $33 \mu\text{m}$ after detachment had taken place (Figure 3d), thus the droplet diameter was about seven times the pore diameter. This ratio is comparable with the experimentally determined droplet/pore diameter ratio of 5 [9]. Hence, assuming rigid spherical droplets growing simultaneously, the distance between two pores must be at least six times the pore diameter to avoid contact, and thus avoid coalescence, between two neighboring droplets. But as expected, the droplet is deformed in the direction of flow of the continuous phase, which is shown in Figure 3. Although only one pore was modeled, it can be seen that due to the deformation of the droplet, a space of almost 10 times the pore diameter is

needed for unhindered droplet growth in the x -direction. In the y -direction the droplet remained almost spherical throughout the formation process; therefore, the space required in that direction is just seven times the pore diameter. From these data we calculated the maximum porosity of an emulsification membrane. The (surface) porosity is the ratio of the total pore cross-sectional area and the total membrane surface area. Figure 4 shows that the maximum porosity depends on the arrangement of the pores in the membrane. For the so-called uniform grid (Figure 4a), the distance of the pores is $50\ \mu\text{m}$ in the x -direction and $33\ \mu\text{m}$ in the y -direction; as a result, the maximum porosity is 1.2%. With a staggered pore arrangement, the maximum porosity can be slightly higher (Figure 4b): 1.5%.

However, it should be borne in mind that we only simulated the formation of one droplet at a single pore with a constant interfacial tension. First, we expect that droplets growing in a multipore system will have a droplet diameter slightly different from the droplet diameter that was calculated for a single pore, since neighboring droplets disturb the laminar flow profile of the cross-flowing water (Figure 3). A droplet that grows in the “shade” of another droplet will experience a different water-flow profile. Second, a constant interfacial tension implies that (dynamical) effects of emulsifiers were not taken into account. Both in a system without emulsifier and in a system with a slow emulsifier (slowly diffusing with respect to the droplet formation time) the interfacial tension will be constant. Addition of a fast emulsifier in a membrane emulsification system will probably affect the droplet shape and the final droplet size. For these reasons, the values for the maximum porosity are only an indication.

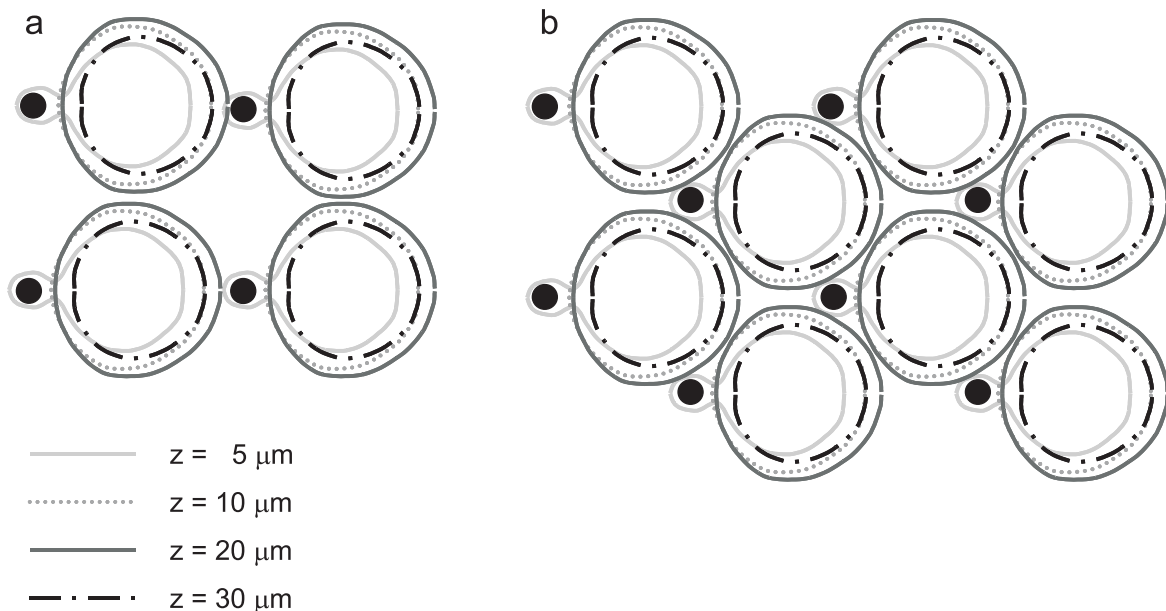


Figure 4: Examples of the arrangement of pores (black) in the membrane with contours of the droplet at 4 distances from the membrane at $t = 1.06 \cdot 10^{-3}$ s. At $z = 20\ \mu\text{m}$ the diameter of the section through the droplet is biggest. a: uniform arrangement; b: staggered arrangement.

Oil flux through the pore

The oil velocity in the pore can be calculated from the pressure drop over the pore (Δp_p) by the Fanning equation (for steady laminar flow in a tubular pipe):

$$\bar{v}_{p,oil} = \frac{d_p^2 \Delta p_p}{32 \eta_{oil} l_p} \quad (2)$$

in which d_p is the pore diameter, η_{oil} the oil viscosity and l_p the length of the pore. Schröder *et al.* [4] reasoned that the velocity of oil in the pore is not constant during the process of droplet formation, because the pressure drop over the pore increases with the size of the droplet. According to them, the total transmembrane pressure can be divided into two parts. One part is the pressure drop over the pore. The other part is the Laplace pressure, being the difference in pressure over the droplet interface, which depends on the curvature of the interface. As Schröder *et al.* [4] assumed a spherical droplet, the Laplace pressure, and thus the pressure drop over the pore, could be calculated. In this section we show that, due to deformation of the droplet, the pressure drop over the pore and the oil velocity in the pore were quite different from those calculated values.

Between 0 and 0.08 ms, the stationary situation is not reached within the iterations per time step, resulting in a decreasing velocity/pressure ratio ($\bar{v}_{p,oil} / \Delta p_p$; Figure 5), but from 0.08 ms onwards, the velocity/pressure ratio is constant; the value follows from equation 2:

$$\frac{\bar{v}_{p,oil}}{\Delta p_p} = \frac{d_p^2}{32 \eta_{oil} l_p} = \frac{(5 \cdot 10^{-6})^2}{32 \cdot 0.003 \cdot 5 \cdot 10^{-6}} = 5.2 \cdot 10^{-5} \text{ m}^2 \text{ s kg}^{-1}$$

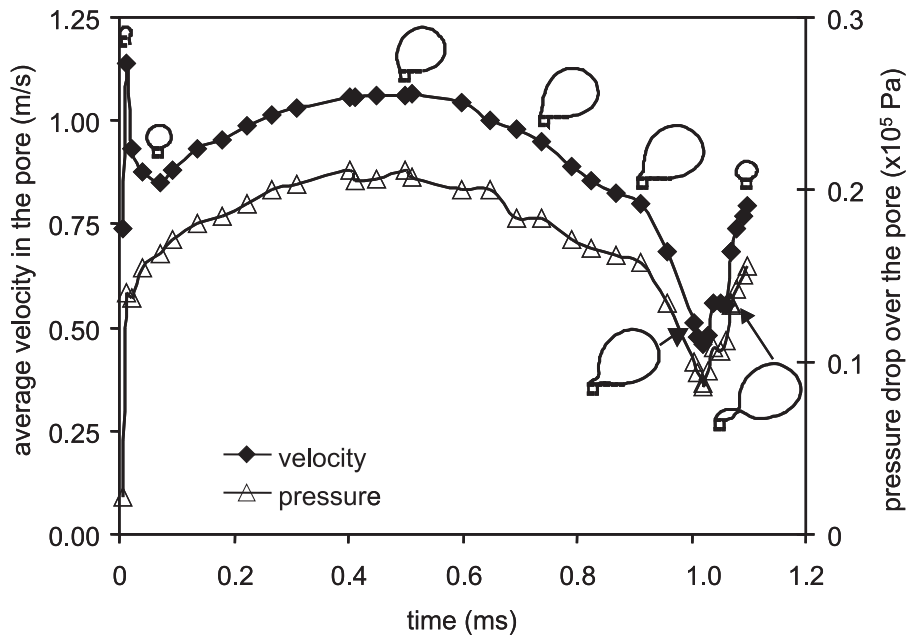


Figure 5: Pressure drop over the pore and average velocity in the pore, both as a function of time. At certain times the droplet shape is depicted.

In Figure 6 the equivalent Laplace pressure calculated with the equivalent sphere diameter (see section model setup), the pressure drop over the pore, the sum of those two pressures, and the transmembrane pressure are shown at several time steps. The droplet formation can be divided into a few stages. In the first stage, until about 0.5 ms, the droplet remained almost spherical (Figure 5). As a result, the Laplace pressure decreased (compare the equivalent Laplace pressure in Figure 6) and the pressure drop over the pore increased. The sum of the equivalent Laplace pressure and the pressure drop over the pore is almost constant during this stage (Figure 6). In the next stage the droplet was that much deformed that the oil was hindered from flowing into the droplet and the oil velocity in the pore started to decrease. After 0.9 ms the velocity decreased sharply, which can be explained by the formation of a neck. Because the neck is only a few micrometers wide, the pressure drop in the neck, between the pore and the droplet, is considerable. This can also be seen in Figure 6: the difference between the sum of the pressures and the transmembrane pressure increases, meaning that there was a resistance against flow somewhere else in the system. At $t = 1.0$ ms, the neck started to widen, which resulted in a higher oil velocity in the pore. After detachment of the droplet, the pressure drop over the pore and the oil velocity in the pore increased further, because the curvature of the newly forming droplet was less sharp than the curvature of the neck. It is important to note that no satellite droplets were formed and that the Laplace pressure in the new droplet is lower than the critical Laplace pressure at the start of the formation of the first droplet, which was $0.24 \cdot 10^5$ Pa ($= 4\gamma/d_p$). This suggests that as soon as one pore is active, no other pores in the neighborhood will become active because the driving force (pressure difference over the pore) is higher for the active pore than for a “starting”

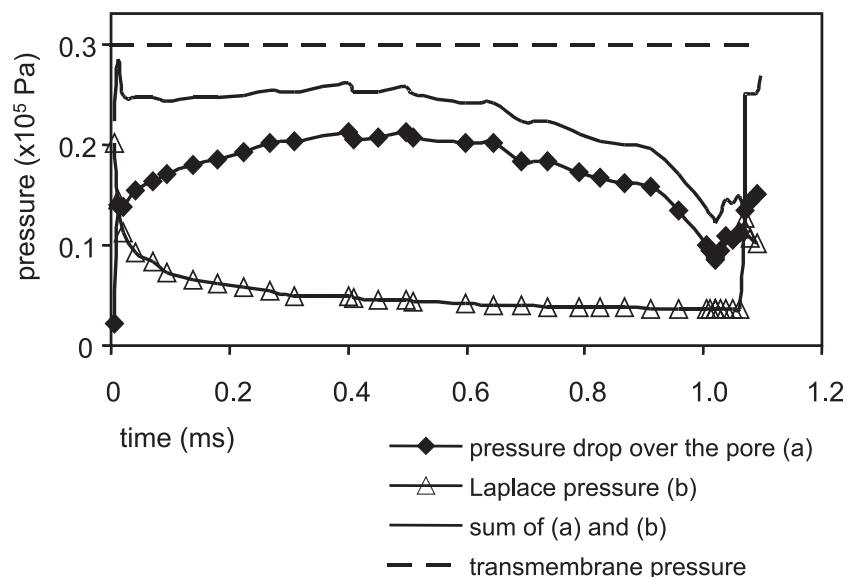
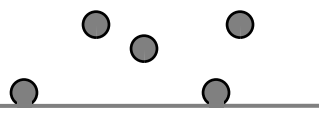


Figure 6: Pressure drop over the pore, calculated from the output data; equivalent Laplace pressure, calculated from the equivalent sphere diameter; sum of both pressures and transmembrane pressure in time.



pore. Qualitative observations (not shown) in a microscopic membrane system point in the same direction: only a few pores were active, although they all had the same pore diameter ($d_p = 5 \mu\text{m}$), and thus the same critical pressure. This is in agreement with Schröder [10]; he found that 3 – 8% of the pores were active at a low transmembrane pressure.

With Figure 6 we show that not only flow in the pore and the Laplace pressure over the interface contribute to the pressure losses in the system, since the sum of these two is never equal to the transmembrane pressure. This is due to viscous dissipation as a result of flow inside the droplet caused by other forces on the droplet (such as drag of the continuous phase). This dissipation term is especially important when the neck is formed, as was explained in the previous paragraph. The pressure drop in the flow channel was negligible.

The time-averaged velocity in the pore ($\bar{v}_{p,oil}$) was 0.92 m/s, which is even higher than the average velocity of the water phase. Due to the high velocity, the droplet formation time was short, only 1.06 ms. The high oil flux through the pore was caused by the low oil viscosity ($\eta_{oil} = 3 \cdot 10^{-3} \text{ Pa s}$) and the extremely short pore chosen ($l_p = 5 \mu\text{m}$). The value for the formation time (1.06 ms) can therefore not directly be compared with calculated droplet formation times (0.09 – 1.05 s) from experiments described in literature because of different conditions [1].

Membrane wetting and fouling

Calculations were performed with a contact angle of 0° for water on the membrane surface, which means that oil will not spread on it. However, in Figure 3b it was shown that the forming oil droplet partly touched the membrane surface, as a result of the deformational forces of the continuous phase on it. In a later stage the membrane was again wetted by water and the droplet completely detached from the membrane surface (although a small part remained at the pore). This formation process indicates that the contact angle with the membrane material should not be too high.

In Figure 7 the pore and part of the flow channel are magnified and oil fractions of 0.5 and 0.99 are given by contour lines. The figure may be an indication of an interesting wetting phenomenon: due to deformation of the droplet in the x -direction, water can enter the pore at the other side. This could have practical implications: when doing experiments with proteins as emulsifier, water entering the pore could cause membrane fouling. For example, proteins can stick with their hydrophilic groups to the surface, in this way making the pore hydrophobic and thereby changing the droplet formation process or ultimately even blocking the pore.

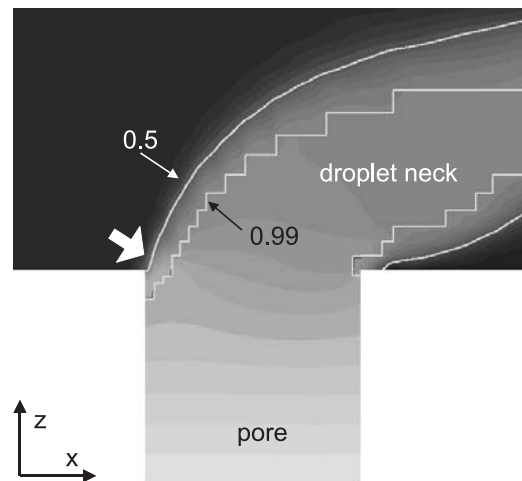
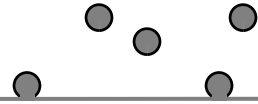


Figure 7: Water entering the pore at $t = 1.05$ ms (indicated with arrow). Velocity profile (m/s) and contour lines at oil fractions 0.5 and 0.99.

Conclusions

Computational fluid dynamics (CFD) was successfully used to calculate the shape of a droplet growing at a pore in a laminar cross-flow. These calculations facilitate the design of a membrane, tailor-made for membrane emulsification. For a cylindrical pore ($d_p = 5 \mu\text{m}$) the resulting droplet diameter was $33 \mu\text{m}$. However, due to deformation during droplet formation, the pores should be placed more than ten times the pore diameter apart in the direction of flow (x -direction), to prevent the coalescence of droplets growing on neighboring pores, under the assumption that the droplets are growing simultaneously. In the y -direction only a distance of seven times the pore diameter is needed. The maximum porosity for a membrane with a staggered arrangement of the pores is about 1.5%. Therefore the porosity of a membrane for emulsification has to be low, and should preferably be different in the x - and y -directions. The velocity of oil through the pore was shown to depend on the shape of the droplet. The velocity sharply decreased at the moment a neck was formed. After detachment of the droplet by further necking, a small droplet remained attached to the pore, which has a Laplace pressure lower than the critical pressure. This will possibly prevent oil from flowing through pores close to a pore that is already active. In case very few pores are active, such that less than 1% of membrane surface area is used, the porosity of the membrane surface is not relevant any more. Anyhow, coalescence of droplets at the membrane surface will be prevented in that case.



Reference list

- 1 V. Schröder and H. Schubert, Production of Emulsions Using Microporous, Ceramic Membranes, *Coll. Surfaces A: Physicochemical Eng. Aspects*, 152 (1999) 103.
- 2 S.M. Joscelyne and G. Trägårdh, Food Emulsions Using Membrane Emulsification: Conditions for Producing Small Droplets, *J. Food Eng.*, 39 (1999) 59.
- 3 S.J. Peng and R.A. Williams, Controlled Production of Emulsions Using a Crossflow Membrane. Part I: Droplet Formation From a Single Pore, *Trans. Inst. Chem. Eng.*, 76 (1998) 894.
- 4 V. Schröder, O. Behrend and H. Schubert, Effect of Dynamic Interfacial Tension on the Emulsification Process Using Microporous, Ceramic Membranes, *J. Colloid Interface Sci.*, 202 (1998) 334.
- 5 S. Omi, Preparation of Monodisperse Microspheres Using the Shirasu Porous Glass Emulsification Technique, *Coll. Surfaces A: Physicochemical Eng. Aspects*, 109 (1995) 97.
- 6 T. Kawakatsu, Y. Kikuchi and M. Nakajima, Regular-Sized Cell Creation in Microchannel Emulsification by Visual Microprocessing Method, *J. Am. Oil Chem. Soc.*, 74 (1997) 317.
- 7 J.U. Brackbill, D.B. Kothe and C. Zemach, A Continuum Method for Modeling Surface Tension, *J. Comput. Phys.*, 100 (1992) 335.
- 8 D.J. Burt, J.W.J. Ferguson and H. Pordal, Numerical Computation of Surface Tension Effects, *Proc. ASME*, 3 (1996) 439.
- 9 R. Katoh, Y. Asano, A. Furuya and M. Tomita, Conditions for Preparation of W/O Food Emulsions Using a Membrane Emulsification System, *Nippon Shokuhin Kagaku Kogaku Kaishi*, 42 (1995) 548.
- 10 V. Schröder, Herstellen von Öl-in-Wasser-Emulsionen mit Mikroporösen Membranen, PhD thesis, Technische Hochschule Karlsruhe, 1999.



3

Analysis of droplet formation

Abstract

During cross-flow membrane emulsification, droplet formation at a micro-engineered membrane with uniform pores was visualized by microscopy. Although the membrane pores were uniform in size, the obtained emulsions were polydisperse. Observations showed this to be due to steric hindrance of droplets forming simultaneously. At some pores close together, the droplet formation frequencies were almost identical (0.86 and 0.88 s⁻¹). This was confirmed by the cross-correlation value (around 0.8). Because the droplets hindered each other during growth, the droplet diameter decreased with an increasing number of active pores. In spite of the uniform pore size and shape, the number of active pores only gradually increased upon increasing transmembrane pressure. We suggest this to be due to the dynamics of the flow of the to-be-dispersed phase towards and through the membrane. Under the process conditions used, interactions can only be prevented by using a membrane with a lower porosity.

Introduction

In cross-flow membrane emulsification a liquid phase is pressed through the membrane pores to form droplets at the permeate side of the membrane; the droplets are carried away by a continuous phase flowing across the membrane surface. Under specific conditions, monodisperse emulsions can be produced using this technique. Substantial research has been carried out how to produce monodisperse emulsions for food, pharmaceutical and cosmetic applications [1-3] and how to produce monodisperse microspheres by polymerization after emulsification e.g. to be used as column packing material. The results were recently reviewed by Joscelyne and Trägårdh [4].

In conventional emulsification processes, severe process conditions are necessary for break-up of the emulsion droplets, which puts high shear on the components and is energy intensive. Especially for producing small droplets ($< 3 \mu\text{m}$) the energy requirement is much lower in membrane emulsification than in conventional processes [5]. Because of the low shear stresses, new products with shear sensitive components can be developed [6, 7].

Unfortunately, the process is not yet commercially feasible because of a low throughput of the to-be-dispersed phase. The throughput is determined by the transmembrane pressure, pore size, membrane porosity and the viscosities of the fluids, among other factors (Figure 1). However, these characteristics affect the obtained average droplet diameter too. For example, the tubular microporous ceramic and glass membranes [8, 9], which are generally used, have a high porosity but quite a thick membrane layer. The second feature is not favorable for a high throughput. A high porosity is favorable for the throughput but not for the droplet size: in an earlier study [10] we have shown that the membrane surface porosity should ideally not be

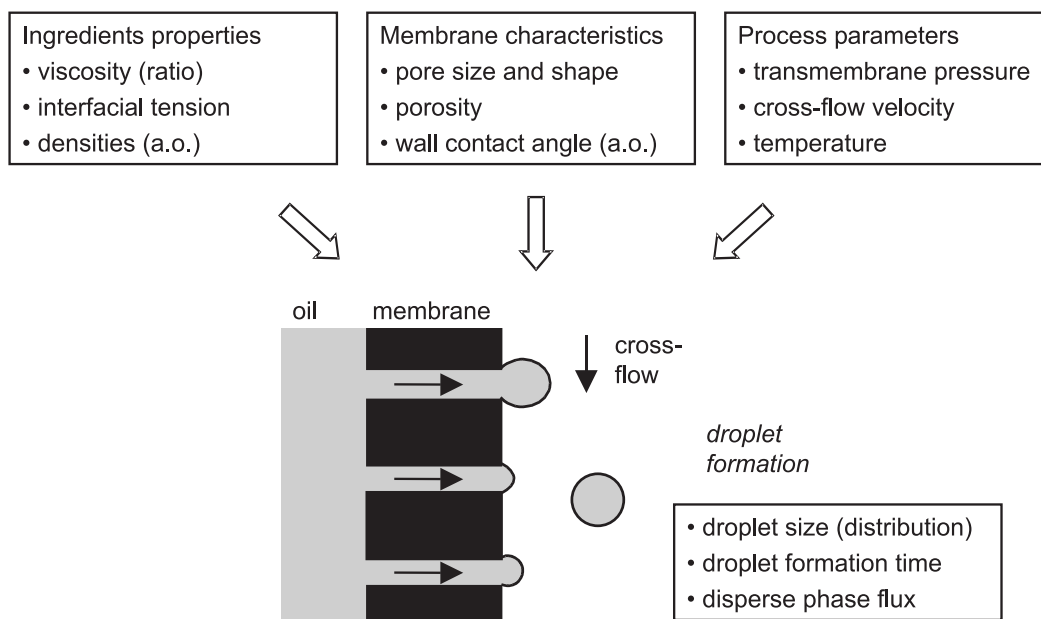
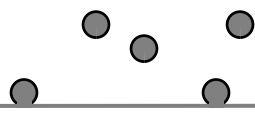


Figure 1: Parameters in membrane emulsification affecting the droplet formation process and thus the droplet diameter and throughput (a.o.: amongst others).



higher than 1.5%. At a higher surface porosity the droplets could touch during droplet formation and possibly coalesce. Moreover, Schröder deduced that depending on pore size and transmembrane pressure, droplets formed at only 3-40% of the pores [5]. This low percentage of active pores is disadvantageous for the overall productivity. In conclusion, we can say that there is a careful balance between the disperse phase throughput and the emulsion droplet diameter.

Direct examination of the formation of individual emulsion droplets using a microscope video system enables one to study the fundamental processes of droplet formation. Visualization experiments with single capillaries in a cross-flow channel show that with an increasing cross-flow velocity both the droplet diameter and the droplet formation time decrease [5, 11]. Increasing the pressure difference also decreases the droplet formation time but results in a larger droplet diameter. In a system with capillaries in a bundle, without emulsifier, coalescence was shown [5]. Droplet formation at membrane surfaces was also studied by the same author, but the pores themselves could not be seen. Further, droplet formation in a microengineered silicon microchannel system was visualized by microscopy [12-14]. However, since the geometry of the cross-flow channel is rather different, it is likely that the mechanism for droplet break-up in this system may not be the same as in the systems described before [15].

In this chapter, we discuss the results of visualization of droplet formation at the surface of a uniform microengineered membrane during cross-flow emulsification. Direct examination provides insight in droplet formation times, the number of active pores and therewith in the oil throughput. We suggest that the low number of active pores is caused by the dynamics of the flow under the membrane. Further, we show that droplets interact due to steric hindrance and collisions, which affects the droplet diameter.

Experimental and Calculation Methods

Chemicals

1% (w/w) Tween 20 (Polyoxyethylene sorbitan monolaurate, for synthesis, Merck) dissolved in demineralized water was used as the continuous phase. The disperse phase was n-hexadecane (for synthesis, Merck) colored with Sudan red (7B for microscopy, Merck). Before the experiment, this solution was passed through a Durapore membrane filter (Millipore) with an average pore diameter of 0.45 μm . Droplet formation was studied with the setup described below.

Membrane

To cancel out the effect of differences in pore diameters in the membrane, we used a microengineered Aquamarijn microsieve[®] [16, 17] which is a uniform membrane, implying: 1. Uniform pore sizes and shapes; 2. The pores are uniformly distributed over the membrane surface. The membrane was a kind gift of S. Kuiper and Aquamarijn. It was made of silicon

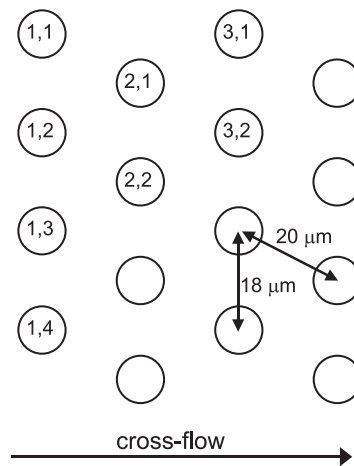


Figure 2: Arrangement and numbering of the pores in the membrane.

nitride of 1 μm thickness and contained circular pores arranged in groups of 100 identical pores with pore diameters ranging from 1.5 to 7 μm [17]. Only droplet formation at the 100 largest pores with a diameter of 7 μm was studied. The arrangement of these pores, the distances between the pores and the numbering, used in the results section, are shown in Figure 2. From the known dimensions, the surface porosity was calculated to be 0.15.

Glueing a hollow glass plate on top of the sieve created the cross-flow channel. The channel height, width and length were 0.26, 10 and 39 mm, respectively. With respect to the height of the cross-flow channel, this module differs from the systems studied in literature. Although the size of some droplets was almost the same as the cross-flow channel height, they did not remain in the channel: all the droplets were removed with the cross-flow.

Experimental methods

Experimental setup: The experimental setup is shown in Figure 3. Hexadecane was pressurized in a pressure vessel. At the outflow of the vessel, the pressure was measured. The continuous (aqueous) phase passed through the membrane module due to a height difference between the in- and outflow vessels, of which the levels were kept constant by a continuous overflow construction. Silicone tubing with a total length of 2.5 m was used.

The cross-flow velocity of the continuous phase (v_c) and the transmembrane pressure (p_{trm}) were calculated from the measured height difference between the continuous phase vessels (Δh) and the measured disperse phase pressure (p_d): $v_c = 1.11\Delta h$; $p_{trm} = p_d - p_c = p_d - \rho_c g(h_{c,in} + h_{c,out})/2$. The pressure of the continuous phase in the module could be calculated in this way, because the friction in the tubes was negligible compared to the friction in the module.

Cleaning: Before the experiments, a detergent solution (5-10% Glorix[®] with hydrogen peroxide) was flushed through the tubing and the module (including the membrane), both through the cross-flow channel and through the disperse phase inlet. Meanwhile the module

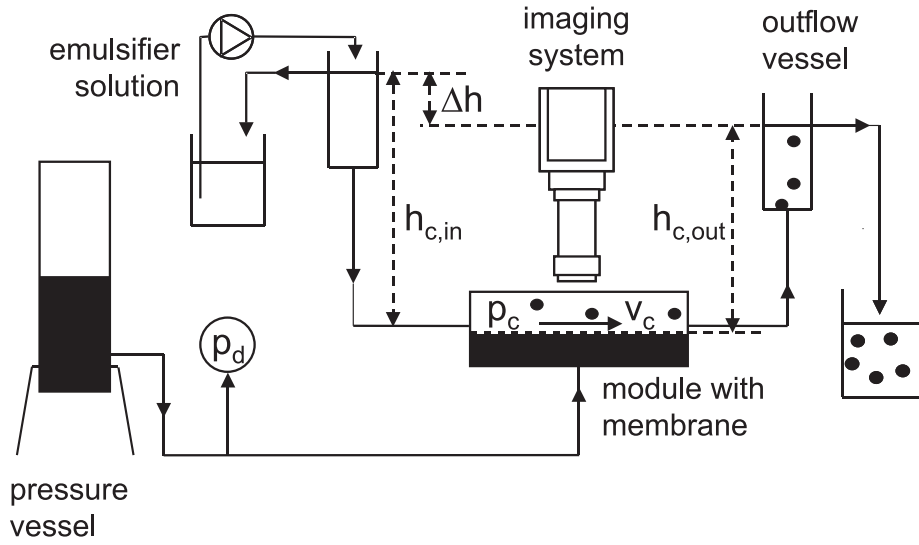


Figure 3: Experimental setup. Symbols concerning the calculation of the cross-flow velocity and the transmembrane pressure are explained in the list of symbols.

was kept at a temperature of 50 °C. After that, the module and tubes were flushed for a day with demineralized water. The pressure vessel was also cleaned with detergent and demineralized water. Tubing, module and pressure vessel were air dried.

Visualization: Images with a magnification of 400x, acquired with a Zeiss Axioplan microscope, were recorded with a Sony CCD video camera (type XC-77CI). The frequency was 25 images per second, which restricted the cross-flow velocity. While replaying, the diameters of the droplets detaching from the membrane were measured manually and the times at which droplet formation started and at which the droplet detached were noted. Each condition (Table 1) was recorded once; per condition between 2.75 and 55 seconds of video was analyzed, depending on the droplet formation time and the width of the droplet size distribution. Maximum measurement errors were 4 μm for the droplet diameter and 0.04 s (being the time between two images) for the time.

Calculation methods

Wall shear stress at the membrane surface in the cross-flow channel (τ_w): To compare the shear stress on the droplets in our geometry with the shear stresses in experiments described in literature, we used the following equations (see list of symbols):

$$f = \frac{16}{Re} = \frac{16\eta_c}{\rho_c v_c D_h} \text{ for } Re = \frac{\rho_c v_c D_h}{\eta_c} < 2300 \quad (-) \quad (1)$$

$$D_h = 4A/O \approx 2h \quad (m) \quad (2)$$

$$\tau_w = 0.5f \rho_c v_c^2 = 8\eta_c \frac{v_c}{2h} \quad (Pa) \quad (3)$$

The calculation of the wall shear stress is only an approximation of the shear stress on the droplets, because in some cases the size of the droplets almost equaled the height of the cross-flow channel.

Cross-correlation: To determine to which extent the detachment of droplets from different pores was coupled, cross-correlation functions were calculated for each pair of pores at which droplets formed. First, a formalized droplet detachment signal was formulated for each active pore. At the moment of droplet detachment the signal is 1 and directly after that it is 0. The signal linearly increases from 0 to 1 until a droplet detached. In this way, a saw wave function is obtained (Figure 4a-b). This signal does not exactly describe droplet formation, but contains the necessary information to calculate whether droplets detached at the same rates. For each pair of active pores the cross-correlation function $\rho_{2,1}(s)$ was calculated (Eq. 4) [18]:

$$\rho_{2,1}(s) = \frac{R_{2,1}(s)}{\sqrt{R_{1,1}(0)R_{2,2}(0)}} \quad (4)$$

In this equation $R_{1,1}(0)$ and $R_{2,2}(0)$ are the variances of both droplet detachment signals at translation 0 and $R_{2,1}(s)$ is the covariance of the two droplet detachment signals as a function of the translation s . The translation of signal 1 with regard to droplet detachment signal 2 was discrete, with steps of 0.01 second.

$$R_{2,1}(s) = \text{cov}\{X_{1,t}, X_{2,t+s}\} = E\{(X_{1,t} - \mu_1) \cdot (X_{2,t+s} - \mu_2)\} \quad (5)$$

In this equation μ_1 and μ_2 are means of the droplet detachment signals 1 and 2, respectively [18].

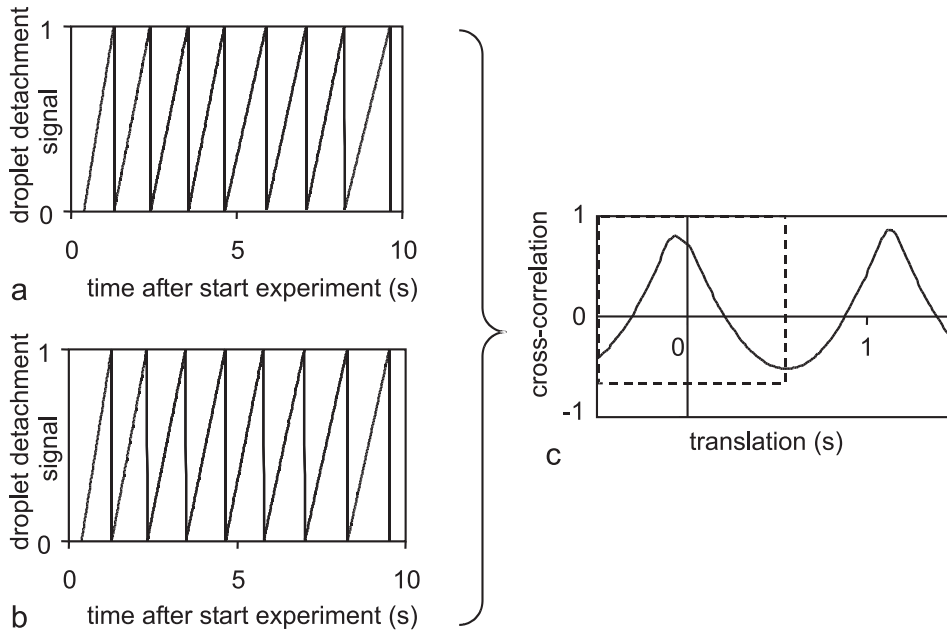
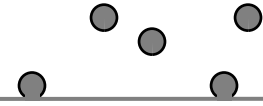


Figure 4: Droplet detachment signals of (a) pore (3,4) and (b) pore (3,8); (c): cross-correlation function for droplet detachment at these pores at $v_c = 0.028$ m/s, $p_{tm} = 7.8$ kPa.



From each resulting cross-correlation function, the maximum cross-correlation and the translation at this maximum value were obtained. Because detachment from one pore is at most half a period behind or before detachment of droplets from the other pore, the maximum cross-correlation value was taken from the range of one period around $s = 0$. This is explained in Figure 4c.

Due to the imposed saw wave on the droplet formation functions experimentally found, the droplet detachment signals are not completely random. Therefore, the maximum cross-correlation value appeared to be at least 0.1.

Results and Discussion

For the conditions listed in Table 1, the droplet diameters were measured and the droplet formation times were calculated. The images (Figure 5) show some important phenomena, which will be discussed further in the next sections. The first thing that attracts attention is the large droplet size. Further, the droplet size varies. Next, it was observed that droplets formed at only a few pores. With the number of active pores, the droplet size and the droplet formation time, the total oil flux through the membrane was calculated. Finally, it will be discussed that the droplets hindered each other sterically (Figure 5).

Table 1: Number of droplets formed (n), number averaged droplet diameter (d_{dr} and standard deviation $SD(d_{dr})$), droplet formation time (t_{form} and standard deviation ($SD(t_{form})$), droplet formation frequency (f), total number of active pores ($N_{p,act}$) and oil throughput (J) for all experimental conditions.

v_c (m/s)	p_{trm} (kPa)	n	d_{dr} (μm)	$SD(d_{dr})$ (μm)	t_{form} (s)	$SD(t_{form})$ (s)	f (s^{-1})	$N_{p,act}$ (-)	J^1 (10^3 $\text{kg m}^{-2} \text{h}^{-1}$)
0.011	7.9	45	130	62	0.60	0.62	1.09	6	1.1
0.017	5.4	21	221	14	2.36	5.09	0.19	2	0.2
0.017	6.6	50	172	76	1.38	3.31	0.19	5	0.3
0.017	7.7	57	152	74	0.37	0.19	1.86	4	1.9
0.017	8.9	55	179	71	0.37	0.14	2.29	3	2.5
0.028	5.5	64	169	43	0.49	0.71	1.17	4	1.2
0.028	6.3	47	196	20	0.78	1.46	0.77	3	0.8
0.028	6.9	58	155	40	0.55	0.71	1.00	5	1.0
0.028	7.3	62	149	50	0.45	0.62	1.56	5	1.5
0.028	7.8	72	134	35	0.77	0.53	1.03	7	0.9
0.028	8.5	53	133	40	0.64	0.50	1.37	7	1.3
0.028	9.0	133	125	48	0.20	0.24	3.05	7	1.1
0.039	7.6	53	125	20	0.69	0.59	1.23	7	0.8
0.039	8.7	51	115	29	0.34	0.32	2.32	8	1.5

$$1. J = \frac{\sum_1^n \frac{1}{6} \pi d_{dr}^3 \rho_d}{\text{time of the experiment } A_m}$$

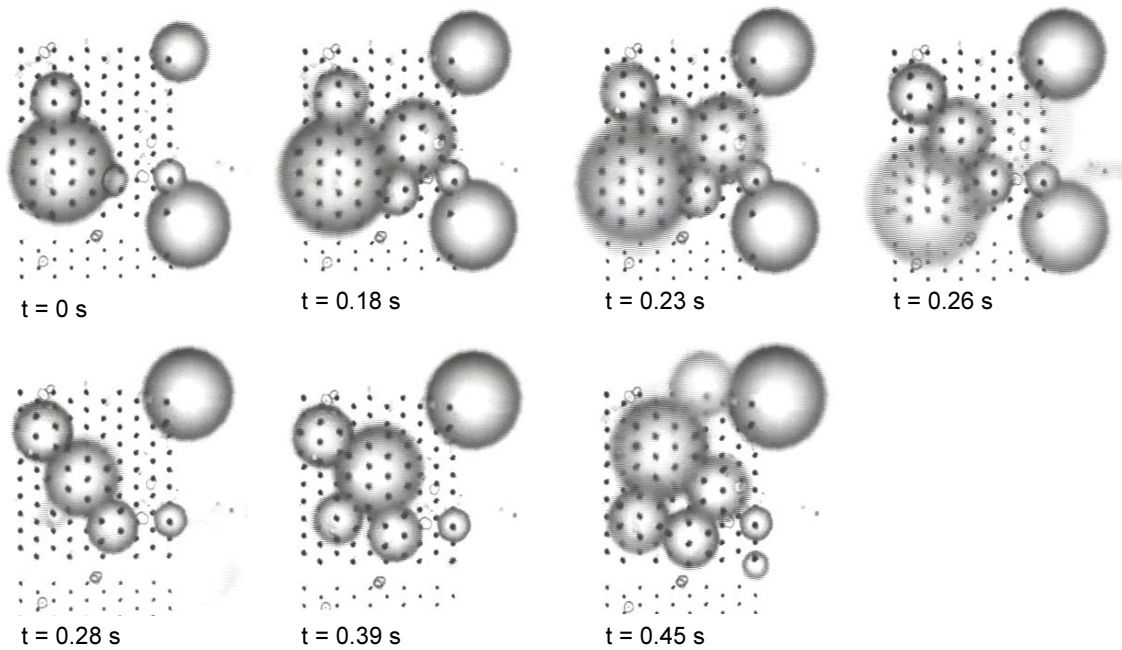


Figure 5: Droplet detachment from the membrane due to contact between droplets growing at neighboring pores at $v_c = 0.028$ m/s and $p_{tm} = 7.8$ kPa.

Droplet size

Droplet sizes varied between 52 and 255 μm . Thus, the droplets were large compared to the pore diameter (7 μm); the droplet/pore diameter ratio was between 7 and 36. In experiments with single pores, droplet/pore diameter ratios of 3 - 10 were found [5, 11] and in membrane emulsification with ceramic or glass membranes this ratio is also between 3 and 10 [2, 19-21]. However, the experimental conditions in our setup were different from the experiments described in literature: the cross-flow velocity was low, besides, the dimensions of the membrane module were different. Because the membrane is very thin, the oil flux through the pores was high; thus, to be able to follow the formation of droplets with microscopy, the cross-flow velocity had to be low. To compare the cross-flow velocity we used, with conditions in different experimental setups, we calculated the wall shear stress (Eq. 3), which was 0.62 Pa at most. With such a low wall shear stress the droplet/pore diameter ratio was found to be high, 10 - 30 [22]; > 80 [3] and the emulsion is less monodisperse than with a high wall shear stress (> 30 Pa) [22]. This is in agreement with our results. In the range of cross-flow velocities used (0.011 - 0.039 m/s), the velocity did not significantly affect the droplet size.

Concerning the dependency of the number averaged droplet diameter (d_{dr} in m) on the transmembrane pressure (p_{tm} in Pa), we found a significant linear *decrease* of the average droplet diameter with increasing pressure at a cross-flow velocity of the continuous phase of 0.028 m/s, $d_{dr} = -A p_{tm} + B$; $A = (2.3 \pm 1.7) \cdot 10^{-8}$ m/Pa; $B = (3.3 \pm 1.2) \cdot 10^{-4}$ m. This equation was obtained using the weighted least squares method [23]; the data were weighted

by the reciprocal of the variance of the data. Schröder did not find significant changes in droplet diameter at low pressures (0.5 – 1.5 kPa) in visualization experiments with single pores and with a bundle of capillaries [5]. Peng and Williams showed that at high pressures (0.35 – 2.1·10⁵ Pa) the droplet diameter increased with increasing transmembrane pressure [11]. This was explained by the increased flux at a higher pressure, which increases the final droplet volume during the second stage of droplet formation, the detachment phase. In the section on droplet-droplet interactions we will discuss that the decreasing diameter with increasing transmembrane pressure in our experiment can be explained by steric hindrance of the droplets.

Droplet size distribution

Direct observation of the droplet formation process gave information on the droplet size distribution for each individual pore. Necessarily, the total number of formed droplets was not very high, due to experimental limitations. Measuring between 21 and 132 droplets revealed that the number averaged droplet diameter was between 115 and 221 μm , depending on the transmembrane pressure and the cross-flow velocity (Table 1). The droplet diameter was only normally distributed for a few conditions. In Figure 6, the number fractions per size class under several process conditions are shown. The width of the size classes was taken constant (17.5 μm). Although it is generally accepted that monodisperse emulsions should be obtained

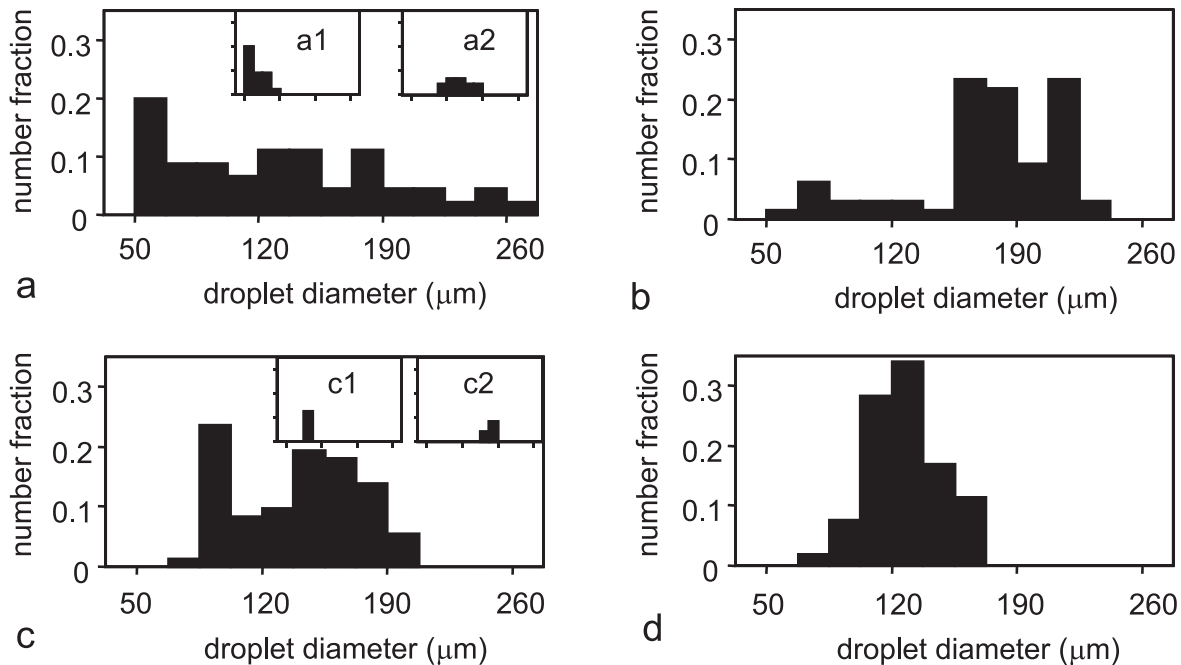


Figure 6: Droplet diameter distributions obtained at different conditions (number fraction of droplets per size class). a. $v_c = 0.011$ m/s, $p_{tm} = 7.9$ kPa; b. $v_c = 0.028$ m/s, $p_{tm} = 5.5$ kPa; c. $v_c = 0.028$ m/s, $p_{tm} = 7.8$ kPa; d. $v_c = 0.039$ m/s, $p_{tm} = 7.6$ kPa. Inserts: droplet size distributions of individual pores (same scales as the total droplet diameter distributions). a1: pore (1,2); a2: pore (5,1); c1: pore (3,4); c2: pore (3,8).

Table 2: Number of droplets formed (n), number averaged droplet diameter (d_{dr} and standard deviation $SD(d_{dr})$), droplet formation time (t_{form} and standard deviation ($SD(t_{form})$), droplet formation frequency (f) and oil throughput (J) for each active pore and for the whole membrane area at $v_c = 0.028$ m/s and $p_{tm} = 7.8$ kPa.

pore	n	d_{dr} (μm)	$SD(d_{dr})$ (μm)	t_{form} (s)	$SD(t_{form})$ (s)	f (s^{-1})	J (10^{-6} kg h^{-1})
(3,4)	9	88	0.0	1.10	0.13	0.86	0.9
(3,8)	9	170	6.7	1.12	0.12	0.88	6.6
(4,6)	9	134	11.3	0.28	0.04	0.86	3.2
(6,8)	11	90	8.2	0.86	0.24	1.06	1.2
(7,7)	22	146	19.2	0.29	0.11	2.22	10.6
(10,1)	7	185	9.4	1.34	0.08	0.75	6.5
(10,10)	5	130	14.4	1.92	0.60	0.49	1.6
Membrane	72	134	34.8	0.77	0.53		30.6

when using a uniform membrane, the emulsions show a high polydispersity and are not normally distributed. The visualization showed that the polydispersity was not caused by coalescence, neither at the membrane surface nor in the bulk phase. The polydispersity could be attributed to differences in droplet formation at the individual pores. Droplet formation was hindered sterically by droplets forming at other pores (Figure 5). Although the droplet diameter distribution of each individual pore was quite narrow, the average droplet diameter varied from pore to pore (Table 2, inserts in Figure 6). To study the non-uniform droplet size distribution, further studies were performed using the results of the process conditions $v_c = 0.028$ m/s and $p_{tm} = 7.8$ kPa (Figure 6c and Table 2).

Droplet formation time, droplet formation frequency and lag time

The *droplet formation time* is defined as the time between the start of droplet formation and detachment of the droplet (Figure 7). The start of droplet formation was defined as the moment at which a droplet could be seen at a certain pore. Conform our expectation, the droplet formation time significantly decreased with increasing transmembrane pressure (Table 1). The average droplet formation time was between 0.37 and 2.36 s, under different conditions, but occasionally single droplets formed within 0.1 s. These droplet formation times have the same order of magnitude as earlier presented values: 1.05 and 1.5 s was calculated for droplet formation with Tween 20 at a ceramic membrane [22]; 0.5 – 1 s with a capillary with a pressure difference of 0.5 kPa [5]; in the order of 1 – 2 s with a capillary of diameter 45.6 μm at low cross-flow velocities [11].

The *droplet formation frequency* was determined by taking the reciprocal of the average time between the successive detachment of two droplets from a pore (Figure 7). The droplet formation frequency varied from pore to pore (Table 2). Yet, the formation frequencies of

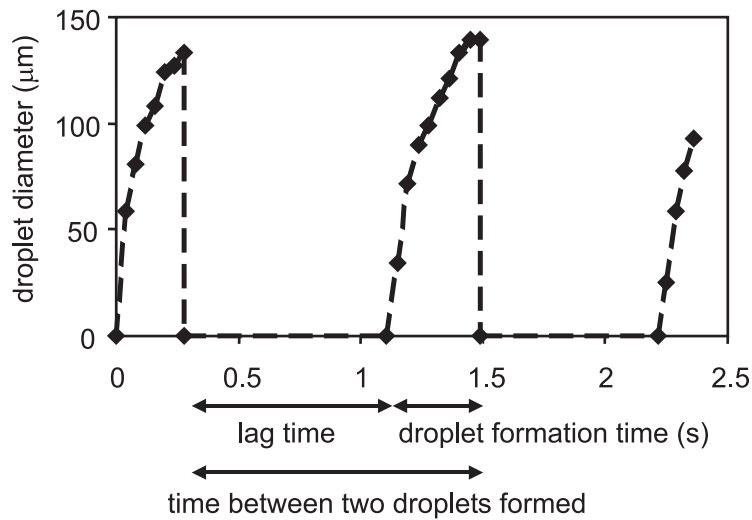


Figure 7: Droplet formation at pore (4,6) at the conditions $v_c = 0.028$ m/s, $p_{tm} = 7.8$ kPa, indicating the droplet formation time, lag time and the time between the consecutive detachment of two droplets.

pores (3,4), (3,8) and (4,6) were very close. This is a result of steric hindrance of the droplets growing close to each other, which will be shown in the last section on droplet-droplet interactions.

Even at the highest pressure there were still pores at which droplet formation was slow. However, the maximum droplet formation frequency increased with transmembrane pressure (Figure 8).

Note that the droplet formation frequency is smaller than the reciprocal of the droplet formation time. This is caused by the fact that sometimes after detachment for a certain time no droplet formed (Figure 7). Under the conditions $v_c = 0.028$ m/s and $p_{tm} = 7.8$ kPa (Table 2), the occurrence of this *lag time* was most pronounced at pores (4,6) and (7,7). The lag time

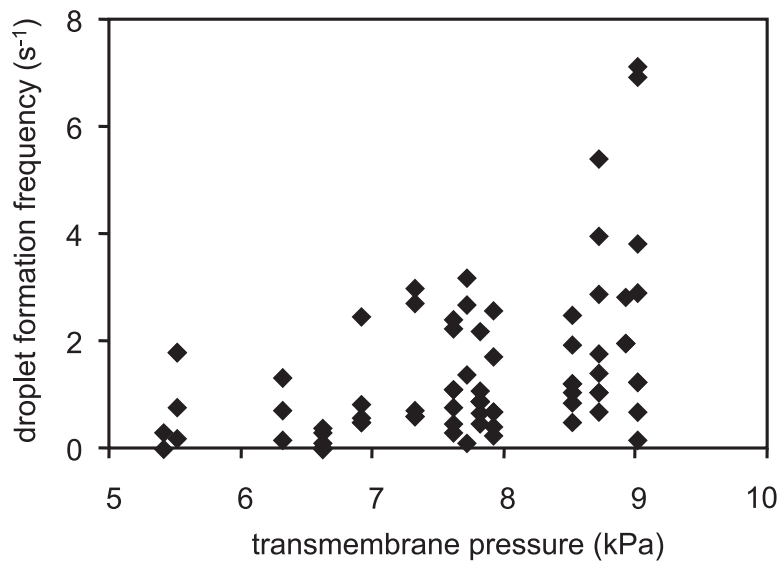


Figure 8: Droplet formation frequency of each pore as a function of transmembrane pressure.

between droplet detachment and renewed droplet formation might be explained by diffusion limitation of emulsifier or by pore refilling after detachment of a droplet. The applied transmembrane pressure was too low to overcome the critical pressure to form a droplet with a clean interface (no emulsifier). Therefore, emulsifier had to diffuse to the interface to reduce the interfacial tension. Usually, the diffusion time of a low-molecular emulsifier like Tween 20 is less than a millisecond, which is much shorter than the observed lag times. However, it might be the case that after detachment the emulsifier is temporarily depleted. The concentration has to be restored by supply of emulsifier with the cross-flowing phase. The second possible explanation is that the pore has to be refilled before a new droplet forms.

Number of active pores and critical pressure

For each condition in Table 1 and for some other conditions, the number of pores at which one or more droplets formed, were counted (Figure 9). From the fact that all the pores had the same diameter, it could be expected that at a certain transmembrane pressure, the critical pressure, all pores should become active. The critical pressure of a pore is defined as the pressure at which just a droplet starts to form at that pore; theoretically this depends on the pore diameter by the Laplace equation: $p_{crit} = 4\gamma/d_p$. In fact, the assumption that pores with the same diameter should become active at the same pressure, is the basis for some standard membrane characterization methods [24]. However, the number of active pores increased linearly with increasing transmembrane pressure and droplets formed only at a few pores. It should be noted that at the highest transmembrane pressure in the experiment (14 kPa), which is approximately 3 times the critical pressure, there were still only 16 out of 100 pores active. Sugiura *et al.* had the same results: below a transmembrane pressure of 2.5 times the critical pressure, the percentage of active pores was below 20% [15]. We considered several

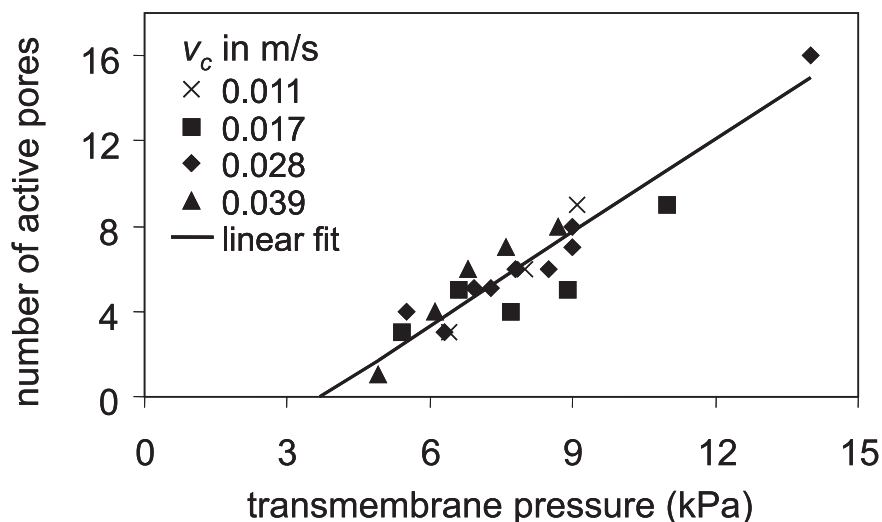
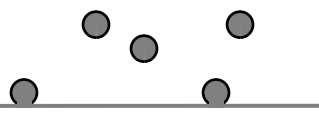


Figure 9: Number of active pores as a function of transmembrane pressure at different cross-flow velocities of the continuous phase.



explanations why only a few pores were active. It cannot be due to slow diffusion of emulsifier, because Tween 20 is a relatively fast emulsifier. Also the effect of the cross-flow, running into a forming droplet, which results in a higher pressure above a pore upstream of that forming droplet is not a satisfying explanation: because the cross-flow velocity is low, the pressure in the cross-flow channel only increases a few Pascals, which affects the transmembrane pressure of pores upstream very slight. Presumably, there is a pressure drop under the membrane as soon as oil flows through a few pores, which prevents other pores to become active. At a higher applied pressure more pores become active, because the pressure difference, which is the driving force for flow through the pores, increases.

During the experiments we observed that pores at which droplets formed, became inactive, while others started to form droplets. After lowering the pressure fewer pores were active; after raising the pressure again, other pores became active. Considering the position of the active pores on the membrane, this suggest that the pores become active at random.

The results in Figure 9 show again that the velocity did not affect the emulsification process, therefore, the dependency of the number of active pores on the transmembrane pressure can be described: $N_{p,act} = (1.46 \pm 0.25) \cdot 10^{-3} p_{tm} - 5.4 \pm 2.0$.

Linear regression with the transmembrane pressure as the dependent variable gives a critical pressure value of 4.8 (± 0.7) kPa. Each time after changing the cross-flow velocity, the critical pressure was determined by increasing the pressure from 0 until a droplet started to form. This value (5.4 (± 0.7) kPa) agrees with the value calculated from the regression line through all the measured data.

Oil throughput as a function of transmembrane pressure

The total oil flux through the membrane increased with increasing transmembrane pressure. Although the droplet size decreased with increasing transmembrane pressure, the total flux through the membrane increased, because both the number of active pores and the droplet formation frequency increased. Although only at a few pores droplets formed under the experimental conditions, the maximum oil throughput in this experiment was $30 \cdot 10^{-12} \text{ m}^3/\text{s}$ ($2500 \text{ kg m}^{-2} \text{ h}^{-1}$) at a transmembrane pressure of 8.9 kPa. It is difficult to compare this result with literature, because membranes with different pore diameters were used. E.g. for a ceramic $0.5 \text{ }\mu\text{m}$ membrane the largest flux found was $200 \text{ kg m}^{-2} \text{ h}^{-1}$ at an effective pressure of 20 kPa (effective pressure = transmembrane pressure – critical pressure) [3].

Droplet-droplet interactions

Visualization showed that droplets forming at different pores sometimes touched each other while they were growing (Figure 5). Due to this steric hindrance, droplets detached. It was observed that pores (3,4), (3,8) and (4,6), being located near each other, had approximately the same droplet formation frequency (Table 2). The cross-correlation between each pair of pores was calculated, to quantify the interaction between pores having the same droplet

Table 3: Maximum cross-correlation value of each pair of pores.

pore	(3,4)	(3,8)	(4,6)	(6,8)	(7,7)	(10,1)	(10,10)
(3,4)		0.80	0.72	0.40	0.26	0.29	0.47
(3,8)	0.80		0.85	0.28	0.27	0.28	0.54
(4,6)	0.72	0.85		0.39	0.34	0.27	0.48
(6,8)	0.40	0.28	0.39		0.27	0.14	0.33
(7,7)	0.26	0.27	0.34	0.27		0.20	0.16
(10,1)	0.29	0.28	0.27	0.14	0.20		0.25
(10,10)	0.47	0.54	0.48	0.33	0.16	0.25	

formation frequency. By definition, the cross-correlation ranges between -1 and 1 . If the absolute value is close to 1 , the droplet formation frequencies can be considered to be identical; 0 implies no correlation at all. Table 3 indeed shows high maximum cross-correlation values between pores (3,4), (3,8) and (4,6) (some of the results are also shown in Figure 10). Therefore, it can be concluded that these pores had the same droplet formation frequency. In other words, there was a binary interaction between each pair of those pores. The maximum cross-correlation value for the pair of pores (3,4) and (3,8) was found at a translation of 0.06 seconds, which means that droplets detached on average 0.06 s later from pore (3,4) than from pore (3,8). Note that the correlation between these three pores and pore (10,10) was around 0.5 . This was due to droplets detaching from pore (3,8); sometimes these droplets collided with droplets attached to pore (10,10) (Figure 5d–e). No values higher than 0.85 or lower than 0.14 were found. This is due to the limited size of the dataset; more data could have made the values somewhat more close to the extremes.

Both pores (7,7) and (10,1) were characterized by low cross-correlations. Although pore (7,7) was close to other active pores, the cross-correlation values with these pores were not high, as we found for the pores (3,4), (3,8) and (4,6). This is caused by the irregular droplet formation at pore (7,7); note the high standard deviation ($SD(t_{form}) = 0.11$ s) compared to the droplet formation time of 0.29 s (Table 2). Video observation showed that the droplet formation at pore (7,7) was influenced by more than one other pore (ternary or higher order interaction). Obviously, this resulted in lower cross-correlations with each pore separately.

Finally, the binary cross-correlations between pore (10,1), which is located at the corner of the membrane, and all other pores were low. Furthermore, the standard deviation of the droplet formation time was small, which means that droplets formed at regular time intervals (of 1.34 s). Video images showed that the other active pores did not influence pore (10,1) because these pores were too far away from pore (10,1). The droplets formed at (10,1) were the biggest formed under these conditions.

Summarizing with Figure 10: droplet detachment at some pores is strongly coupled. In the case of binary interactions, this is shown by a high cross-correlation value (area I). No

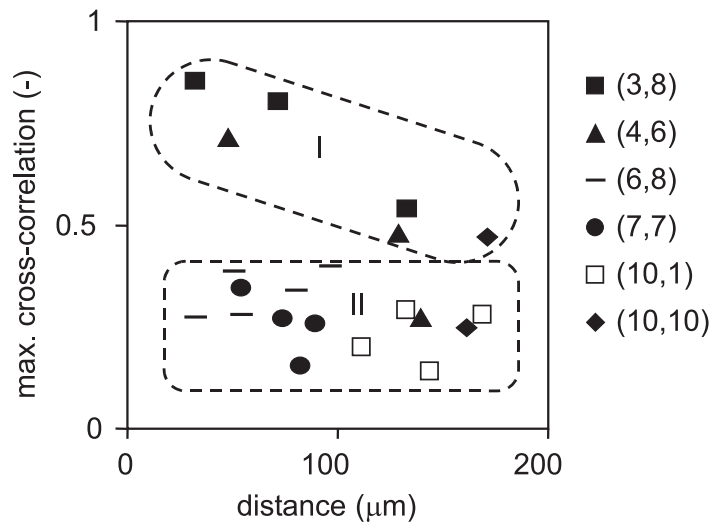


Figure 10: Maximum cross-correlation value as a function of the distance between two pores. Area I: binary interaction; area II: ternary or higher order interaction or no interaction.

interaction during detachment or ternary or higher interaction result in low cross-correlation values (area II).

With increasing transmembrane pressure, we found a decreasing droplet diameter. This can now be explained: at a higher transmembrane pressure more pores were active, so the chance that two active pores were close together will have been bigger. As a result, steric hindrance and detachment of droplets will have occurred at a smaller droplet size. Therefore, at a higher transmembrane pressure, smaller droplets were obtained.

Conclusion

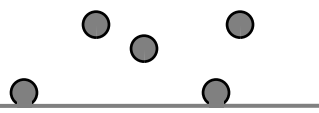
In this study of droplet formation at a uniform membrane we found two types of interactions which affected droplet formation at the membrane surface: at the cross-flow channel side of the membrane, droplets interacted through steric hindrance and collisions downstream. In this way, the droplet detachment rates of pores were sometimes coupled. Steric hindrance can be prevented by using a membrane with a low porosity. The distance between the pores should be larger than the droplet diameter. However, collisions cannot be prevented by this measure. Secondly, droplets formed only at a few pores. The number of active pores increased linearly with the transmembrane pressure. We think this is due to a pressure drop under the membrane, resulting from flow of oil through the active pores, thus preventing the other pores to become active. Due to steric hindrance the droplet size decreased with an increasing number of active pores.

The interactions, combined with the very low cross-flow velocity, caused the emulsion to be polydisperse even though the membrane had uniform pores. Notwithstanding, the flux of the to-be-dispersed phase was quite high ($2.5 \cdot 10^3 \text{ kg m}^{-2} \text{ h}^{-1}$), even with a low number of active pores and a low transmembrane pressure.

Clearly, our experiments show that to obtain monodisperse emulsions, choosing a uniform membrane is not sufficient. In this study we have attempted to provide a first quantification of the complexity of droplet formation during cross-flow emulsification. Use of microengineered membranes will help clarify all the important effects, and will also offer the possibility to design the best possible system that can provide mild emulsification to produce emulsions with the right properties.

Nomenclature

A	area of the channel cross-section	$A = 2.6 \cdot 10^{-6}$	(m ²)
A	help parameter		(m/Pa)
A_m	surface area of the membrane	$A_m = 3.24 \cdot 10^{-8}$	(m ²)
B	help parameter		(m)
D_h	hydraulic diameter	$D_h = 5.1 \cdot 10^{-4}$	(m)
d_{dr}	droplet diameter		(m)
d_p	pore diameter		(m)
f	Fanning friction factor		(-)
f	droplet formation frequency		(s ⁻¹)
g	gravitational constant		(m/s ²)
h	height of the cross-flow channel	$h = 2.6 \cdot 10^{-4}$	(m)
Δh	height difference between the continuous phase vessels		(m)
$h_{c,in}$	height of the inflow continuous phase vessel		(m)
$h_{c,out}$	height of the outflow continuous phase vessel		(m)
J	oil throughput		(kg m ⁻² h ⁻¹ or kg h ⁻¹)
$N_{p,act}$	total number of active pores		(-)
n	number of droplets formed		(-)
O	perimeter of the channel cross-section	$O = 2.1 \cdot 10^{-2}$	(m)
p_c	continuous phase pressure		(Pa)
p_{crit}	critical pressure		(Pa)
p_d	disperse phase pressure		(Pa)
p_{trm}	transmembrane pressure		(Pa)
$R_{i,i}(0)$	variance of droplet formation signal i		(-)
Re	Reynolds number		(-)
s	translation of a signal		(s)
SD	standard deviation		(m or s)
t_{form}	droplet formation time		(s)
v_c	cross-flow velocity of the continuous phase		(m/s)
$X_{i,t}$	value of signal i at time t		(-)



γ	interfacial tension		(N/m)
η_c	viscosity of the continuous phase	$\eta_c = 1 \cdot 10^{-3}$	(Pa s)
μ_i	mean of the droplet detachment signal i		(-)
ρ_c	density of the continuous phase	$\rho_c = 1000$	(kg/m ³)
ρ_d	density of the disperse phase	$\rho_d = 773$	(kg/m ³)
$\rho_{i,j}$	cross-correlation between two functions i and j		(-)
τ_w	wall shear stress		(Pa)

Acknowledgements

We would like to thank Stein Kuiper for the Aquamarijn microsieves and modules. We are grateful for the advices of Cees van Rijn and Wietze Nijdam of Aquamarijn, on the use and cleaning of the modules during this research.

Reference list

- 1 V. Schröder, O. Behrend and H. Schubert, Effect of Dynamic Interfacial Tension on the Emulsification Process Using Microporous, Ceramic Membranes, *J. Colloid Interface Sci.*, 202 (1998) 334.
- 2 R.A. Williams, S.J. Peng, D.A. Wheeler, N.C. Morley, D. Taylor, M. Whalley and D.W. Houldsworth, Controlled Production of Emulsions Using a Crossflow Membrane. Part II: Industrial Scale Manufacture, *Trans. Inst. Chem. Eng.*, 76 (1998) 902.
- 3 S.M. Joscelyne and G. Trägårdh, Food Emulsions Using Membrane Emulsification: Conditions for Producing Small Droplets, *J. Food Eng.*, 39 (1999) 59.
- 4 S.M. Joscelyne and G. Trägårdh, Membrane Emulsification - a Literature Review, *J. Membrane Sci.*, 169 (2000) 107.
- 5 V. Schröder, Herstellen von Öl-in-Wasser-Emulsionen mit Mikroporösen Membranen, PhD thesis, Technische Hochschule Karlsruhe, 1999.
- 6 G. Muschiolik and S. Dräger, Emulsionsbildung mittels Mikroporösem Glas (MPG). Vergleich der Emulgiereigenschaften Unterschiedlicher Molkenproteine., *Dtsch. Milchwirtsch.*, 46 (1995) 1041.
- 7 H. Schubert and V. Schröder, Mechanical Emulsification with Minimum Energy Input, in *Proceedings of the Minimal Processing of Food: a Challenge for Quality and Safety*, 1996, 53.
- 8 T. Nakashima, M. Shimizu and M. Kawano, Articles of Porous Glass and Process for Preparing the Same, *US 4 657 875*, 1987.
- 9 K. Kandori, Applications of Microporous Glass Membranes: Membrane Emulsification, in A.G. Gaonkar (Ed.), *Food Processing: Recent Developments*, Elsevier science B.V., Amsterdam, 1995.
- 10 Chapter 2, published as: A.J. Abrahamse, A. van der Padt, R.M. Boom and W.B.C. de Heij, *Process Fundamentals of Membrane Emulsification: Simulation With CFD*, *AIChE Journal*, 47 (2001) 1285.
- 11 S.J. Peng and R.A. Williams, Controlled Production of Emulsions Using a Crossflow Membrane. Part I: Droplet Formation From a Single Pore, *Trans. Inst. Chem. Eng.*, 76 (1998) 894.
- 12 T. Kawakatsu, Y. Kikuchi and M. Nakajima, Regular-Sized Cell Creation in Microchannel Emulsification by Visual Microprocessing Method, *J. Am. Oil Chem. Soc.*, 74 (1997) 317.
- 13 T. Kawakatsu, Y. Kikuchi and M. Nakajima, Visualization of Microfiltration Phenomena Using Microscope Video System and Silicon Microchannels, *J. Chem. Eng. Jpn.*, 29 (1996) 399.
- 14 J. Tong, M. Nakajima, H. Nabetani and Y. Kikuchi, Surfactant Effect on Production of Monodispersed Microspheres by Microchannel Emulsification Method, *J. Surf. Det.*, 3 (2000) 285.

- 15 S. Sugiura, M. Nakajima, J. Tong, H. Nabetani and M. Seki, Preparation of Monodispersed Solid Lipid Microspheres Using a Microchannel Emulsification Technique, *J. Colloid Interface Sci.*, 227 (2000) 95.
- 16 S. Kuiper, C.J.M. van Rijn, W. Nijdam and M.C. Elwenspoek, Development and Applications of Very High Flux Microfiltration Membranes, *J. Membrane Sci.*, 150 (1998) 1.
- 17 S. Kuiper, C.J.M. van Rijn, W. Nijdam, G.J.M. Krijnen and M.C. Elwenspoek, Determination of the Critical Pressure in Microfiltration: a Simple Single Particle Model Tested on a Model Membrane, *J. Membrane Sci.*, 180 (2000) 15.
- 18 M.B. Priestley, Multivariate and Multidimensional Processes, in M.B. Priestley (Ed.), *Spectral Analysis and Time Series*, Academic Press, London, 1981.
- 19 R. Katoh, Y. Asano, A. Furuya, K. Sotoyama and M. Tomita, Preparation of Food Emulsions Using a Membrane Emulsification System, *J. Membrane Sci.*, 113 (1996) 131.
- 20 Y. Mine, M. Shimizu and T. Nakashima, Preparation and Stabilization of Simple and Multiple Emulsions Using a Microporous Glass Membrane, *Coll. Surfaces B: Biointerfaces*, 6 (1996) 261.
- 21 V. Schröder and H. Schubert, Emulsification Using Microporous, Ceramic Membranes, in *Proceedings of the First European Congress on Chemical Engineering ECCE1, 1997*, 2491.
- 22 V. Schröder and H. Schubert, Production of Emulsions Using Microporous, Ceramic Membranes, *Coll. Surfaces A: Physicochemical Eng. Aspects*, 152 (1999) 103.
- 23 R.H. Myers, *Classical and Modern Regression With Applications*, PWS Publishers, Boston, 1986.
- 24 M. Mulder, *Basic Principles of Membrane Technology*, Kluwer Academic Publishers, Dordrecht, 1991.

4 Effect of membrane morphology on pore activation

Abstract

The low throughput of the disperse phase is one of the issues in cross-flow membrane emulsification. This is apparent in the low percentage of pores at which droplets are formed (few active pores). To determine the effect of membrane morphology on pore activation, we developed and experimentally validated a model that describes the flow phenomena in and under a membrane with uniform pores (microsieve). In this model the membrane is divided into two parts: the top layer and the membrane substructure. The model was validated with a larger-scale physical analogon. It predicts a linear increase of the number of active pores with increasing transmembrane pressure, while the pressure difference over the active pores is independent of the transmembrane pressure as long as not all pores are active. Although the resistance of the microsieve substructure was found to be 4 times lower than the resistance of a single pore, the resistance of the membrane substructure had a large effect on the activation of pores. Hence, the number of active pores can be increased by increasing the ratio of flow resistance in the pores and the flow resistance in the membrane substructure. Preliminary experiments show that the gradual increase in active pores at a ceramic membrane surface can be explained in the same way.

Introduction

In cross-flow membrane emulsification a to-be-dispersed phase is pressed through a membrane. At the membrane surface droplets are formed, which are detached by the cross-flowing continuous phase. With this technique it is possible to produce emulsions with quite a narrow droplet size distribution with relatively low shear and low energy input [1-3]. Membrane emulsification is shown to be applicable to manufacture food: a very low fat spread has been developed and commercialized [4]; to synthesize microspheres [5]; and to produce drug delivery systems [6, 7]. In cross-flow membrane emulsification research usually the emphasis is laid on obtaining the required droplet size and a narrow droplet size distribution. Because of that, the oil fluxes for production of especially O/W emulsions have been quite low [8]. Because different membrane types with various average pore sizes are used at different maximum transmembrane pressures, it is difficult to compare the fluxes obtained. Some results are listed in Table 1.

Schröder and Schubert [2] suggest that the disperse phase flux may be increased by increasing the transmembrane pressure, but in many cases that will result in larger droplets. Another important factor influencing the disperse phase flux is the percentage of pores at which droplets are formed, so-called active pores [2]. From the ratio of the to-be-dispersed phase flux and the oil flux through an in oil submerged membrane, they estimated that only 3% of the pores were active in a ceramic membrane with average pore size of 0.05 μm at transmembrane pressures (p_{trm}) between 1 and $3 \cdot 10^5$ Pa. In a membrane with pore size 0.5 μm , the estimated percentage of active pores increased from 8% at $p_{trm} = 1 \cdot 10^5$ Pa to 40% at $p_{trm} = 3 \cdot 10^5$ Pa [2, 3]. In an earlier study we analyzed droplet formation at the surface of a microsieve with uniform pores. We expected all the pores to become active at the same transmembrane pressure, because they all had the same pore diameter. However, we observed that the percentage of active pores linearly increased with the transmembrane pressure (Figure

Table 1: Disperse phase fluxes obtained in several studies with different membrane types, average pore sizes (d_p) and transmembrane pressures (p_{trm}).

membrane type	d_p (μm)	p_{trm} (10^5 Pa)	disperse phase	flux ($1 \text{ m}^{-2} \text{ h}^{-1} \text{ bar}^{-1}$)	Ref.
ceramic	0.2	2.5	vegetable oil	> 40 ¹	[9]
ceramic	0.5	15	vegetable oil	33	[3]
SPG	0.52	3.5	kerosene	19	[1]
SPG	1	0.7	styrene, divinyl- benzene, hexadecane	16	[10]
SPG	3	0.15	aqueous colloidal silica	8000	[11]
silicon microsieve	7	0.09	n-hexadecane	21000	[12]

1. disperse phase flux in $\text{kg m}^{-2} \text{ h}^{-1} \text{ bar}^{-1}$

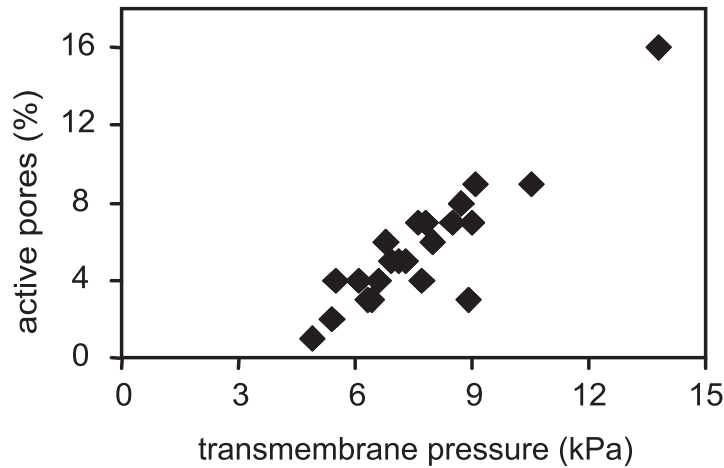


Figure 1: Percentage of active pores as a function of the transmembrane pressure when using a microsieve [12].

1) [12]. Observation of droplet formation in a microchannel emulsification system also shows a gradual increase in pore activity with increasing transmembrane pressure [13].

To guarantee an optimal flux, all pores should be active. Up till now the mechanism of pore activation is not understood. In this chapter we describe how the number of active pores depends on the membrane morphology, or more specific on the pore resistance (determined by the pore diameter and length) and the membrane sublayer resistance. For that we developed a model that describes the flow phenomena in and under a membrane with uniform pores as a function of the transmembrane pressure and the membrane morphology. This model is validated on a physical analogon: flow of nitrogen through 27 parallel needles in water. Next to that, the model is used to describe the results of earlier membrane emulsification experiments [12]. With the obtained insights, the effect of membrane design on the process performance (pore activation and droplet formation) is discussed. Furthermore, we show that although the model equations were derived for membranes with uniform pores, the theory can be applied adequately to predict pore activation in membranes with interconnected pores. This is demonstrated with preliminary experimental results with a ceramic membrane.

Theory

To describe the flow through N equally sized parallel pores in the toplayer of a membrane, we adapted the model of Ho and Zydney [14, 15]. The membrane is assumed to be composed of two distinct structural layers, each having a given resistance to fluid flow (Figure 2). We assume the following:

1. Fluid flow can be described with Darcy's law (eq. 1, modified from [16]):

$$\phi_s = \frac{\Delta p}{\eta R} \quad (\text{m}^3/\text{s}) \quad (1)$$

in which ϕ_s is the volume flux, Δp the pressure difference over the membrane layer that is considered (in Pa), η is the fluid viscosity (in Pa s) and R (in m^{-3}) is either the resistance against flow in the membrane sublayer (R_s) or the resistance in a single pore (R_p).

- The pores are equally sized and in parallel, which means that both R_p and the critical pressure are identical for all the pores.

R_p can be calculated from the Fanning equation (for steady laminar flow in a tubular pipe) and the cross sectional area of the pore, giving:

$$R_p = \frac{128l_p}{\pi d_p^4} \quad (\text{m}^{-3}) \quad (2)$$

in which d_p is the pore diameter and l_p the length of the pore. In case of flow through pores with a small length/diameter ratio, the entrance effect adds to the resistance of the pore. For microsieves the following equation applies (R_{p+e} describes the resistance due to the friction in the pore together with the entrance effect):

$$R_{p+e} = \left(\frac{128l_p}{\pi d_p^4} + \frac{24}{d_p^3} \right) f(\kappa) \quad (\text{m}^{-3}) \quad (3)$$

$$f(\kappa) = 1 - \sum_{i=1}^{\infty} a_i \kappa^{i+1/2} \quad (-) \quad (4)$$

With κ being the porosity of the membrane. The values for a in the first three terms is: $a_1 = 0.344$, $a_2 = 0.111$ and $a_3 = 0.066$ [17].

The critical pressure is the pressure difference over a pore just enough to form a droplet at that pore. The critical pressure can be estimated with the Laplace equation (5):

$$p_{crit} = 2\gamma \left(\frac{1}{d_1} + \frac{1}{d_2} \right) \cos \theta \quad (\text{Pa}) \quad (5)$$

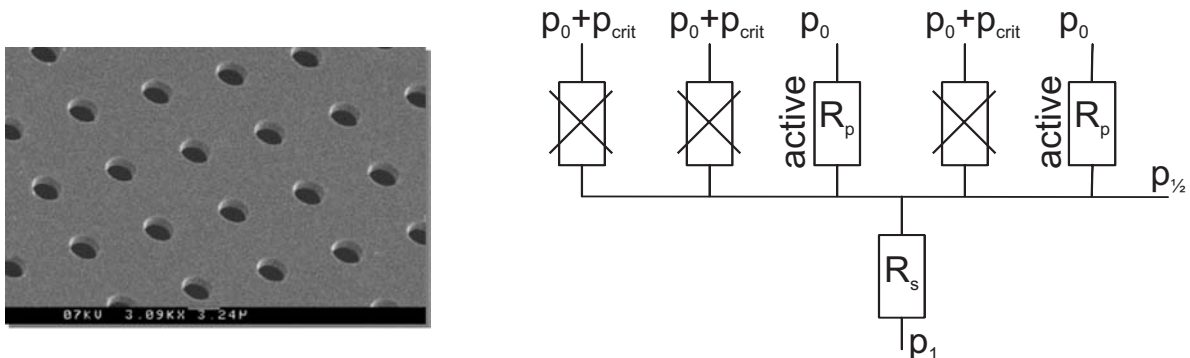


Figure 2: a. Scanning Electron Micrograph of a microsieve [18] b. Scheme of the resistances against flow in the membrane and the corresponding pressures. R_p : pore flow resistance; R_s : membrane substructure resistance; p_1 : disperse phase pressure; p_0 : continuous phase pressure; $p_{1/2}$: pressure just below the pores; p_{crit} : critical pressure.

in which γ is the interfacial tension (N/m), d_1 and d_2 the respective perpendicular diameters of the pore opening and θ the wall contact angle. In the case of a spherical pore with straight edges the equation can be simplified, with d_p the diameter of the pore. $\cos \theta$ is taken to be 1, because for a pore with straight edges the pressure inside the forming droplet is maximal when the droplet is hemispherical. This reduces equation 5 to $p_{crit} = 4\gamma/d_p$. The effect of wetting properties and the shape of the pore opening on the critical pressure, is described elsewhere [19].

3. Because the toplayer pores are parallel to each other, the pressure under the pores is everywhere the same: $p_{1/2}$. In case a pore is not active, there is no disperse phase flow through the pore, so the disperse phase pressure at the top of the pore is equal to $p_{1/2}$. The pressure of the continuous phase is p_0 . A pore starts to form droplets (becomes active) when the pressure difference $p_{1/2} - p_0$ equals the critical pressure (eq. 5). It is assumed that at the moment a pore becomes active, the disperse phase pressure at the top of the membrane is p_0 . Thus the pressure drop over the pore is $p_{1/2} - p_0$, resulting in a specific disperse phase flow. This is an approximation, because the pressure inside the droplet will actually be in between p_0 and $p_{1/2}$ as long as the pore is active. The exact value depends on the size and shape of the droplet, which increases in time until the droplet detaches (see e.g. [20]).
4. The pressures in the system are determined by the balance in flow through the membrane substructure (determined by R_s) and the flow through the pores ($N \cdot R_p$):

$$\frac{p_1 - p_0}{\eta} = \frac{p_1 - p_{1/2}}{\eta} + \frac{p_{1/2} - p_0}{\eta} = \frac{\phi_s}{N} R_p + \phi_s R_s \quad (\text{s}^{-1}) \quad (6)$$

Rewriting equation 6 leads to equation 7 to calculate the number of active pores and to equations 8 – 10 to calculate the flux through the system:

$$N = \frac{R_p}{R_s} \left(\frac{p_1 - p_0}{p_{1/2} - p_0} - 1 \right) \quad (-) \quad (7)$$

$$\phi_s = \frac{p_1 - p_0}{\eta \left(\frac{R_p}{N} + R_s \right)} \quad \text{for } p_1 > p_{1/2} \quad (\text{m}^3/\text{s}) \quad (8)$$

$$\phi_s = N \phi_p = N \frac{p_{1/2} - p_0}{\eta R_p} \quad (\text{m}^3/\text{s}) \quad (9)$$

$$\phi_s = \frac{p_1 - p_{1/2}}{\eta R_s} = \frac{p_1 - p_0}{\eta R_s} - \frac{p_{1/2} - p_0}{\eta R_s} \quad (\text{m}^3/\text{s}) \quad (10)$$

Using the equations above, the parameters R_p and R_s can be estimated to fit experimental data using a non-linear least squares problem solver. The 95% confidence intervals on the parameters were calculated with the residuals and the Jacobian matrix.

Experimental

To validate the model, results published in literature were used [12] and experiments in an analogous larger-scale system were performed: a bubble column with needles. In Figure 3 the experimental set-up is shown schematically. Nitrogen gas was used as the to be dispersed phase. The nitrogen flow was varied with read-out and control electronics of Brooks Instrument (model 0154/CC1A1) and controlled by a mass flow controller (Brooks, 5850E series) with a range of 0 – 60 l/h. The pressure was measured before (p_1) and after ($p_{1/2}$) the clamp (both pressure sensors: WIKA, Klingenberg, Germany). The clamp, representing the membrane substructure resistance, was screwed to obtain a certain resistance against flow in the tubing. The bubble column had an inner diameter of approximately 6 cm. Between the upper and lower part of the bubble column, a silicon rubber disc, with 27 needles pierced through, was clamped. The needles were of BD Microlance™ 3; 27 GA $\frac{3}{4}$ Nr. 20, with an outer diameter of 0.4 mm and a given length of 19 mm, but it was measured to be approximately 25 mm. The inner diameter was measured to be approximately 0.2 mm. The bubble column was filled with water until a height of 1.5 cm above the needles.

In four series of measurements the nitrogen gas flow was increased while the pressure before and after the clamp and the observed number of active needles were noted. In the first measurement series there was no clamp present, in the following series the clamp was screwed tighter. If the pressure drop in the system is larger than 10% of the inlet pressure, then the flow is considered to be compressible [21]. In this event, formulas which make proper allowance for this change in both density and velocity should be used. To keep the calculations straightforward, only data with an inlet pressure lower than an absolute pressure of $1.1 \cdot 10^5$ Pa were used.

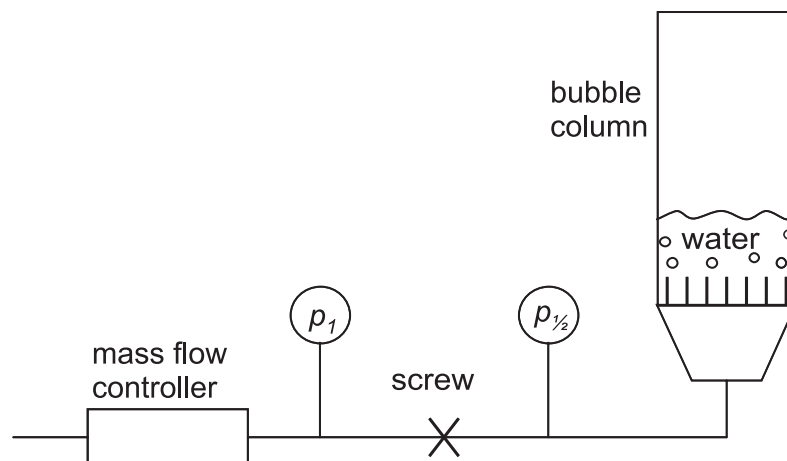


Figure 3: Set-up used in the experiments with needles in a bubble column.

Results and discussion

Scaled-up analogon

The results of the measurements in the scaled-up analogon, the bubble column, are presented in Figure 4a-b. In Figure 4b two domains can be distinguished: the first part in which the pressure under the needles ($p_{1/2}$) is approximately constant and the number of active needles increases; and the second part in which the number of active needles is constant because the maximum is reached ($N = 27$) and the pressure under the needles increases. $p_{1/2}$ and N as a function of the nitrogen flow are for all four series quite similar.

To verify the model, equations 9 and 10 were used to estimate the parameters R_p and for each measurement series a separate R_s . However, in a real membrane system, $p_{1/2}$ cannot be measured easily. Therefore, we also estimated the same parameters with equation 8 in which it is not necessary to know the value of $p_{1/2}$. In both procedures we used $p_0 = 150$ Pa, since this is the hydrostatic pressure of the water column of 1.5 cm above the needles. The viscosity of nitrogen was taken to be $17 \cdot 10^{-6}$ Pa s. The parameter values found using the two procedures are given in Table 2. The values estimated for the resistance against flow through the tubing with the clamp (R_s) are significantly different for the four measurement series. However, we did not find significant differences for these values using the two fitting procedures. As expected the resistance against flow through the tubing approximates 0 when there is no clamp present and increases with screwing the clamp.

The same 27 needles were used in all the measurement series. This means that the R_p -values of all the series should be the same, because R_p is an intrinsic needle property (eq. 2). The R_p -values (Table 2) estimated using equation 9 and using equation 8 are in good agreement, $R_p = (675 \pm 11) \cdot 10^{12}$ and $(700 \pm 67) \cdot 10^{12} \text{ m}^{-3}$ respectively. Of course the R_p -value estimated using equation 9 was more reliable, since it is determined directly. Theoretically, the resistance against flow through a needle in case of laminar flow ($Re_{max} = 166$), is (eq. 2):

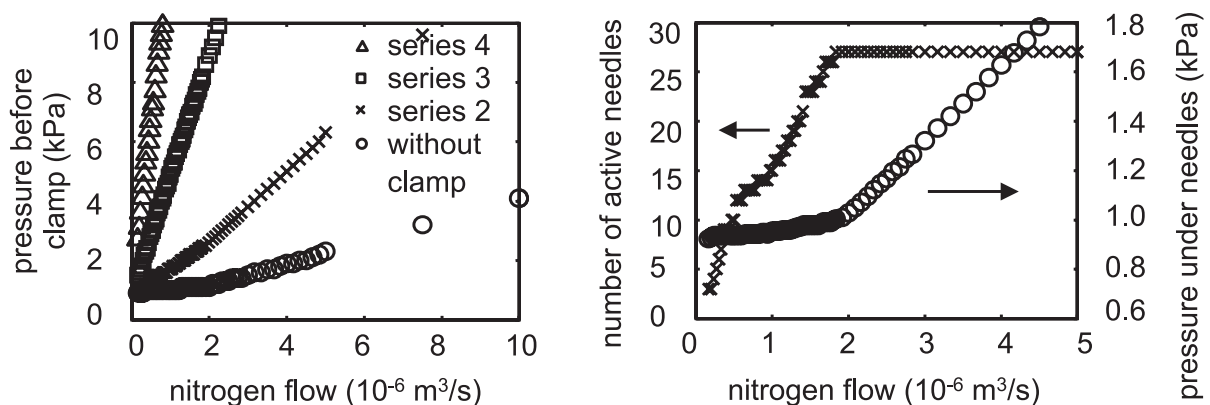


Figure 4: a. Pressure measured before the clamp as a function of nitrogen flow rate in 4 series in which the clamp was screwed tighter after the measurement series. b. number of active needles counted and pressure before the bubble column measured as a function of nitrogen flow rate of series 2.

$$R_p = \frac{128I_p}{\pi d_p^4} = \frac{128 \cdot 25 \cdot 10^{-3}}{\pi \cdot (0.2 \cdot 10^{-3})^4} = 637 \cdot 10^{12} \text{ m}^{-3}. \text{ This value is of the same order of magnitude as}$$

the estimated values. From the measured pressure values just under the needles ($p_{1/2}$) and the estimated pressure above the needles (150 Pa) the critical pressure follows: $p_{1/2} - p_0 \approx 950 - 150 = 800$ Pa. Calculating the theoretical value of the critical pressure with equation 5 gives $p_{crit} = 840$ Pa, with $\gamma = 72$ mN/m, the surface tension of water with nitrogen gas; $d_1 = 0.2$ mm and because the needle opening is elliptical $d_2 = 1.2$ mm. Actually, assuming completely identical needles, $p_{1/2}$ should have been exactly constant with increasing number of active pores. Instead, $p_{1/2}$ increased slightly, which thus can be explained by small differences in the sizes and shapes of the needles. The difference in critical pressure between the first needle that became active, which is the largest needle, and the 27th active needle is only $997 - 922 = 75$ Pa. This implies that the diameters of the largest and the smallest needle differed only $75/840 \cdot 100\% = 9\%$.

We conclude that the data can be described well with the model and the theoretical resistance of a single pore is of the same order of magnitude as the estimated value of R_p . The value of $p_{1/2} - p_0$ in the first part of the graph in Figure 4b was shown to be quite constant and could be estimated by calculating the critical pressure with equation 5.

Table 2: Estimated parameter values with their confidence intervals resulting from fitting the four needle experiments data with the model using different loss functions. The estimated parameters are: R_p (pore flow resistance) and R_s (resistance of the tubing and clamp against flow).

equation numbers	series number	R_p (10^{12} m^{-3})	R_s (10^{12} m^{-3})
9 and 10 ¹	1		3.8 ± 0.2
	2	675 ± 11	50 ± 0.6
	3		232 ± 0.7
	4		673 ± 6
8 ²	1		
	2	700 ± 67	46 ± 3
	3		234 ± 9
	4		694 ± 92

1. To estimate R_p : $RSS = \sum_{series1}^{series4} (\hat{N} - N_i)^2$

to estimate R_s of series k , with $1 < k < 4$ $RSS_{series k} = \sum (\hat{\phi}_s - \phi_{s,i})^2$

2. To estimate R_p and separate R_s for each series $RSS = \sum_{series1}^{series4} (\hat{\phi}_s - \phi_{s,i})^2$

with RSS : residual sum of squares; i : experimental value.

Microsieve emulsification

In a previous paper [12] we described the formation of oil droplets in a cross-flow system studied with microscopy. The oil was pressed through a microsieve with 100 uniform cylindrical pores (pore diameter $d_p = 7 \mu\text{m}$). The total number of pores at which droplets were formed during the emulsification time was analyzed by microscopy (Figure 1). These numbers of active pores were found to be independent of other parameters, such as the cross-flow velocity. The transmembrane pressure ($p_1 - p_0$) was calculated from the measured disperse phase pressure (p_1) and the continuous phase pressure (p_0).

For 22 different conditions the number of active pores was determined as a function of the transmembrane pressure. For 14 of these experiments also the droplet sizes were determined and thus the oil fluxes were calculated. The pressure just under the membrane pores ($p_{1/2}$) could not be measured, but in the preceding section we concluded that $p_{1/2} - p_0$ can be estimated by calculating the critical pressure (eq. 5): $p_{crit} = 2857 \text{ Pa}$, assuming $\gamma = 5 \text{ mN/m}$, the equilibrium interfacial tension of hexadecane with 1%-Tween in water.

To estimate the parameters R_p and R_s in this system, the dataset with the known fluxes was fitted using equation 8, the other dataset was fitted using equation 7. The part of the loss function using equation 8, was the same as in the experiments with the needles (see Table 2). To get residuals of the same order of magnitude, the residuals were either weighted by the average flux determined or by the average of the number of active pores observed:

$$RSS = \sum \left\{ \left(\frac{\hat{\phi}_s - \phi_{s,i}}{\bar{\phi}_s} \right)^2 + \left(\frac{\hat{N} - N_i}{\bar{N}} \right)^2 \right\}.$$

We used a hexadecane viscosity of $3 \cdot 10^{-3} \text{ Pa s}$.

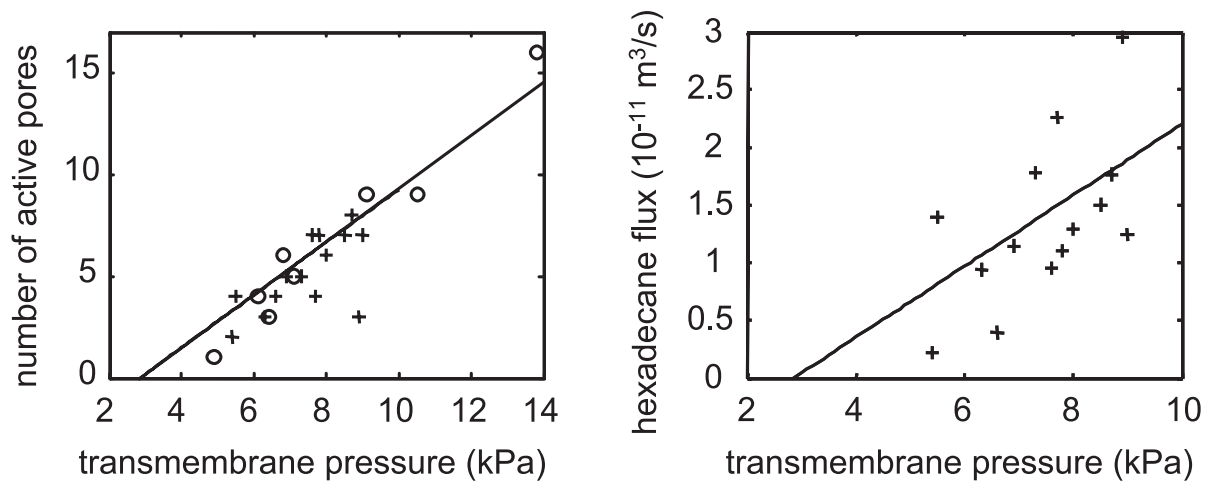


Figure 5: a. Data and fit of the number of active pores against the transmembrane pressure (+: datapoint of which also the flux was determined). b. Data and fit of the hexadecane flux through the microsieve as a function of the transmembrane pressure.

The values found were $R_p = (40 \pm 11) \cdot 10^{16} \text{ m}^{-3}$ and $R_s = (10.8 \pm 2.8) \cdot 10^{16} \text{ m}^{-3}$. With these values the fluxes are in the same order of magnitude as the experimental fluxes (Figure 5b). In comparison, the experimentally determined numbers of active pores are described quite well (Figure 5a). Theoretically, the resistance against flow through a pore is (eq. 2)

$$R_p = \frac{128l_p}{\pi d_p^4} = \frac{128 \cdot 1 \cdot 10^{-6}}{\pi \cdot (7 \cdot 10^{-6})^4} = 1.7 \cdot 10^{16} \text{ m}^{-3}.$$

This is an order of magnitude lower than the estimated value. However, the length/diameter ratio of the pore is small, so the entrance effect may not be neglected. With equation 3 we find $R_{p+e} = 8.6 \cdot 10^{16} \text{ m}^{-3}$. Still, the entrance effect only cannot account for the difference between the estimated value and the theoretical value. An explanation may be that flow through these micron scale channels cannot be described adequately by equations 2 – 4, which are developed for flow through larger tubes [22]. A different expression might be developed by taking scaling effects into account [23]. Alternatively, the presence of a cake layer of (dust) particles of the size of the pore diameter (7 μm) could have increased the experimental R_p . However, this is not very likely, considering the cleaning procedure used and the filtering of the oil before the experiment [12]. With these results it becomes clear that the membrane substructure has quite a large effect on the activation of the pores, even though the resistance of the substructure is almost 4 times smaller than the resistance of a single pore.

General discussion

In the results section it was shown that the gradual activation of membrane pores with increasing pressure can be described adequately by the developed model, based on dividing the membrane in two parts with resistances against flow. With the obtained insights we will discuss the influence of the membrane characteristics on the number of active pores and on droplet formation, thus on the overall process performance. Secondly, we will consider pore activation in a porous membrane.

Membranes with uniform pores straight through the membrane layer

Pore activation: With equation 7 the number of active pores is calculated as a function of the ratio R_p/R_s and the pressure ratio; the pressure ratio is the transmembrane pressure divided by the critical pressure. In order to compare different membranes (next section), the ratio of the resistances is expressed per square meter of membrane area (R_p/R_s^*). Thus, the number of active pores per square meter of membrane area is calculated; it is however plotted in Figure 6 as the number of active pores per $3.24 \cdot 10^{-8} \text{ m}^2$, which was the evaluated microsieve area. To put this figure into perspective the results of the microsieve are shown. The ratio of the resistance against flow in a pore over the resistance in the membrane substructure (R_p/R_s) was 3.7, with the microsieve area giving: $R_p/R_s^* = 1.1 \cdot 10^8 \text{ m}^{-2}$. The critical pressure was 2857 Pa. Therefore, a pressure of 26 times the critical pressure ($= 0.74 \cdot 10^5 \text{ Pa}$) would have been

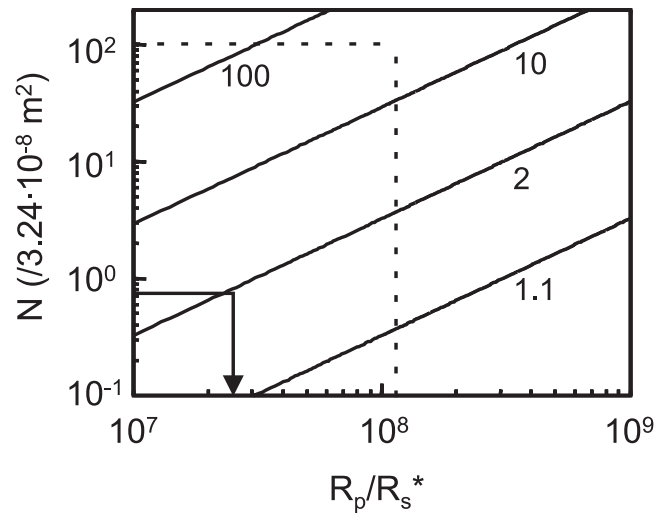


Figure 6: Number of active pores divided by the microsieve membrane area as a function of the ratio of pore flow resistance and substructure resistance per m^2 membrane area and of the pressure ratio (ρ_{tm}/ρ_{crit} ; numbers close to the lines). The dotted line indicates the microsieve, the arrows show the ceramic membrane.

required to activate all 100 pores in the membrane (Figure 6). From the figure it is clear that a higher critical pressure (either due to smaller pores or to a higher interfacial tension) while keeping the transmembrane pressure constant, leads to a lower pressure ratio and thus to less active pores. Furthermore, the ratio of the pore resistance and the membrane substructure resistance should be as high as possible. That is, either the toplayer resistance should be high, or the membrane substructure resistance should be low. When designing a membrane, it should be taken into account to what extent a structure is needed to support the membrane [17, 24]. When there is almost no substructure present the resistance will be very low, and only very moderate pressures are needed to activate all the membrane pores. On the other hand, when a tighter support structure is designed, a stronger membrane is obtained, but then a higher transmembrane pressure is needed.

Droplet formation: an interesting finding is that the pressure difference over the pores is constant and independent of the applied transmembrane pressure as long as not all the pores are active and when there is a specific membrane substructure resistance. This implies that the droplet formation velocity at each individual pore is constant and the droplet sizes are the same for all the pores. Therefore, when only a fraction of the pores is active, fluctuations in the transmembrane pressure do not affect the droplet size. Moreover, the rate at which droplets are formed at each pore can be influenced with the toplayer design. Increasing the pore resistance results in a lower droplet formation rate and a larger number of active pores. The pore resistance may be increased by increasing the length of the pores or by decreasing the pore diameter. However, the last measure will affect the droplet diameter as well [1, 25, 26]. A slower droplet formation rate probably decreases the impact of surfactant dynamics and interface rheology. It should be borne in mind that activating all the pores in a membrane

with a high porosity can result in a polydisperse emulsion, due to coalescence or steric hindrance of droplets forming simultaneously close to each other [12].

Pore activation in a porous membrane with interconnected pores

Although in ceramic and glass membranes the pores are interconnected and feature a size distribution, the same trend in pore activation was observed. Preliminary results of visualizing droplet formation at the surface of an isotropic ceramic membrane (Figure 7), show a linear relation between the number of active pores and the transmembrane pressure. Hence, it is likely that there is a membrane sublayer resistance. In that case the critical pressures of the pores are much smaller than the applied transmembrane pressures at the moment a pore becomes active. Of course one can argue whether the gradual activation of pores results from the membrane sublayer resistance or from a different pore size. If there was no membrane sublayer resistance, the critical pressure would have been equal to the transmembrane pressure. So, the pore diameter, calculated from the transmembrane pressure with eq. 5, of the 7th active pore would have been around two times as large as the diameter of the pore that becomes active first. Because the 7 active pores were only a small fraction of the pores (less than 0.2%), it is not convincing that the diameters differed so much. Therefore, we come to the conclusion that the theory behind the model also holds for a membrane with interconnected pores, because most probably the effect of a sublayer resistance is dominant over the effect of different pore sizes. Note that the number of active pores were determined at two different spots on the membrane surface, and at the second spot with decreasing and increasing transmembrane pressure (Fig. 7), which results in hysteresis.

Because of the thickness of a ceramic or glass membrane, we expect the resistance of the sublayer to be considerably higher than that of a microsieve, while the toplayer pore resistance is probably only somewhat larger (because l_p is larger) than in a microsieve. Hence, it is expected that at the same transmembrane pressure a ceramic membrane will have much

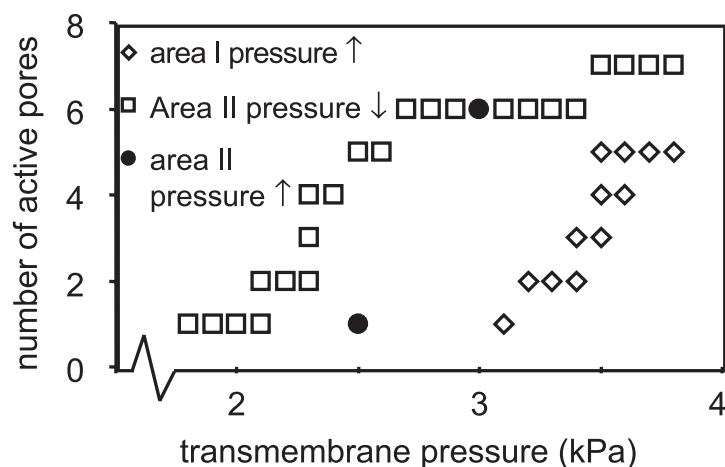
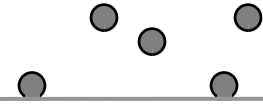


Figure 7: Number of active pores as a function of the transmembrane pressure in an isotropic ceramic membrane with an average pore diameter of 3 μm .



less active pores than a microsieve. Assuming that the 7 active pores were approximately equally sized, we can use Figure 6 to compare this ceramic membrane with the microsieve. The pressure ratio was almost 2 (critical pressure ≈ 1.8 kPa, transmembrane pressure when 7th pore becomes active = 3.5 kPa). The number of active pores should be corrected for the difference in membrane areas: the area of the ceramic membrane we observed was $3 \cdot 10^{-7} \text{ m}^2$, which results in 0.8 active pores per $3.24 \cdot 10^{-8} \text{ m}^2$ membrane area. In Figure 6 it can be seen that R_p/R_s^* for the ceramic membrane is $2.5 \cdot 10^7 \text{ m}^{-2}$. Comparing this value with R_p/R_s^* for the microsieve, we conclude that indeed the resistance of the sublayer is higher in a ceramic membrane. Due to the differences in morphology, the number of active pores per unit of membrane area will be higher for a microsieve than for a ceramic membrane at the same transmembrane pressure. A microsieve will thus give a better process performance.

Conclusion

To obtain a high throughput of the to-be-dispersed phase through the membrane, the fraction of pores at which droplets are formed, should be as high as possible. In this study we show that this can be done by increasing the ratio of flow resistance in the pores itself and the flow resistance in the membrane substructure (R_p/R_s). This can either be done by increasing the resistance of the pores (R_p), by choosing a longer channel, or, more efficiently, a smaller diameter. However, the last measure will also affect the droplet diameter, whereas the channel length does probably not influence the droplet diameter so much. Because the resistances in the membrane not only affect the pore activation, but also the droplet formation process, the total membrane should be designed carefully.

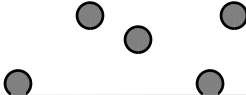
Nomenclature

d_p	diameter	(m)
l_p	length	(m)
N	number of active pores/needles	(-)
p_0	continuous phase pressure	(Pa)
$p_{1/2}$	pressure just below the pores/needles	(Pa)
p_1	disperse phase pressure at the inlet of the system	(Pa)
Δp	pressure difference	(Pa)
p_{crit}	critical pressure	(Pa)
p_{trm}	transmembrane pressure	(Pa)
R_p	pore flow resistance	(m^{-3})
R_{p+e}	resistance against flow due to the entrance effect and friction in the pore	(m^{-3})
R_s	membrane substructure resistance against flow	(m^{-3})
R_s^*	product of membrane substructure resistance and membrane area	(m^{-1})
Re	Reynolds number	(-)

ϕ_p	flux of disperse phase through a pore	(m ³ /s)
ϕ_s	total flux of disperse phase through the system	(m ³ /s)
γ	surface or interfacial tension	(N/m)
η	viscosity	(Pa s)
κ	porosity	(-)

Reference list

- 1 T. Nakashima, M. Shimizu and M. Kukizaki, Membrane Emulsification by Microporous Glass, *Key Eng. Mater.*, 61 & 62 (1991) 513.
- 2 V. Schröder and H. Schubert, Production of Emulsions Using Microporous, Ceramic Membranes, *Coll. Surfaces A: Physicochemical Eng. Aspects*, 152 (1999) 103.
- 3 V. Schröder, Herstellen von Öl-in-Wasser-Emulsionen mit Mikroporösen Membranen, PhD thesis, Technische Hochschule Karlsruhe, 1999.
- 4 T. Nakashima, M. Shimizu and M. Kukizaki, Particle Control of Emulsion by Membrane Emulsification and Its Applications, *Adv. Drug Delivery Rev.*, 45 (2000) 47.
- 5 H. Yuyama, K. Yamamoto, K. Shirafuhi, M. Nagai, G.H. Ma and S. Omi, Preparation of Polyurethaneurea (PUU) Uniform Spheres by SPG Membrane Emulsification Technique, *J. Appl. Polym. Sci.*, 77 (2000) 2237.
- 6 J.O. You, S.B. Park, H.Y. Park, S. Haam, C.H. Chung and W.S. Kim, Preparation of Regular Sized Ca-Alginate Microspheres Using Membrane Emulsification Method, *J. Microencapsulation*, 18 (2001) 521.
- 7 S. Higashi and T. Setoguchi, Hepatic Arterial Injection Chemotherapy for Hepatocellular Carcinoma With Epirubicin Aqueous Solution As Numerous Vesicles in Iodinated Poppy-Seed Oil Microdroplets: Clinical Application of Water-in-Oil-in-Water Emulsion Prepared Using a Membrane Emulsification System, *Adv. Drug Delivery Rev.*, 45 (2000) 57.
- 8 S.M. Joscelyne and G. Trägårdh, Membrane Emulsification - a Literature Review, *J. Membrane Sci.*, 169 (2000) 107.
- 9 S.M. Joscelyne and G. Trägårdh, Food Emulsions Using Membrane Emulsification: Conditions for Producing Small Droplets, *J. Food Eng.*, 39 (1999) 59.
- 10 H. Yuyama, T. Watanabe, G.H. Ma, M. Nagai and S. Omi, Preparation and Analysis of Uniform Emulsion Droplets Using SPG Membrane Emulsification Technique, *Coll. Surfaces A: Physicochemical Eng. Aspects*, 168 (2000) 159.
- 11 T. Fuchigami, M. Toki and K. Nakanishi, Membrane Emulsification Using Sol-Gel Derived Macroporous Silica Glass, *J. Sol-Gel Sci. Tech.*, 19 (2000) 337.
- 12 Chapter 3, published as: A.J. Abrahamse, R. van Lierop, R.G.M. van der Sman, A. van der Padt and R.M. Boom, Analysis of Droplet Formation and Interactions During Cross-Flow Membrane Emulsification, *J. Membrane Sci.*, 204 (2002) 125.
- 13 S. Sugiura, M. Nakajima, J. Tong, H. Nabetani and M. Seki, Preparation of Monodispersed Solid Lipid Microspheres Using a Microchannel Emulsification Technique, *J. Colloid Interface Sci.*, 227 (2000) 95.
- 14 C.C. Ho and A.L. Zydney, Protein Fouling of Asymmetric and Composite Microfiltration Membranes, *Ind. Eng. Chem. Res.*, 40 (2001) 1412.
- 15 C.C. Ho and A.L. Zydney, Effect of Membrane Morphology on the Initial Rate of Protein Fouling During Microfiltration, *J. Membrane Sci.*, 155 (1999) 261.
- 16 M. Mulder, *Basic Principles of Membrane Technology*, Kluwer Academic Publishers, Dordrecht, 1991.
- 17 C.J.M. van Rijn and M.C. Elwenspoek, Micro Filtration Membrane Sieve With Silicon Micro Machining for Industrial and Biomedical Applications, *Proc. IEEE*, 83 (1995) 83.

- 
-
- 18 C.J.M. van Rijn, W. Nijdam, L.A.V.G. van der Stappen, O.J.A. Raspe, L. Broens and S. Hoof, Innovation in yeast cell filtration: cost saving technology with high flux membranes, in Proceedings of the Proceedings of European Brewery Conference 1997, 501.
 - 19 A.J. Gijsbertsen-Abrahamse, A. van der Padt and R.M. Boom, Membrane emulsification: the influence of pore geometry and wall contact angle on process performance, in Proceedings of the CME (World Congress on Emulsions) 3, 24 – 27 September 2002, Lyon, in press.
 - 20 Chapter 2, published as: A.J. Abrahamse, A. van der Padt, R.M. Boom and W.B.C. de Heij, Process Fundamentals of Membrane Emulsification: Simulation With CFD, *AIChE Journal*, 47 (2001) 1285.
 - 21 R.H. Perry and D. Green, *Perry's Chemical Engineers' Handbook*, McGraw-Hill Book Company, New York, 1984.
 - 22 T. Hasegawa, M. Suganuma and H. Watanabe, Anomaly of Excess Pressure Drops of the Flow Through Very Small Orifices, *Phys. Fluids*, 9 (1997) 1.
 - 23 H. Herwig, Flow and Heat Transfer in Micro Systems: Is Everything Different or Just Smaller?, *Z. Angew. Math. Mech.*, 82 (2002) 579.
 - 24 S. Kuiper, C.J.M. van Rijn, W. Nijdam and M.C. Elwenspoek, Development and Applications of Very High Flux Microfiltration Membranes, *J. Membrane Sci.*, 150 (1998) 1.
 - 25 Y. Mine, M. Shimizu and T. Nakashima, Preparation and Stabilization of Simple and Multiple Emulsions Using a Microporous Glass Membrane, *Coll. Surfaces B: Biointerfaces*, 6 (1996) 261.
 - 26 R.A. Williams, S.J. Peng, D.A. Wheeler, N.C. Morley, D. Taylor, M. Whalley and D.W. Houldsworth, Controlled Production of Emulsions Using a Crossflow Membrane. Part II: Industrial Scale Manufacture, *Trans. Inst. Chem. Eng.*, 76 (1998) 902.



5 Estimating pore size distributions of interconnected porous materials with liquid displacement methods

Abstract

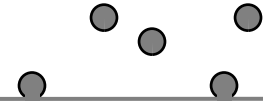
The liquid displacement method is a commonly used method to determine the pore size distribution of micro- and ultrafiltration membranes. One of the assumptions for the calculation of the pore sizes is that the pores are parallel, hence, not interconnected. To show that the estimated pore size distribution is affected if this assumption is not satisfied, we developed two models. Firstly, a model describing the flow through an isotropic porous membrane with uniform pores, and secondly a two-layer model for uniform pores that approximates the first model if the membrane thickness is larger than 10 times the pore radius. In the two-layer model the membrane skin layer is divided into two parts: the unconnected pore layer and a sublayer. This model is extended to describe pore activation as a function of pressure with a pore size distribution in the unconnected pore layer (read membrane surface). It is shown that, depending on the membrane thickness or the sublayer resistance, the transmembrane pressure needs to be much larger than the critical pressure of the pores, to activate all the pores. If the sublayer resistance is over 10% of the resistance of the unconnected pore layer, the pore size is underestimated with the liquid displacement method, hence the number of pores is overestimated. Because the sublayer resistance is always larger than the unconnected pore layer resistance in an isotropic membrane with interconnected pores, we conclude that using the liquid displacement method for this type of membrane always results in underestimation of the pore size distribution. To use the liquid displacement method correctly, we suggest either to count the number of (active) pores or to measure the flux-pressure curve several times, while covering each time a different fraction of the membrane surface.

Introduction

To characterize filtration membranes, several methods have been developed to determine pore size, pore size distribution and porosity. They can be classified into: 1. methods to determine pore size and pore size distribution of a membrane; 2. methods based on rejection performance using reference molecules and particles [1]. The liquid displacement method, falling in class 1, is commonly used to determine membrane pore size distributions because it is close to (ultra)filtration practice: dead-end pores are not evaluated; the membrane is characterized in wet conditions; in addition the pressure is kept as low as possible, hence no alteration of the membrane occurs [1]. The method was first described by Erbe [2] and Kesting [3] and further developed by Capannelli et al. [4, 5]. It is based on the measurement of the flux of a displacing liquid through the membrane as a function of the pressure applied. From the flux-pressure curve the pore size distribution is calculated using the Hagen-Poiseuille equation. Although many researchers investigated the liquid displacement method and improvements were suggested [6-8], no one studied how the pore size distribution determination is affected by pore connections, that is, if the pores are not straight through the whole membrane layer. Nevertheless, the method is not only used to determine the pore size distribution of membranes with straight-through pores [9-12], but also for symmetric membranes and asymmetric membranes with a thin skin layer with more or less interconnecting pores [4, 10, 13-15]. In this chapter we show that wrong results are obtained when the pores are connected to each other. First, the main points and assumptions of the liquid displacement method are recapitulated. Then flow through an isotropic membrane with uniform pores is modeled, and the effect of a pore size distribution of the surface pores is modeled in a two-layer model: the membrane skin layer is assumed to be divided in an unconnected pore layer and a sublayer. Furthermore, we suggest two methods to modify the liquid displacement method to take pore connections into account.

Theory of the liquid displacement method

The liquid displacement method is an indirect method to determine the pore size distribution of a membrane, because first a flux-pressure curve is measured, from which the pore size distribution is calculated subsequently. To measure the flux-pressure curve a pair of immiscible liquids with a low interfacial tension is used. The membrane is wetted with one of the liquids. By a stepwise increase of the transmembrane pressure, the non-wetting liquid is pressed through the membrane. With increasing pressure, first the liquid in the largest pores is displaced, then, at higher pressures more and more smaller pores are opened [2-4]. Eventually, a pressure is reached at which further increases result only in an increase in flux which is proportional to the increase in pressure [3]. Alternatively, a low surface tension liquid may be displaced by pressurized nitrogen to characterize microfiltration membranes. From the flux-pressure curve the pore size distribution can be calculated assuming the following [2]:



1. the pores are cylindrical;
2. the pores are parallel to each other and not interconnected, thus straight through the whole membrane layer;
3. the pores all have a length l , usually l is taken to be the thickness of the membrane (or the thickness of the membrane skin layer in case of an asymmetric membrane) [4, 9].

With assumption 2 (parallel pores) and the implicit assumption that nowhere in the measuring set-up a resistance against flow is present, the transmembrane pressure at which the liquid in a pore is displaced is equal to the critical pressure of that pore. Assuming a cylindrical pore (assumption 1), the critical pressure of a pore can be calculated with the Laplace equation:

$$p_{crit} = \frac{2\gamma \cos \theta}{r_p} \quad (\text{Pa}) \quad (1)$$

in which γ is the interfacial tension between the two liquid phases, r is the radius of the pore and θ is the wall contact angle. For convenience, usually the contact angle θ is taken to be zero. Actually, this is the only value giving correct results in case of pores with sharp edges, because the droplet always has to go through the hemispherical stage [7, 16]. In that stage the pressure is maximal and can be calculated with:

$$p_{crit} = \frac{2\gamma}{r_p} \quad (\text{Pa}) \quad (2)$$

With assumptions 1 and 3, the number of pores in a certain size class (N) can be calculated from the increase in the measured flux ($d\phi_s$) upon the increase in transmembrane pressure (dp_{tm}) (see e.g. [2-4]):

$$N(r_p) = \frac{8\eta l}{\pi r_p^4} \frac{d\phi_s}{dp_{tm}} \quad (-) \quad (3)$$

with η the viscosity of the displacing liquid. If l is not known, a relative pore size distribution can be calculated.

Effect of interconnected pores on pore size estimation

Most membranes are not characterized by parallel, unconnected pores. Most symmetric membranes have highly interconnected, tortuous pores, as is the case for the skin layer of asymmetric membranes (Figure 1a). In this section we will show that this has a strong effect on the estimation of the pore size distributions by liquid displacement. In the first section we will model the flux-pressure curve with an isotropic membrane model. Then the similarity between this model and a simpler two-layer model for uniform pores is shown (schematically in Figure 1b). The two-layer model was developed to describe pore activation in membrane emulsification [17]. Finally, to include the effect of different pore sizes in the model, the two-layer model is extended.

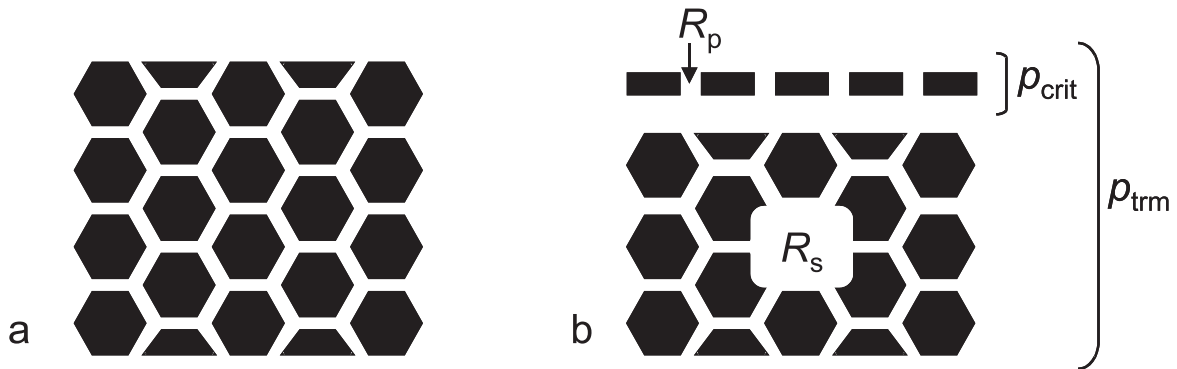


Figure 1: a. isotropic membrane with uniform pores, schematically; b. two-layer model for uniform pores.

Isotropic membrane model

To determine the effect of pore connections, the flux through an isotropic membrane with uniform pores (equal pore radii and pore lengths) is calculated as a function of the transmembrane pressure and the membrane thickness. Figure 2 schematically shows that more and more pores are activated upon increasing transmembrane pressure. Due to the flow through an active pore, the pressure just below that pore drops to a value lower than the critical pressure and the pressures below the pores close to the active pore decrease too (Figure 2c). The pressure decreases least under the pores which are furthest away from an active pore; these pores will be activated next (Figure 2d). With this in mind, we assumed that the space around an already active pore can be approximated by a cylinder (Figure 3). The pressure under the surface pores at the edge of the cylinder and the flux through the cylinder were calculated as a function of the cylinder radius and the membrane thickness. From these results the fraction of active pores and the flux can be determined as a function of the membrane thickness and the ratio of the transmembrane pressure and the critical pressure of the pores.

The model: Analogous to the model of Ho and Zydney [18] for pore blockage during filtration, we modeled the pressure profile in the cylindrical part of the porous membrane (Figure 3b). With Darcy's law and the continuity equation a second-order partial differential equation for the local pressure is obtained [18]:

$$\frac{k_r}{r} \frac{\partial}{\partial r} \left(r \frac{\partial p}{\partial r} \right) + k_z \frac{\partial^2 p}{\partial z^2} = 0 \quad (\text{s}^{-1}) \quad (4)$$

in which k_r and k_z are the permeabilities in the radial and transverse directions.

The boundary conditions are given by:

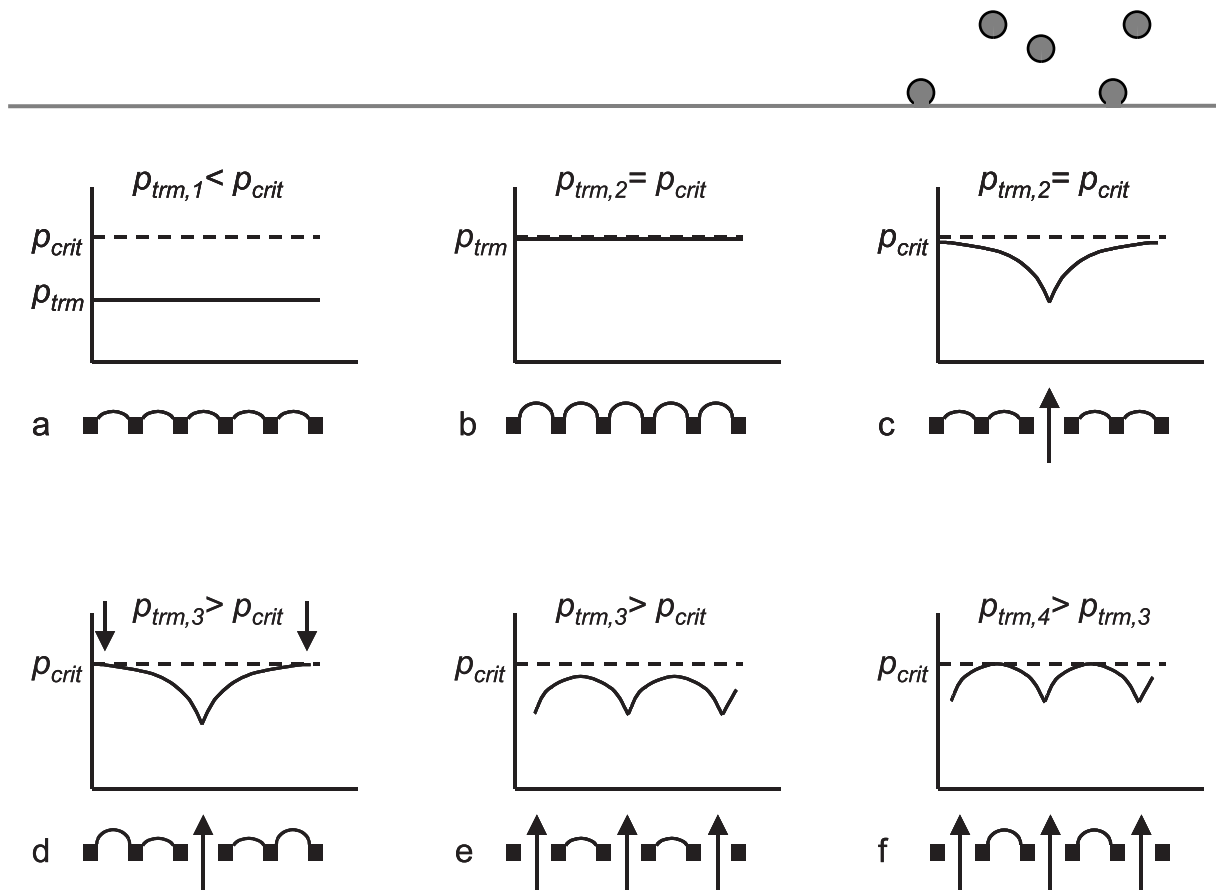


Figure 2: Schematic of gradual activation of pores with increasing transmembrane pressure (p_{tm}); on the x-axes the position of the surface pores, on the y-axes the pressure just below the surface pores. Schematical representation of the surface pores, either a droplet is present or the pore is active (depicted by arrows).

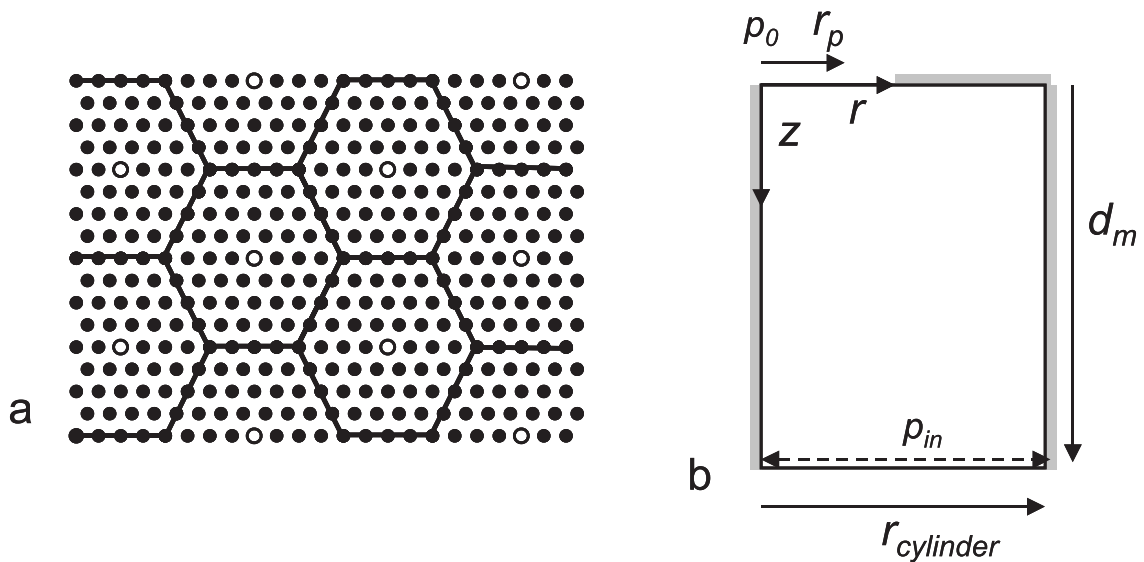


Figure 3: a. top surface of a membrane with active pores (○) and non-active pores (●), schematically; b. approximation of the hexagon around an active pore in (a) by a cylinder. Dimensions and boundary conditions are shown (in grey boundary conditions: $\partial p/\partial r = 0$ or $\partial p/\partial z = 0$). Symbols are explained in the section nomenclature.

$$r = 0: \quad \frac{\partial p}{\partial r} = 0 \quad (5)$$

$$r = r_{cylinder}: \quad \frac{\partial p}{\partial r} = 0 \quad (6)$$

$$z = d_m: \quad p = p_{in} = p_{trm} + p_0 \quad (7)$$

$$z = 0: \quad p = p_0 \quad 0 \leq r \leq r_p \quad (8a)$$

$$\frac{\partial p}{\partial z} = 0 \quad r_p < r \leq r_{cylinder} \quad (8b)$$

We assume an isotropic membrane, implying equal permeabilities in the radial and transverse directions: $k_r = k_z$, hence they both can be removed from equation 4. The problem was non-dimensionalized in the radial and transverse directions using the pore radius (r_p): $\rho = r/r_p$ and $Y = z/r_p$, so $\rho_{cyl} = r_{cylinder}/r_p$ and $\delta_m = d_m/r_p$. A typical result of the pressure profile in the cylinder is shown in Figure 4 ($\rho_{cyl} = 8$, $\delta_m = 20$, $p_{in} = 1$, $p_0 = 0$).

Results: In Figure 5a the ratio of the transmembrane pressure ($p_{trm} = p_{in} - p_0$) and the pressure under the pores at the edge of the cylinder, is shown as a function of the cylinder radius and the membrane thickness. A decreasing cylinder radius means that the distance between active pores decreases and the fraction of active pores increases. To activate a pore, the pressure under the pore should be equal to the critical pressure. Figure 5a thus shows that to increase the number of active pores, the transmembrane pressure should increase considerably. This was schematically shown in Figure 2. In the case of a membrane with a dimensionless

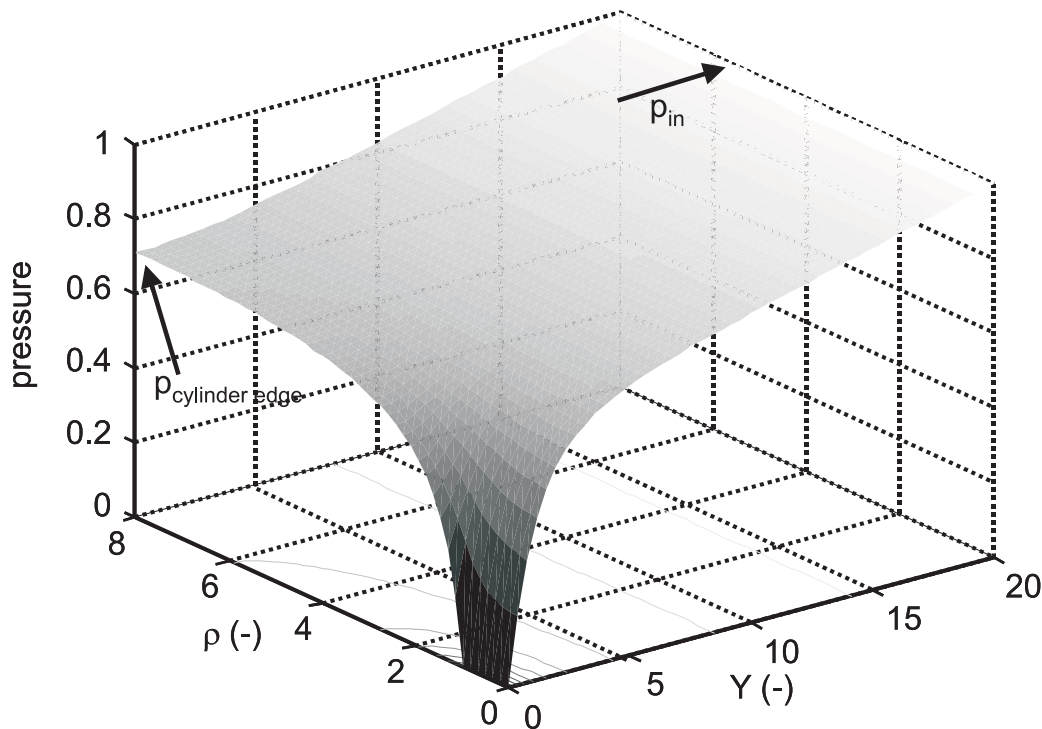


Figure 4: Pressure profile in a cylinder ($p_{in} = 1$, $p_0 = 0$, $\rho_{cyl} = 8$, $\delta_m = 20$).

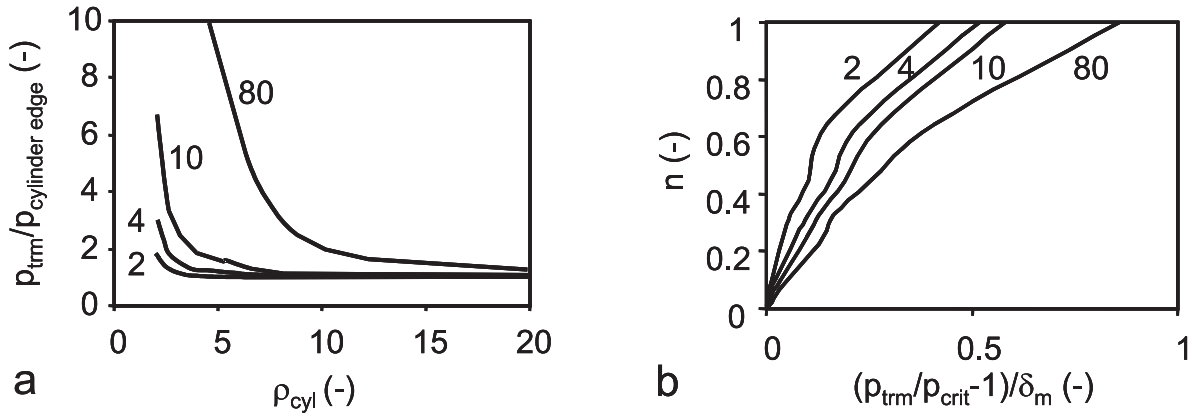


Figure 5: Results obtained with the isotropic membrane model with several membrane thicknesses. a. ratio of transmembrane pressure and the pressure under the pores at the edge of the cylinder as a function of the dimensionless cylinder radius; b. fraction of active pores as a function of the dimensionless pressure divided by δ_m .

thickness of 80, the transmembrane pressure should even be increased to about 70 times the critical pressure to activate all the pores.

The fraction of active pores (n) at a certain ratio of transmembrane pressure and critical pressure, was calculated by:

$$n \Big|_{\frac{p_{trm}}{p_{crit}}} = \frac{A_{active}}{A_m} = \frac{\pi r_p^2}{\pi (0.5 r_{cylinder})^2} = \left(\frac{1}{0.5 \cdot \rho_{cyl}} \right)^2 \quad (-) \quad (9)$$

n was calculated using $0.5 \cdot \rho_{cyl}$, because it was assumed that at the value of p_{trm}/p_{crit} (calculated using ρ_{cyl}), some pores at the edge of the cylinder just become active. Thus, the distance between two active pores was reduced to half the cylinder radius. n is plotted as a function of $(p_{trm}/p_{crit}) - 1$ divided by the dimensionless membrane thickness (δ_m) (Figure 5b).

With this figure it is clearer that to activate all the pores, the transmembrane pressure should be many times the critical pressure, depending on the membrane thickness, even for uniform pores! Because the transmembrane pressure at which a pore becomes active is no longer only a function of the pore radius, using the liquid displacement method will introduce errors in the estimation of the pore size distribution. To estimate these errors, we calculated the flux-pressure curves using the following equation to determine the pressure gradient at the bottom of the cylinder:

$$\frac{\Delta p}{\Delta Y} \Big|_{p=p_m} = \int_0^{\rho_{cyl}} \frac{\Delta p}{\Delta Y} \Big|_{Y=\delta_m} d\rho \quad (\text{Pa}) \quad (10)$$

From this pressure gradient the flux of the non-wetting liquid phase was calculated according to Darcy's law:

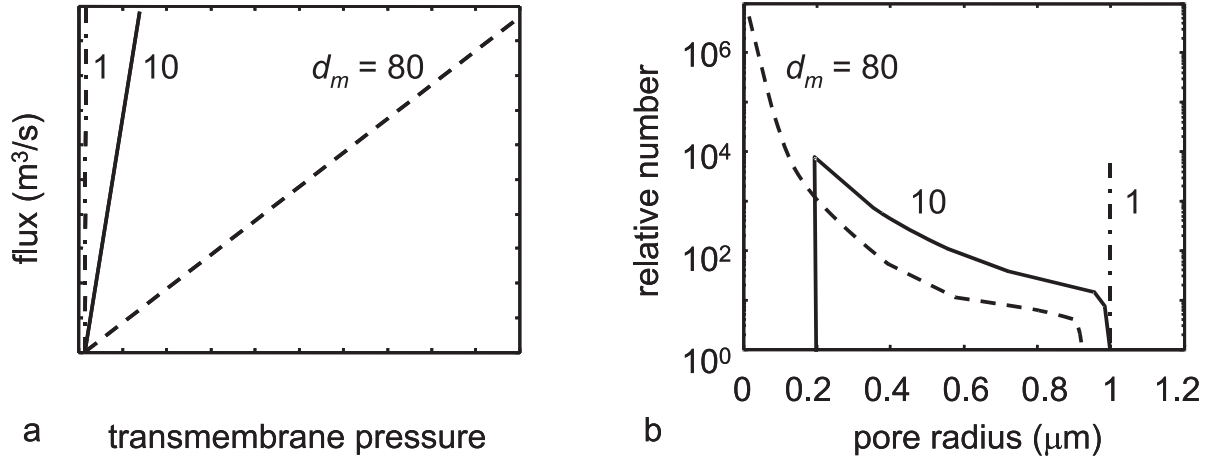


Figure 6: a. flux-pressure curves calculated with the isotropic membrane model ($r_p = 1 \mu\text{m}$, ($K = 1.8 \cdot 10^{-14} \text{ m}^2$), $d_m = 1, 10$ and $80 \mu\text{m}$); b. original pore size distribution and pore size distributions estimated from the flux-pressure curves in (a) with the liquid displacement method.

$$\phi_s = A_m k_z \frac{\Delta p}{\Delta Y} \bigg|_{p=p_m} \frac{1}{r_p} = A_m k_z \frac{\Delta p}{\Delta Y} \bigg|_{p_{crit}=1} \frac{p_{crit}}{r_p} \quad (\text{m}^3/\text{s}) \quad (11)$$

In which A_m is the membrane area considered, and k_z can be written as K/η ; K is the permeability in m^2 and can be determined by measuring the membrane flux and using the Hagen-Poiseuille equation or the Kozeny-Carman equation [19]. The permeability, and thus the flux, will be a function of the membrane porosity. In Figure 6a-b, flux-pressure curves of two membranes with the same uniform pore size, but different thicknesses, and the apparent pore size distributions estimated with the liquid displacement method (described in the section theory) from those flux-pressure curves, are shown. It is clear that the obtained pore size distributions are not correct: the estimated pore sizes are much too small. The thicker the membrane compared to the pore radius, the worse the estimation of the pore size distribution.

Isotropic membrane model and two-layer model compared

Both the fraction of active membrane surface pores and the pressure gradient at the bottom of the cylinder are roughly linearly dependent on the dimensionless transmembrane pressure (Figures 5b and 7). This is especially true for the flux, which is approximately linearly dependent on the pressure gradient when $\delta_m > 10$. These linear dependencies show large resemblance with the two-layer model, developed to describe pore activation in membrane emulsification [17]. In the two-layer model, the membrane is assumed to be composed of two distinct structural layers, an unconnected pore layer having parallel pores, and a sublayer; each layer having a given resistance to fluid flow (Figure 1b). In the next section it will be shown that the two-layer model can easily be extended to describe the effect of different pore sizes on the estimation of the pore size distribution. Therefore, in this section we compare the

two models and give equations to convert the isotropic membrane model in the two-layer model.

In the two-layer model for uniform pores, the number of active pores (N) is given by:

$$N = \frac{R_p}{R_s} \left(\frac{p_{trm}}{p_{crit}} - 1 \right) \quad (-) \quad (12)$$

In which R_p is the resistance of a single pore in the unconnected pore layer and R_s is the resistance of the sublayer, which is in series with the unconnected pores. The fraction of active pores (n) is calculated by dividing both N and the single pore resistance (R_p) by the total number of pores in the surface (N_{tot}):

$$n = \frac{N}{N_{tot}} = \frac{R_p/N_{tot}}{R_s} \left(\frac{p_{trm}}{p_{crit}} - 1 \right) = \frac{R_{up}}{R_s} \left(\frac{p_{trm}}{p_{crit}} - 1 \right) \quad (N < N_{tot}) \quad (-) \quad (13)$$

In which R_{up} is the total resistance of the pores in the unconnected pore layer. The ratio of resistances R_{up}/R_s for a membrane with interconnected pores can now be calculated from the slopes (a) of the graphs in Figure 5b. In this Figure n is shown as a function of $(p_{trm}/p_{crit} - 1)/\delta_m$ and thus:

$$\frac{R_{up}}{R_s} = \frac{a}{\delta_m} = \frac{a r_p}{d_m} \quad (-) \quad (14)$$

a ranges from around 2 for a very thin membrane to 1 for a thick membrane. This means that R_{up}/R_s is always smaller than 1 for a membrane with interconnected pores. From this result it will be concluded in the next section that the estimation of the pore size distribution with the liquid displacement method is always incorrect with such a type of membrane, as is already partly shown in Figure 6.

In order to make an estimation of R_s of a membrane with interconnected pores, the equations for the flux in the two-layer model,

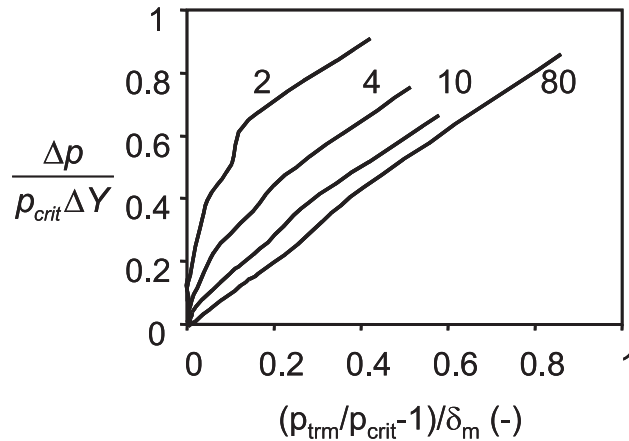


Figure 7: Dimensionless pressure gradient at the bottom of the cylinder, as a function of the dimensionless pressure divided by δ_m . Until the point where $n = 1$.

$$\phi_s = \frac{P_{trm}}{\eta R_s} - \frac{P_{crit}}{\eta R_s} = \frac{P_{crit}}{\eta R_s} \left(\frac{P_{trm}}{P_{crit}} - 1 \right) \quad (\text{m}^3/\text{s}) \quad (15)$$

should be substituted in the flux equation of the isotropic membrane model (eq. 11), giving:

$$\frac{\Delta p}{\Delta Y} \Big|_{P_{crit}=1} = \frac{r_p}{R_s A_m K} \left(\frac{P_{trm}}{P_{crit}} - 1 \right) \quad (-) \quad (16)$$

Now the resistance of the sublayer R_s can be calculated from the slopes (b) of the graphs in Figure 7:

$$R_s = \frac{r_p}{A_m K} \frac{\delta_m}{b} = \frac{d_m}{A_m K b} \quad (\text{m}^{-3}) \quad (17)$$

b is close to 1 and not dependent on the membrane thickness as long as the membrane thickness is more than 10 times the pore radius ($\delta_m > 10$). This implies that in a microfiltration membrane with a maximum average radius of 2.5 μm and a thickness (of the skin layer) of 25 μm the two-layer model can be used instead of the isotropic membrane model. Usually the membrane or membrane skin layer will be thicker or the pore radius will be smaller, thus in most cases pore activation and the flux-pressure curve can be determined by the two-layer model.

Two-layer model with pore size distribution

As the isotropic membrane model is not convenient for determining the effect of interconnected pores on the estimation of the pore size distribution if the pores are not uniform, the two-layer model is extended to describe flow through an unconnected pore layer with pores that are not uniform, and a sublayer. In the preceding section it was shown that in many practical cases the isotropic membrane model can be approximated by the two-layer model.

The model: The transmembrane pressure necessary to displace the liquid from the i -th pore can be calculated by assuming that there is no accumulation of fluid in the membrane. Thus, the total flow through the unconnected pore layer (equation 18) must equal the flow through the sublayer, described by equation 15.

$$\phi_{up} = \sum_{i=1}^N \phi_p = \frac{P_{crit,i}}{\eta R_{up,i}} \quad (\text{m}^3/\text{s}) \quad (18)$$

in which ϕ_p is the flux through a pore, ϕ_{up} the total flux through the unconnected pore layer, and $R_{up,i}$ the resistance of the unconnected pore layer, which depends on the number and sizes of the pores from which the liquid is displaced, according to equation 19:

$$R_{up,i} = \frac{1}{\sum_{i=1}^i R_{p,i}} = \frac{8l}{\pi \sum_{i=1}^i r_i^4} \quad (\text{m}^{-3}) \quad (19)$$

With l being the unconnected pore length; a best guess for the value of l is probably the diameter of the nodular structure of the membrane. Combining equations 18 and 15 gives:

$$P_{trm,i} = P_{crit,i} \left(\frac{R_s + R_{up,i}}{R_{up,i}} \right) \quad (\text{Pa}) \quad (20)$$

Hence, the transmembrane pressure at which the liquid from the i -th pore is displaced is a function of the ratio of the resistance of the two layers ($R_s + R_{up}$) and the resistance in the unconnected pore layer. With this equation it can be explained that even uniform pores do not become active at the same transmembrane pressure. If liquid is displaced from an increasing number of pores, R_{up} decreases and thus the transmembrane pressure needs to be increased to activate additional pores.

Results: In Figure 8a two calculated flux-pressure curves are given: one of a membrane in which the pores (with a log-normal size distribution) are straight through the membrane (or through the skin layer, in case of an asymmetric membrane) and a membrane with the same log-normal pore size distribution, but with a sublayer resistance in series (calculated with equations 18 and 20). In Figure 8b the pore size distributions calculated with the commonly used liquid displacement method (described in the theory) are shown. The results clearly show that if there is a sublayer present, the determination of the pore size distribution from the flux-pressure curve results in a smaller average pore radius, a larger standard deviation and a larger number of membrane pores. In the same way we explored different average pore sizes, values of the standard deviation of the pore size distribution at different values of the sublayer resistance (R_s). The resulting errors in average pore radius, standard deviation and number of pores using the liquid displacement method are plotted (Figure 9a-c) as the ratio of the calculated value over the input value. On the x-axis the input is shown: the total

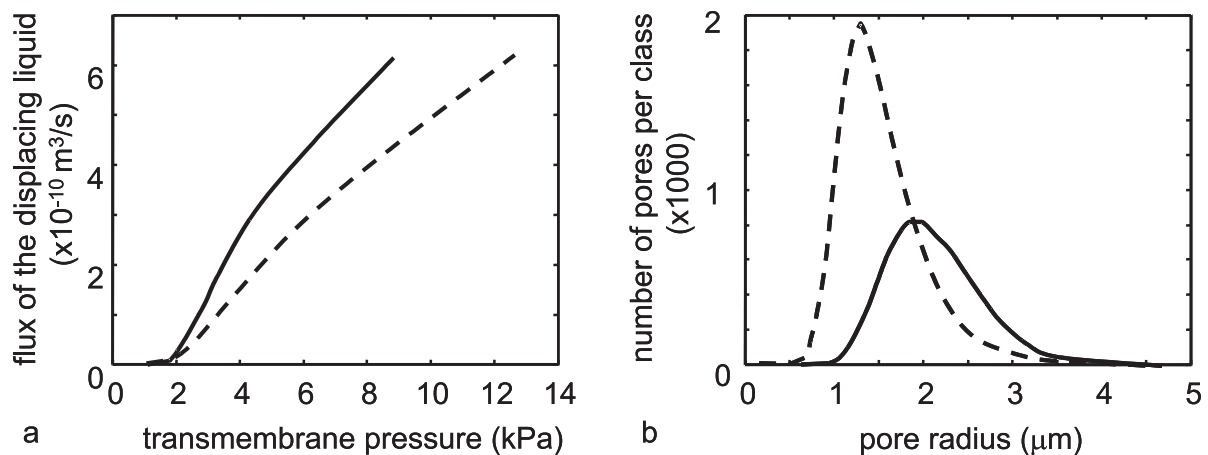


Figure 8: a. flux of the displacing liquid as a function of transmembrane pressure for $R_s = 0$ (—) and $R_s = 2 \cdot 10^{13} \text{ m}^{-3}$ (.....); b. pore size distributions calculated with the liquid displacement method from the flux-pressure curves in a. (class width $1 \cdot 10^{-7} \text{ m}$). Values of the original pore size distribution and of the displacing liquid: $\bar{r} = 2 \cdot 10^{-6} \text{ m}$, $\sigma = 0.25$, $n = 1 \cdot 10^4$, $l = 5 \cdot 10^{-6} \text{ m}$, $R_{up} = 4.77 \cdot 10^{13} \text{ m}^{-3}$, $\gamma = 0.35 \cdot 10^{-3} \text{ N/m}$, $\eta = 30 \cdot 10^{-3} \text{ Pas}$.

unconnected pore layer resistance (R_{up}) over the sublayer resistance (R_s).

As long as the sublayer resistance is less than 10% of the resistance of the unconnected pore layer, the membrane can be considered as consisting of just the unconnected pore layer; then the liquid displacement method can be used to determine the pore size distribution without making any errors. However, a larger R_s (relatively to R_{up}) results in an increasing underestimation of the pore radii. As a result, the number of pores is overestimated. From Figure 9b it follows that the pore size distribution estimated with the liquid displacement method is much wider than it is in reality. This is due to the fact that pores with the same radius do not become active at the same transmembrane pressure, which was explained with equation 20. In the preceding section it was shown that R_{up}/R_s is always smaller than 1 in a membrane with interconnected pores, which means that the pores cannot be assumed to be straight through the whole membrane layer. Therefore, the liquid displacement method needs to be modified to take the membrane morphology into account, which is discussed below. However, if the membrane is not at all isotropic, $k_r \ll k_z$, or even $k_r = 0$ (which is the case for Nuclepore[®] track-etched membranes), the liquid displacement method in its original form is correct. Yet, in the two-layer model it is assumed that the liquid is displaced in the pores from the bottom up. However, also channelling through the porous matrix may occur. Then the resistance in the sublayer will be much higher and it cannot be assumed that the pores in the

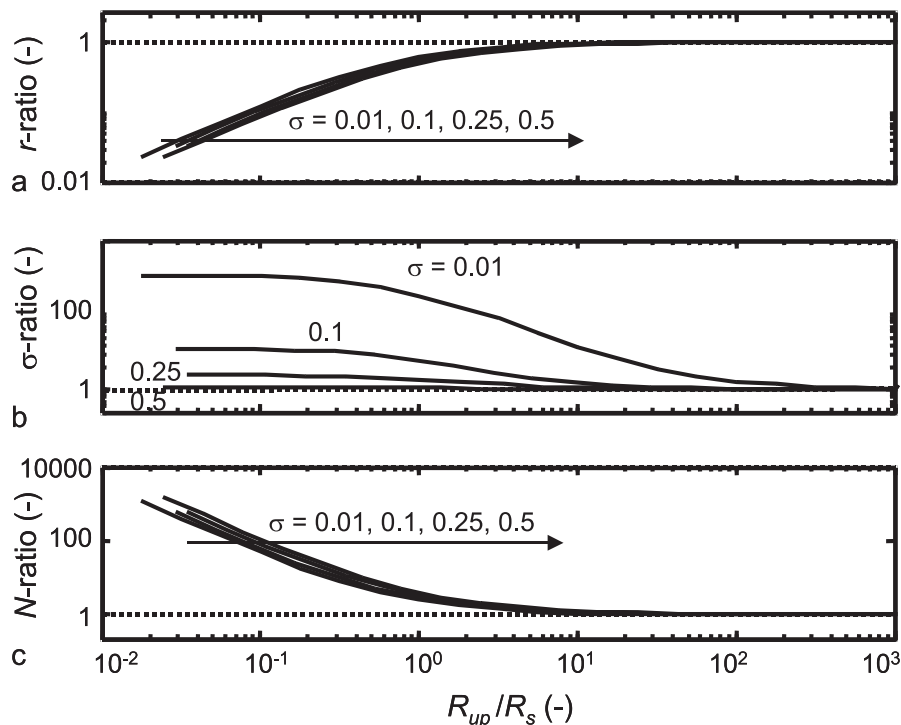
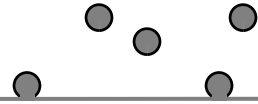


Figure 9: Ratios of the calculated value over the original value as a function of the ratio of the unconnected pore layer resistance (R_{up}) and the sublayer resistance (R_s). a. ratio of the average pore radius; b. ratio of the standard deviation of the pore size distribution; c. ratio of the total number of pores. Note that the ratios should be 1 for correct estimation of the pore size distribution (dotted line).



surface layer experience the same critical pressure. So in the case of channelling, the model is not valid.

Discussion: Modification of the liquid displacement method

In this section two options are presented to adjust the liquid displacement method, thus including the effects of interconnectivity. In the theory the basis of the liquid displacement method was presented (equations 2 and 3). From the measured flux and pressure vectors, only two of three variables (r , l and n) can be determined. Therefore, usually l is assumed to have a constant value for all the pores. If a sublayer resistance should be taken into account, there is an extra variable: R_s . In order to determine the pore size distribution decently (with the equations given in the preceding section), R_s has to be estimated, either by determination of the number of (active) pores or by repeating the experiment with a partially covered membrane surface. These methods are discussed in more detail in this section.

Determination of the number of (active) pores to estimate R_s

Determination of the number of active pores by visualization would yield the required extra information. However, this is not very easy to do. It might be possible to include a microscope in the set-up, but observing the displacement of liquid from the smallest pores will be difficult, because of the flow of liquid through the other pores. In ultrafiltration membranes it will not be possible to visualize the pores, due to their small sizes. Nevertheless with microfiltration membranes, only observing the number of pores from which liquid is displaced in a part of the low pressure range, gives already enough information: because if it is exactly known how much pores cause the measured flux at a certain pressure, the sublayer resistance can be calculated with equations 15 and 18-20. This R_s -value can be used to determine the remainder of the pore size distribution. Perhaps one can think of another method to determine the number of active pores as a function of pressure or to determine the total number of pores in the membrane surface. One of these methods would be to increase the transmembrane pressure very slowly and with very small steps to make just one pore active at a time. The flux needs to be measured very accurately, because then not only the pressure and flux, but also the number of active pores is known and again R_s can be determined.

Repeated flux measurements with partially covered membrane surface to estimate R_s

If the flux as a function of the transmembrane pressure is measured several times with different levels of coverage of the membrane surface, different flux-pressure curves are obtained. The covering material could for example be a grid with known dimensions. With a metal grid it is also assured that flexible membranes are sufficiently supported. It is assumed that covering the surface only changes the resistance of the unconnected pore layer (R_{up}) and not R_s . This assumption is probably only valid if the pieces that cover the membrane are not

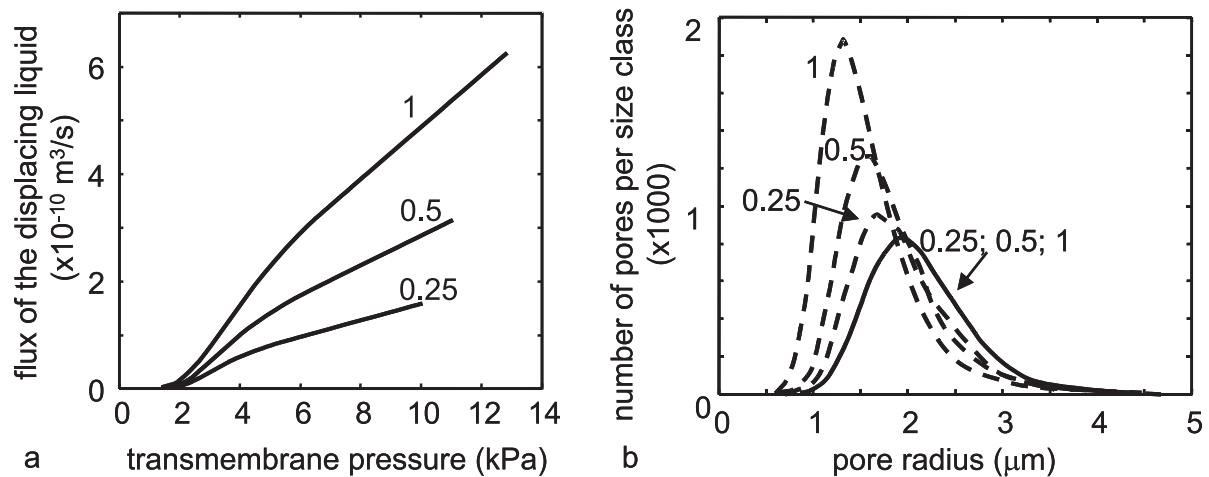
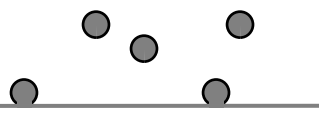


Figure 10: a. flux-pressure curves calculated with the two-layer model for a partially covered membrane surface, with $R_s = 2 \cdot 10^{13} \text{ m}^{-3}$ and further the same data as in Figure 8; b. pore size distributions estimated with the modified liquid displacement method with ($R_s = 0 \text{ m}^{-3}$ (—)) and $R_s = 2 \cdot 10^{13} \text{ m}^{-3}$ (.....), divided by the uncovered fraction. Numbers denote f_{uncov} .

much larger than the average pore radius, because otherwise a lot of fluid has to flow in the transversal direction through the membrane, resulting in pressure loss. Furthermore, it is expected that the shape of the pore size distribution is not changed by partly covering the membrane, while the number of pores will be a fraction of the total number of pores in the unconnected pore layer ($f_{uncov} = \text{uncovered area}/\text{total membrane area}$). If there is no sublayer resistance, the flux-pressure curve obtained by partly covering the membrane surface divided by the uncovered fraction coincides with the flux-pressure curve obtained without covering the membrane surface. The flux-pressure curves with different uncovered membrane surface fractions, calculated for the “membrane” in Figure 8, are shown in Figure 10a. Starting at $R_s = 0 \text{ m}^{-3}$, the pore size distribution can be estimated from this curve by iteratively changing R_s until the ratio of the number of pores of the distributions is equal to the uncovered fraction (Figure 10b). Note that at this R_s ($= 2 \cdot 10^{13} \text{ m}^{-3}$), the pore size distribution curves divided by the uncovered fraction coincide. In reality statistics are essential to determine the best R_s -value.

Conclusion

Determining the pore size distribution with membrane characterization methods using liquid displacement is incorrect if the pores are connected to each other or if there is a resistance against flow in the membrane sublayer or in the measurement apparatus. As a result of the additional resistance, the estimated pore size distribution shifts towards smaller pores and a larger number of pores. To overcome this, two methods are suggested to modify the liquid displacement method: either the sublayer resistance is estimated by determining the number of active pores or by repeated measurement of the flux-pressure curves with different levels of coverage of the membrane surface.



Nomenclature

a	slope	(-)
A_m	membrane area	(m ²)
b	slope	(-)
d_m	membrane thickness	(m)
f_{uncov}	uncovered fraction of the membrane surface	(-)
K	membrane permeability	(m ²)
k	membrane permeability	(kg m s ⁻¹)
l	unconnected pore length	(m)
N	number of pores	(-)
N_{tot}	total number of pores	(-)
n	fraction of active pores	(-)
p_0	pressure in the displaced liquid	(Pa)
p_{in}	disperse phase pressure at the inlet of the system	(Pa)
p_{crit}	critical pressure	(Pa)
$p_{cylinder\ edge}$	pressure at the edge of the cylinder	(Pa)
p_{trm}	transmembrane pressure	(Pa)
$r_{cylinder}$	cylinder radius	(m)
r_p	pore radius	(m)
R_p	pore flow resistance	(m ⁻³)
R_{up}	total resistance of the unconnected pore layer against flow	(m ⁻³)
R_s	sublayer resistance against flow	(m ⁻³)
Y	dimensionless axial coordinate	(-)
δ_m	dimensionless membrane thickness	(-)
ϕ_p	flux of displacing liquid through a pore	(m ³ /s)
ϕ_{up}	flux of displacing liquid through the unconnected pore layer	(m ³ /s)
ϕ_s	total flux of the displacing liquid through the membrane	(m ³ /s)
γ	surface or interfacial tension	(N/m)
η	viscosity	(Pa s)
θ	wall contact angle	(-)
ρ	dimensionless radial coordinate	(-)
ρ_{cyl}	dimensionless cylinder radius	(-)
σ	standard deviation of the pore size distribution	(-)

Reference list

- 1 S.I. Nakao, Determination of Pore Size and Pore Size Distribution 3. Filtration Membranes, *J. Membrane Sci.*, 96 (1994) 131.
- 2 F. Erbe, Die Bestimmung Der Porenverteilung Nach Ihrer Größe in Filtern Und Ultrafiltern, *Kolloid-Zeitschrift*, 63 (1933) 277.
- 3 R.E. Kesting, Characterization, in R.E. Kesting (Ed.), *Synthetic Polymeric Membranes*, McGraw-Hill Book Company, New York, 1971, 12-54.
- 4 G. Capannelli, F. Vigo and S. Munari, Ultrafiltration Membranes - Characterization Methods, *J. Membrane Sci.*, 15 (1983) 289.
- 5 G. Capannelli, I. Becchi, A. Bottino, P. Moretti and S. Munari, Computer driven porosimeter for ultrafiltration membranes, in *Proceedings of the Studies in surface science and catalysis*, 1987, 283.
- 6 I.M. Wienk, B. Folkers, Th. van den Boomgaard and C.A. Smolders, Critical Factors in the Determination of the Pore Size Distribution of Ultrafiltration Membranes Using the Liquid Displacement Method, *Sep. Sci. Technol.*, 29 (1994) 1433.
- 7 W. Piatkiewicz, S. Rosinski, D. Lewinska, J. Bukowski and W. Judycki, Determination of Pore Size Distribution in Hollow Fibre Membranes, *J. Membrane Sci.*, 153 (1999) 91.
- 8 A.M. Vaidya and N.J. Haselberger, A Novel Technique for the Characterization of Asymmetric Membranes by Permoporometry, *Sep. Sci. Technol.*, 29 (1994) 2523.
- 9 S. Munari, A. Bottino, P. Moretti, G. Capannelli and I. Becchi, Permoporometric Study on Ultrafiltration Membranes, *J. Membrane Sci.*, 41 (1989) 69.
- 10 S. Munari, A. Bottino, G. Capannelli and P. Moretti, Membrane Morphology and Transport Properties, *Desalination*, 53 (1985) 11.
- 11 E. Jakobs and W.J. Koros, Ceramic Membrane Characterization Via the Bubble Point Technique, *J. Membrane Sci.*, 124 (1997) 149.
- 12 W. Kujawski, P. Adamczak and A. Narebska, A Fully Automated System for the Determination of Pore Size Distribution in Microfiltration and Ultrafiltration Membranes, *Sep. Sci. Technol.*, 24 (1989) 495.
- 13 P. Mikulášek and P. Dolecek, Characterization of Ceramic Tubular Membranes by Active Pore-Size Distribution, *Sep. Sci. Technol.*, 29 (1994) 1183.
- 14 A. Bottino, G. Capannelli, A. Grosso, O. Monticelli and M. Nicchia, Porosimetric Characterization of Inorganic Membranes, *Sep. Sci. Technol.*, 29 (1994) 985.
- 15 A. Bottino, G. Capannelli, P. Petit-Bon, N. Cao, M. Pegoraro and G. Zoia, Pore Size and Pore-Size Distribution in Microfiltration Membranes, *Sep. Sci. Technol.*, 26 (1991) 1315.
- 16 A.J. Gijsbertsen-Abrahamse, A. van der Padt and R.M. Boom, Membrane emulsification: the influence of pore geometry and wall contact angle on process performance, in *Proceedings of the CME (World Congress on Emulsions) 3*, 24 – 27 September 2002, Lyon, in press.
- 17 Chapter 4, A.J. Gijsbertsen-Abrahamse, A. van der Padt and R.M. Boom, Influence of Membrane Morphology on Pore Activation in Membrane Emulsification, *J. Membrane Sci.*, in press.
- 18 C.C. Ho and A.L. Zydney, Theoretical Analysis of the Effect of Membrane Morphology on Fouling During Microfiltration, *Sep. Sci. Technol.*, 34 (1999) 2461.
- 19 M. Mulder, *Basic Principles of Membrane Technology*, Kluwer Academic Publishers, Dordrecht, 1991.

6 Discussion and outlook for industrial application

Abstract

Cross-flow membrane emulsification has great potential to produce monodisperse emulsions and emulsions with shear sensitive components. However, until now, only low disperse phase fluxes were obtained. A low flux may be a limiting factor for emulsion production on a commercial scale. Therefore, the effects of membrane parameters on the disperse phase flux are estimated. Besides, the effects of these parameters on the droplet size and droplet size distribution are qualitatively described. Wetting properties, pore size and porosity mainly determine the droplet size (distribution). Membrane morphology largely determines the disperse phase flux. As an example, industrial-scale production of culinary cream was chosen to evaluate the required membrane area of different types of membranes: an SPG membrane, an α -Al₂O₃ membrane and a microsieve. Due to the totally different morphologies of these membranes, the fraction of active pores is 1 for a microsieve and is very low for the other membranes. The choice of the optimal membrane did not depend on the production strategy: either to produce large quantities or to produce monodisperse emulsions, the best suitable was a microsieve with an area requirement of around 1 m². In general, the total membrane resistance should be low to obtain a large disperse phase flux. In contrast, the membrane resistance should be high to obtain monodisperse emulsions when using membranes with a high porosity.

This chapter is a part of the paper submitted as: A.J. Gijsbertsen-Abrahamse, A. van der Padt and R.M. Boom, Membrane and pore dimensions for cross-flow membrane emulsification. Part of the section *critical pressure* was published in: A.J. Gijsbertsen-Abrahamse, A. van der Padt and R.M. Boom, Membrane emulsification: the influence of pore geometry and wall contact angle on process performance, in Proceedings of the CME (World Congress on Emulsions) 3, 24 – 27 September 2002, Lyon.

Introduction

Literature shows that cross-flow membrane emulsification has potential to produce monodisperse emulsions, perhaps even nanosized, and emulsions with shear sensitive components with relatively low energy input (see chapter 1). However, a limiting factor for emulsion production on a commercial scale will be a low disperse phase flux [1].

This thesis explores droplet formation (chapters 2 and 3) and disperse phase fluxes (chapters 4 and 5). Based on these studies we discuss the effects of membrane parameters on membrane emulsification performance in this chapter. In Table 1 membranes used for emulsification and some of their characteristics are summarized. The effects on the droplet size (distribution) are described qualitatively, while the effects on the disperse phase flux are discussed in more detail by model calculations. The choice of the optimal membrane, either existing or newly designed, depends on both the required droplet size and the required disperse phase flux, which is illustrated by an example: industrial-scale culinary cream production.

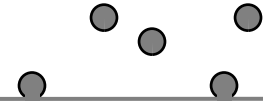
Table 1: Characteristics of membranes used for emulsification (d_p : pore diameter; SD: width of pore size distribution; ε : porosity; d_m : membrane thickness (in case of an asymmetric membrane: thickness of the skin layer)). With references to literature about the characteristics of these membranes and about experiments in which they were used.

membrane	d_p (μm)	SD	ε	wetting ¹	structure ²	d_m (μm)	Ref.
SPG	0.1-18	small	0.5-0.6	W	IS	700-1000	[2-11]
$\alpha\text{-Al}_2\text{O}_3$	0.2-3		0.35	W	IA	20-40	[12-14]
zirconium oxide	0.02-0.1		0.6	W	IA	8	[12, 13]
microsieve	0.2-20	<1%	var.	W	P	0.1-10	[15, 16]
straight through MC ³	17.3	<1%	low	W	P	200	[17]
silicon MC ³	5.8-30	small		W / O	P	~100	[18-26]
PTFE	0.5-5		0.79	W / O	IS	35-75	[3, 27]
polycarbonate	0.05-12	small	0.05-0.2	W	P	10-22	[28, 29]

1. W: wetted by the water phase (hydrophilic); O: wetted by the oil phase (hydrophobic).
2. IS: symmetric membrane with interconnected pores; IA: asymmetric membrane with interconnected pores; P: parallel pores.
3. MC: microchannel; the average pore diameter is expressed as the equivalent diameter [17].

Droplet size (distribution)

Table 1 of the introduction (chapter 1) shows the parameters influencing the droplet size and its distribution. In this section we discuss qualitatively how membrane parameters influence the droplet size. Finally, we summarize which parameters are most important when choosing or designing a membrane for emulsification.



Pore size

The average droplet size is mainly determined by the size of the pore opening. Generally, the pore openings at the membrane surface are not circular, but an equivalent pore diameter can be calculated. Many studies show a linear dependency of the droplet size (d_{dr}) on the pore diameter (d_p):

$$d_{dr} = x d_p \quad (m) \quad (1)$$

in which x is usually between 2 and 10 [1], depending on the ingredients used. To obtain these results, in many cases a minimum cross-flow velocity (or wall shear stress) is required. If this requirement is not met, x can become an order of magnitude larger and the obtained emulsions are more polydisperse. However, Christov *et al.* [5] claim that under specific conditions, theoretically the droplet size should be 3 times the pore size without a cross-flow. In this case, the transmembrane pressure must be very close to the critical pressure of the pores (within 10%) which will yield a very low flux (shown below). Besides, the dynamic wall contact angle should be small, which is discussed in more detail below.

Shape of the pore opening

Kobayashi *et al.* found a ratio of droplet size over pore size of 2, using a silicon membrane with oblong pores and very low cross-flow velocities [17]. This ratio was independent from the cross-flow velocity and the transmembrane pressure. With the same membrane type with circular pores, droplet formation depended on these variables and the droplets obtained were much larger (about 10 times the pore diameter) [17]. Christov *et al.* [5] did their experiments with SPG-membranes, which are made by spinodal decomposition of a mixture of glasses. It may well be that the surface pores have a somewhat oblong shape (see SEM images in [7, 9]). Further study towards the effect of the pore shape could be carried out with microengineered membranes.

Membrane surface porosity

Experiments with a microsieve show that steric hindrance of droplets forming simultaneously results in polydisperse emulsions [15, 28]. Therefore, the surface porosity should be low enough to prevent any hindrance. CFD calculations show that to prevent coalescence or steric hindrance of droplets the porosity should indeed be low (around 1% for a ratio of droplet diameter over pore diameter of 7) [30]. Furthermore, the droplets will be deformed in the direction of flow depending on the cross-flow velocity, thus a larger distance is needed between the pores in the direction of flow than in the direction normal to the flow. Although many experiments were carried out with membranes with a high porosity (SPG, ceramic, see Table 1), probably the droplets did not hinder each other, because the fraction of active pores was low and the obtained droplets were small compared to the pore size [9, 11]. However, it will be necessary to increase the transmembrane pressure, to obtain a disperse phase flux that

makes industrial application feasible. Consequently the fraction of active pores will increase (see section on disperse phase flux), and thus the chance of steric hindrance will increase.

Membrane thickness

The total membrane thickness, or pore length, has an indirect effect on the droplet size obtained. Increasing the effective transmembrane pressure (= transmembrane pressure - critical pressure), may increase the average droplet diameter [31, 32]. This is explained by a changing interfacial tension. On increasing the transmembrane pressure, the disperse phase flux increases. The increased droplet expansion rate may lead to the dynamic interfacial tension to become higher than the equilibrium value. The interfacial tension force thus increases and keeps the droplet attached at the pore until it has reached equilibrium with the detaching forces, which is at a larger droplet size. The membrane thickness is one of the factors determining the expansion rate.

Wall contact angle

In general the membrane should be wetted with the continuous phase to obtain droplets of the disperse phase; hence the wall contact angle (measured in the continuous phase) α_{scd} , should be smaller than 90° . From Young's equation [33] it follows that the wall contact angle (α_{scd}) is a function of the properties of the two immiscible liquids and the solid:

$$\gamma_{sc} - \gamma_{sd} + \gamma_{cd} \cos \alpha_{scd} = 0 \quad \text{or} \quad \cos \alpha_{scd} = \frac{\gamma_{sd} - \gamma_{sc}}{\gamma_{cd}} \quad (2)$$

in which γ_{sd} and γ_{sc} are the interfacial tensions of respectively the boundary solid/disperse phase and the boundary solid/continuous phase; γ_{cd} is the interfacial tension between the two liquid phases. The interfacial tensions between the liquids and the solid may be different for different emulsifiers. The interfacial tension between the two liquids largely depends on the expansion rate of the forming interface, determined by the disperse phase flux, and depends on the concentration and type of emulsifier (see e.g. [28, 34]). The lower the interfacial tension between the two liquid phases, the smaller the wall contact angle.

To investigate the effect of the wall contact angle on droplet formation, we simulated droplet formation at a single pore with varying wall contact angles ($\alpha_{swo} = 0, 30$ or 60° , cross-flow velocity 2 m/s; geometry and other parameters as in [30]; simulated with CFX 4.3). In Figure 1 it is shown that the droplet spreads over the membrane surface at a wall contact angle of 60° , which is considerably smaller than the earlier mentioned 90° , above which spreading is expected to occur. This can be explained by the fact that the cross-flowing continuous phase deforms the droplet towards the membrane surface.

The wetting properties of the membrane can be manipulated by pre-soaking the membrane in the continuous phase. In this way even water-in-oil emulsions were made with an originally hydrophilic SPG membrane [6]. However, it is not known for what period of time the wall contact angle will remain constant with this method. For practical application, it would be

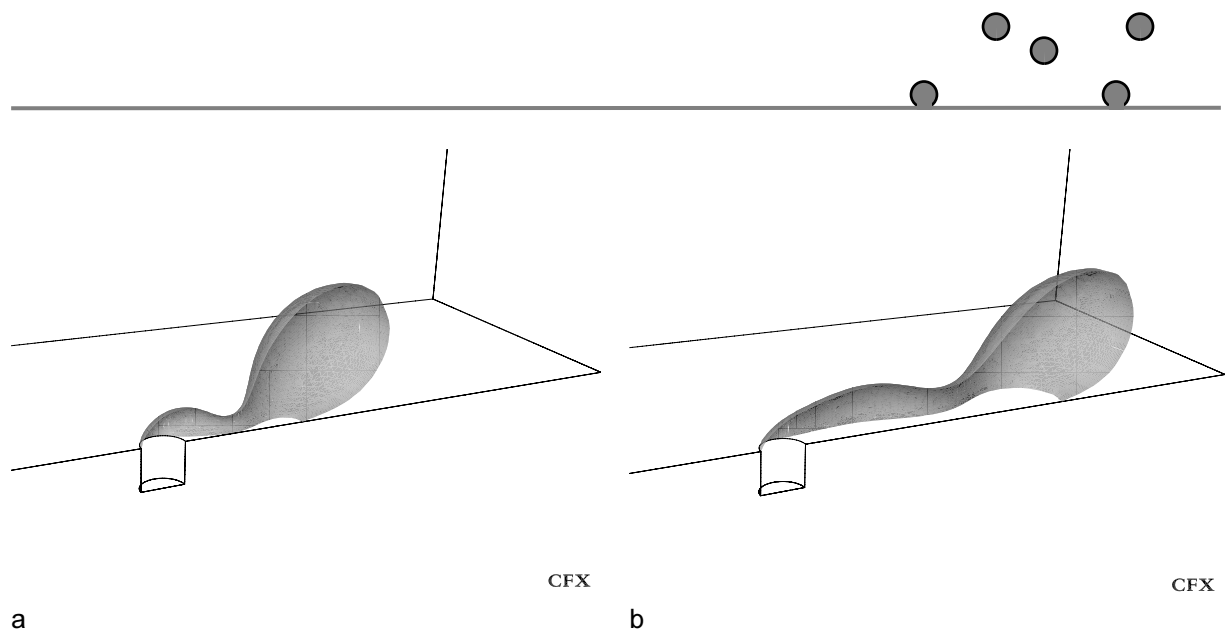


Figure 1: Droplet deformation calculated with CFD. a: wall contact angle 30° , after $180 \mu\text{s}$; b: wall contact angle 60° , after $322 \mu\text{s}$.

preferable to covalently modify the membrane surface. For example, an SPG membrane could be made hydrophobic by a silicone coupler reagent [10] and microchannels were modified with several silicone coupler reagents, resulting in wall contact angles between 46 and 124° depending on the continuous and disperse phases [18, 20]. Note that to prevent fouling and changes in the wall contact angle, emulsifier molecules should not adsorb to a large extent to the membrane surface.

Summary

When choosing or designing a membrane for emulsification, the most important characteristics affecting the droplet size (distribution) are the wall contact angle, which should be as low as possible, and the average pore size, which can be estimated from the required emulsion droplet size and a value for x . From the ratio of droplet diameter over pore diameter (x) the maximum allowable porosity can be calculated, yet, it is more useful to take the fraction of active pores into account (next section). When optimizing the membrane and the applied transmembrane pressure for high disperse phase fluxes, it should be kept in mind that the membrane structure affects the droplet formation time, which may affect the droplet size.

Disperse phase flux

In this section the effects of membrane parameters on the flux of the to-be-dispersed phase (in this chapter called the disperse phase flux) are discussed. The disperse phase flux is determined by the critical pressure and the membrane resistance [35], which is described in the next sections. At the end of this section equations to calculate the required membrane area as a function of the transmembrane pressure are derived.

Critical pressure

Both pore size and wetting properties affect the critical pressure of a pore. The minimum pressure difference over a pore, necessary to start producing droplets from that pore, is called the critical pressure. When the contact angle is smaller than 90° , the critical pressure does not depend on the contact angle for a pore with sharp edges, and can be calculated with the Laplace equation (Figure 2):

$$p_{crit} = \gamma \left(\frac{2}{d_1} + \frac{2}{d_2} \right) \quad (\text{Pa}) \quad (3)$$

in which d_1 and d_2 are the diameters of the pore in two directions perpendicular to each other. Thus, the critical pressure of each pore is inversely proportional with its diameter (d_p). This directly shows that in a membrane with uniform pores with sharp edges, all the pores should become active at the same transmembrane pressure. This was not at all the case in experiments with a microsieve (standard deviation of the pore size was less than 1% [15, 16]) or in microchannel emulsification experiments [17, 37], which could be explained by the presence of a membrane substructure resistance (discussed below). Of course, in a membrane with a pore size distribution, the critical pressures also depend on the width of the distribution.

The wetting properties of an individual pore do not affect the critical pressure of that pore if it has straight edges. However, the contact angle does affect the critical pressure in the case the pore edges are rounded. We did two-dimensional, two phase computational fluid dynamic (CFD) simulations to quantify the effect of the wall contact angle on the critical pressure. For that purpose we used CFX 4.3, in which we modeled the pore as shown in Figure 3. In this Figure also the boundary types are given. The physical parameters of the two phases had the same values as in [30]. We varied the wall contact angle between 0 and 90° and varied the pressure at pressure boundary 1 (Figure 3). In Figure 4 the results are shown: at a pressure

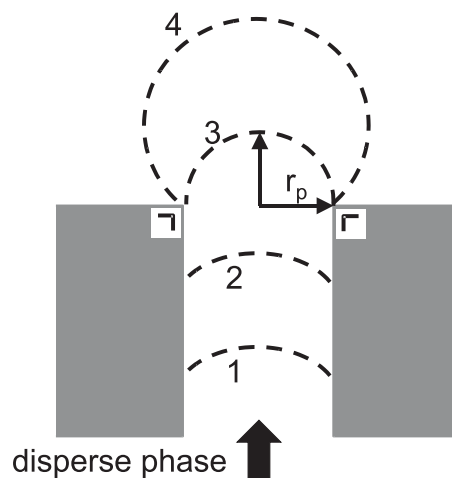


Figure 2: Droplet formation at several stages of time (schematically) at a pore with sharp edges. The critical pressure (eq. 3) is the pressure inside the hemispherical droplet at stage 3.

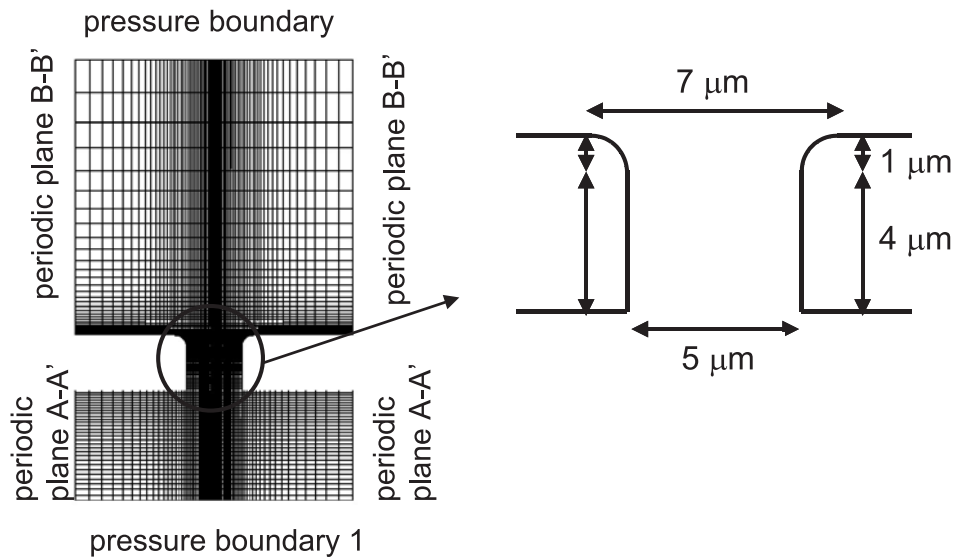


Figure 3: Geometry (pore with rounded edges) used in 2D CFD calculations.

above 11 kPa, at all wall contact angle values the oil-water interface was moved through the pore by the flowing disperse phase to form a 2D-droplet (o). With small contact angles and lower pressures, the interface reached a steady state in the pore (-). In some cases a steady state was not reached: on average (over a few 100 time steps) the interface remained at the same place, but the interface shape was not constant (□). When the wall contact angle was close to 90°, the critical pressure of the pore was determined by the diameter of the (2D) pore opening $p_{crit} = 2\gamma/d_p = 2 \times 30 \cdot 10^{-3} / 7 \cdot 10^{-6} = 8.6$ kPa. With a wall contact angle of 0°, the pressure at which a droplet was formed (11 kPa) was lower than the critical pressure expected for a pore with a diameter of 5 μm (12 kPa). This may have resulted from the difficulties in defining the (rectangular) grid at the (rounded) edges. Altogether, the wetting properties of the pores have a slight effect on the critical pressure, but only when the size of the pore

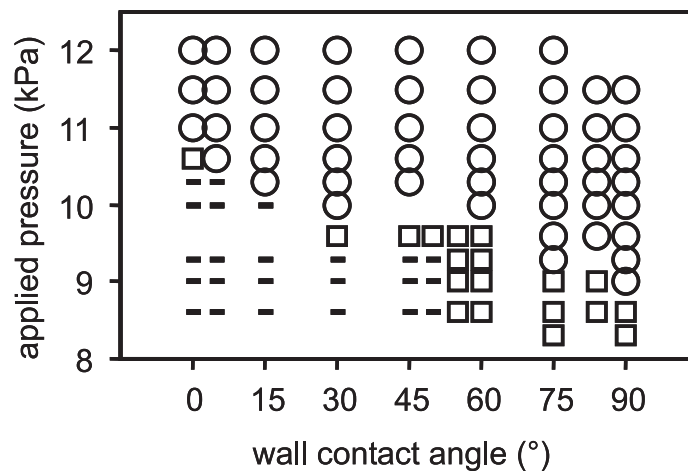


Figure 4: Results of 2D CFD calculations with different wall contact angles and transmembrane pressures (o: 2D-droplet formation at that condition; -: interface steady state; □: ambiguous).

opening differs from the smallest pore size. In this 2D geometry, the decrease in critical pressure is 20% at maximum. For a cylindrical pore (3D) with the same dimensions, we assume the critical pressures to be a factor of 2 larger than calculated for the 2D geometry. Hence, the decrease in critical pressure due to differences in wetting conditions in a 3D geometry will also be 20% at maximum. In membranes produced by certain methods (e.g. sintering of spheres of the membrane material) it can be expected that the size of the pore opening differs from the average of the pore radius, but it is not very likely that the wetting conditions differ much between separate pores. Thus, pores with approximately the same diameter will have comparable critical pressures, which can be estimated without taking the wall contact angle into account. Furthermore, a variation of 20% (or even less) affects the estimation of the required membrane area only very slightly if the applied transmembrane pressure is much larger than the critical pressure. This can be established from equation 11a (shown below).

Membrane resistance

In most cases the disperse phase flux through the membrane can be described using two hydrodynamic resistance parameters: R_s being the resistance of the membrane substructure or sublayer and R_{up} the resistance against flow of the unconnected (upper) pore layer [35, 36]. In Table 2 the equations are given to estimate the values of R_s and R_{up} for two different membrane structure types. We assume that either the membrane consists of a layer with parallel pores with a certain support structure below it, or that the membrane has interconnected pores. Microsieves and silicon microchannels are examples of the first type (Table 1). Many other membranes fall in the second category: either the whole membrane is symmetric, as is the case in SPG membranes, or the membrane is asymmetric, with a skin

Table 2: Equations to estimate the resistance of the sublayer (R_s) and the resistance of the unconnected pore layer (R_{up}) depending on the membrane structure [35, 36]. Symbols are explained in the section nomenclature.

membrane type ^a	R_s (m ⁻³)	R_{up} (m ⁻³)
P [35]	^b	$R_{up} = \frac{1}{N_{tot}} \left(\frac{8l_p}{\pi r_p^4} + \frac{3}{r_p^3} \right) \left(1 - \sum_{i=1}^{\infty} a_i \kappa^{i+\frac{1}{2}} \right)^c$ (4)
IS / IA [36]	$R_s = \frac{d_m}{A_m K b}$ ^d (5)	$R_{up} = \frac{R_s a r_p}{d_m}$ ^d (6)

a. P: parallel pores; IS: symmetric membrane with interconnected pores; IA: asymmetric membrane with interconnected pores; see Table 1.

b. depending on membrane design, see comments in text.

c. for equally sized cylindrical pores and laminar flow; with $a_1 = 0.344$, $a_2 = 0.111$ and $a_3 = 0.066$ [16].

d. 1 (thick membrane) $< a < 2$ (very thin membrane); $b = 1$ if $d_m/r_p > 10$ [36].

layer having interconnected pores, e.g. ceramic membranes.

In the case of microsieves, R_s depends on the design of the substructure. That structure may be very open [16]. However, since the value of R_{up} in these membranes can be very low, the resistance of the substructure may still be quite important [35]. When using microsieves with a small pore diameter and an emulsifier with a high equilibrium interfacial tension, transmembrane pressures of several bars are needed. To prevent rupture, a dense support structure is necessary, resulting in a higher R_s [38].

The sublayer resistance of a membrane with interconnected pores can be estimated with equation 5. The fact that b in that equation approaches 1, actually implies that the value of R_s is very close to the total membrane resistance (R_m , unit: m^{-1}). The total membrane resistance can either be estimated with the Carman-Kozeny equation, or determined experimentally. The experimentally determined R_m , by measuring the clean water flux of an SPG membrane with $d_p = 5 \mu m$, $d_m = 0.7 mm$ and $\varepsilon = 0.6$, was $3.2 \cdot 10^9 m^{-1}$ [11]. This is in close agreement with the calculation of R_m with the Carman-Kozeny equation:

$$R_s (A_m = 1) \approx \frac{d_m}{K} = R_m = \frac{C(1-\varepsilon)^2 S_m^2 d_m}{\varepsilon^3} = 1.5 \cdot 10^9 m^{-1} \quad (7)$$

with $C = 2$ for membranes with uniform cylindrical pores and $S_m = 2\varepsilon/(r_p(1-\varepsilon))$ [39].

Required membrane area

In this section equations to calculate the required membrane area are given for membranes with equally sized pores. For membranes with a pore size distribution, it is not possible to give analytical equations, however, the general idea will be the same. From Darcy's law and the balance of flow through the two separate layers in the two-layer model, the following equations were derived to estimate the disperse phase flux [35]:

$$\phi_s = \frac{p_{trm} - p_{crit}}{\eta R_s} \text{ for } N < N_{tot} \equiv n < 1 \quad (m^3/s) \quad (8a)$$

$$\phi_s = \frac{p_{trm}}{\eta(R_{up} + R_s)} \text{ for } N = N_{tot} \equiv n = 1 \quad (m^3/s) \quad (8b)$$

with p_{trm} is the transmembrane pressure, N_{tot} is the total number of pores and n is the fraction of active pores (N/N_{tot}). The fraction of active pores is a function of the ratio of the resistances R_{up} and R_s and of the dimensionless transmembrane pressure:

$$n = \frac{R_{up}}{R_s} \left(\frac{p_{trm}}{p_{crit}} - 1 \right) \text{ for } n < 1 \quad (-) \quad (9)$$

Substituting $n = 1$ in equation 9 gives the dimensionless transmembrane pressure at which just all the pores are active:

$$\frac{p_{trm}}{p_{crit}} = \frac{R_s}{R_{up}} + 1 \quad (-) \quad (10)$$

To calculate the membrane area required to produce a certain amount of emulsion per unit of time, we make use of the fact that both R_{up} and R_s scale with the membrane area (A_m) used. $R_i A_m = \text{constant}$: $R_i = R_i' / A_m$ in which R_i' is the resistance of the sublayer (index $i = s$) or the resistance of the unconnected pore layer ($i = up$) of a membrane piece of 1 m². Using equations 8 and 10, we derive:

$$A_m = \frac{\eta \phi_s R_s'}{P_{crit}} \left(\frac{P_{trm}}{P_{crit}} - 1 \right)^{-1} \quad \text{for } \frac{P_{trm}}{P_{crit}} < \frac{R_s'}{R_{up}'} + 1, \quad (\text{m}^2) \quad (11a)$$

$$A_m = \frac{\eta \phi_s (R_s' + R_{up}')}{P_{crit}} \left(\frac{P_{trm}}{P_{crit}} \right)^{-1} \quad \text{for } \frac{P_{trm}}{P_{crit}} \geq \frac{R_s'}{R_{up}'} + 1 \quad (\text{m}^2) \quad (11b)$$

These equations are used below to estimate the membrane area required of different membranes.

Outlook for industrial application

Technologically, the choice of the optimal membrane, either existing or newly designed, depends on both the required droplet size and the required disperse phase flux. To determine which membrane is most suitable, there may be different criteria, depending on the aim of the emulsion production. The following strategies are discussed below:

1. minimize the membrane area;
2. minimize the standard deviation of the droplet size distribution;
3. ensure a stable operation of the process.

First, the implications of these strategies are illustrated by an example and secondly, membrane choice and optimization are generalized.

Case: culinary cream production

The requirements for culinary cream production are: a droplet size between 1 and 3 μm and a production volume of 20 m³/h containing 30% disperse phase. We assume the viscosity of the milk fat to be 22·10⁻³ Pas at an emulsification temperature of 50 °C. Milk proteins are used as emulsifiers in the continuous phase. The equilibrium interfacial tension is assumed to be 25·10⁻³ N/m. The disperse phase is oil, so a hydrophilic membrane should be used. Either SPG, α-Al₂O₃ membranes or a microsieve can be used. To produce droplets with a diameter of 1 – 2 μm, an average pore diameter of 0.2 μm would probably be appropriate (equation 1, assuming $x = 5 - 10$). Note that this pore diameter is (almost) the smallest possible with these membrane types. Actually, to be able to produce the required droplet size, the cross-flow velocity should be chosen sufficiently high. The necessary parameters to calculate the required membrane area are given and explained in Table 3. For the microsieve we can choose the porosity. To prevent steric hindrance of droplets, the porosity should be 0.01 with

Table 3: Parameters of the membranes suitable for culinary cream production (d_p : pore diameter; SD: standard deviation of the log-normal pore size distribution; ε : porosity; d_m : membrane thickness; R_s' : sublayer resistance; R_{up}' : unconnected pore layer resistance).

code in Figure 5	membrane type	d_p (μm)	SD (μm)	ε (-)	d_m (μm)	R_s' (10^9 m^{-1})	R_{up}' (10^9 m^{-1})
SPG	SPG	0.2	0	0.6	700	1400 ^c	0.2 ^f
A11	$\alpha\text{-Al}_2\text{O}_3$	0.2	0	0.35	30	70 ^d	0.3 ^f
A12	$\alpha\text{-Al}_2\text{O}_3$	0.2	0.1	0.35	30	70 ^d	0.3 ^f
A13	$\alpha\text{-Al}_2\text{O}_3$	0.2	0.25	0.35	30	70 ^d	0.3 ^f
m1	microsieve	0.2	0	0.01 ^a	0.2 ^b	3.5 ^e	25 ^g
m2	microsieve	0.2	0	0.01 ^a	0.2 ^b	3.5 ^e	125 ^h

- $\varepsilon = 0.25\pi(d_p/d_{dr})^2 = 8 \cdot 10^{-3} \approx 1 \cdot 10^{-2}$ assuming a square array of pores.
- a thickness of 0.2 μm is chosen, because, as a rule, the thickness of the membrane and the pore size are of the same order of magnitude.
- with $R_m = 0.056d_p^{-2}$ [11].
- estimated with equation 7 under the assumption that only the skin layer adds to R_s .
- estimated with data in [35]: $R_s' = R_s A_m = 10.8 \cdot 10^{16} \times 3.24 \cdot 10^{-8} = 3.5 \cdot 10^9 \text{ m}^{-1}$.
- with equation 6.
- with equation 4 (cylindrical pores).
- Because of the discrepancy of equation 4 with experimental results [35] with a factor 5, the R_{up}' of "m1" is multiplied by 5.

the assumed value of x . That's why the resistance of the unconnected pore layer of the microsieve is much larger than that of the other membranes having a much higher porosity.

Figure 5a shows the membrane area required for the mentioned culinary cream production for the three different membrane types assuming equally sized cylindrical pores, calculated with equation 11. Furthermore, the area required of an $\alpha\text{-Al}_2\text{O}_3$ membrane was calculated for two log-normal pore size distributions with different standard deviations (0.1 and 0.25), using the equations in [36]. In Figure 5b the fraction of active pores, calculated with equation 9, is shown to be totally different for the three membranes due to the different ratios R_{up}'/R_s . The percentage of active pores in the SPG membrane even remains below 0.1%. The low fraction of active pores using the $\alpha\text{-Al}_2\text{O}_3$ or the SPG membrane, makes the assumption of equally sized pores more acceptable. However, from the results of the $\alpha\text{-Al}_2\text{O}_3$ membrane with pore size distributions (A12 and A13; Table 3 and Figure 5a) it can be concluded that only pores larger than the average pore diameter will be active.

Note that the transmembrane pressure ranges up to $25 \cdot 10^5 \text{ Pa}$ in Figure 5. Tests should reveal whether the membranes can cope with this pressure. Due to the thickness of the SPG membrane, it can withstand much larger pressures [2, 7]; the microsieve can probably be designed in such a way that rupture can be prevented, but this still has to be realised.

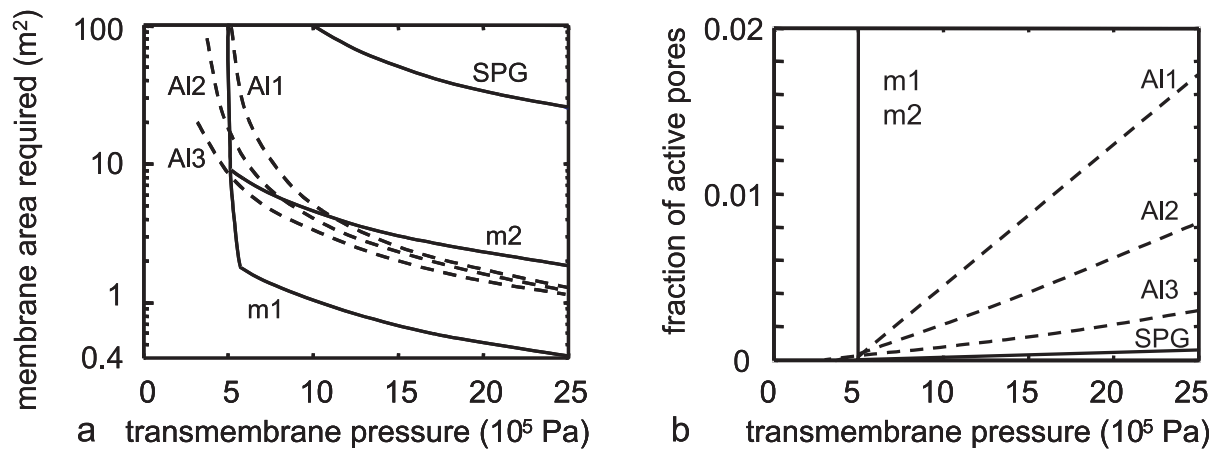
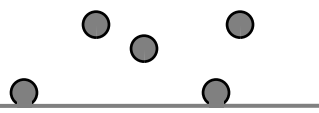


Figure 5: a. Membrane area required to produce culinary cream ($20 \text{ m}^3/\text{h}$ with 30% disperse phase) with different membranes (Table 3) as a function of the transmembrane pressure. b. Fraction of active pores as a function of the transmembrane pressure.

The implications of the three different strategies mentioned above will now be discussed:

1. If minimizing the membrane area is the main requirement and the monodispersity of the droplet size distribution is not so much an issue, then the best choice would probably be a microsieve with an area of around 1 m^2 . Because the criterion of “no steric hindrance” is not so strict in this case, also a microsieve with a higher porosity could be used. Because R_{up} will be lower then, even a smaller area would be needed.
2. Minimize the standard deviation of the droplet size distribution. This could be achieved by using a membrane in which the active pores are far enough away from each other and in which the pores are equally sized. Both a pore size distribution and touching of simultaneously growing droplets result in emulsions which are more or less polydisperse [15, 28]. The smallest pore size distribution is present in the microsieve and its porosity was chosen to be low enough to prevent steric hindrance, which makes it the preferred membrane.
3. Ensure a stable operation of the process. A stable operation implies that the same droplet size is obtained even if the transmembrane pressure varies a little. However, probably the transmembrane pressure can be controlled within $0.1 \cdot 10^5 \text{ Pa}$. Such a pressure difference will hardly affect the emulsification in this case. Thus, the best choice would be to use the membrane with the smallest area required, again the microsieve.

A few remarks: microsieves with a pore diameter of $0.2 \text{ }\mu\text{m}$ having the desired properties (thickness, mechanical stability) do not yet exist, even though their realisation seems possible. Therefore, the conclusions may change depending on the exact specifications of newly designed membranes. Furthermore, after the choice of a membrane, the membrane module and emulsification set-up should be designed in such a way that the conditions (e.g. the continuous and disperse phase pressures) do not vary in the set-up. Additionally, the disperse



phase content probably has to be controlled by recirculation of the continuous phase. Of course, for commercial production the cost and life span of the membranes and the cost of modules and additional equipment should be compared. E.g. if a microsieve is more than roughly 5 times as expensive as an α -Al₂O₃ membrane per m², it may be cheaper to use an α -Al₂O₃ membrane of which a larger surface area is required (under the condition that the life spans of these membranes are comparable). The life span of the membranes will be restricted by the resistance against fouling and cleaning agents. These factors are outside the scope of this chapter.

Membrane choice and optimization

In this section we discuss how the membranes can be optimized for emulsification. Equation 11 shows that the required membrane area is determined by R_s' if not all pores are active, and by the total membrane resistance ($R_s' + R_{up}'$) if all pores are active. For membranes with interconnected pores, like the SPG and the α -Al₂O₃ membrane, the membrane resistance is mainly determined by R_s' . Therefore, to decrease the required membrane area, R_s' should be reduced. For a given pore size, this can be done by increasing the membrane porosity or by decreasing the membrane thickness. Due to the production methods of SPG and α -Al₂O₃ membranes it is not possible to choose the porosity independently. In case of an α -Al₂O₃ membrane decreasing the thickness implies decreasing the thickness of the skin layer. The resistance of the SPG membrane may be reduced considerably by developing an asymmetric SPG membrane, or just by decreasing the thickness of the membrane. The last measure may be feasible for pore sizes in the range of micrometers, when the transmembrane pressures needed are low. From Table 3 it seems that in microsieves R_{up}' is most important. With increasing pore diameter, R_{up}' decreases according to equation 4. Logically, R_s' may decrease along with R_{up}' , because with larger pore sizes a less dense substructure is needed. So, a balance between the strength of the toplayer, strength of the substructure and the sum of both resistances should be found to obtain a maximum disperse phase flux. Design of the pore shape can reduce the resistance in two ways: either the pore diameter may vary through the upper layer of the microsieve; or the shape of the pore opening can be changed from circular to rectangular. As mentioned before with oblonged (rectangular) pore openings x was 2. Because of that, the same droplet size could possibly be produced with larger pores and a higher porosity. This reduces R_{up}' considerably.

With regard to minimizing the standard deviation of the droplet size distribution, the membrane surface porosity should be low. Presumably, SPG and α -Al₂O₃ membranes with a sufficiently low porosity (< 0.05) cannot be developed. Therefore, the fraction of active pores should be low for these membranes with a high porosity. Hence, the ratio of R_{up}'/R_s' should be small (eq. 9), meaning that the ratio of d_m/r_p should be large (eq. 6). Consequently, R_s' should be large to obtain a monodisperse emulsion, while R_s' should be as small as possible to

obtain a high flux. For this reason it is very important to determine the technological strategy before choosing and designing the membrane.

When using a microsieve or straight-through microchannel, stable operation can be achieved when $n < 1$ [17], because then the pressure under the pores always equals the critical pressure [35]. An increase in pressure only results in a larger number of active pores and not in a higher flux through each pore individually. This effect is especially important if the pore size is large (around 5 μm), because then the transmembrane pressure applied will be quite low, which makes it more difficult to control.

Although the required disperse phase flux and the ingredients properties (disperse phase viscosity and interfacial tension) have great impact on the membrane area required, they do not favor one membrane above the others.

Concluding remarks

The cross-flow membrane emulsification process has potential to produce: 1. monodisperse emulsions; 2. emulsions with shear sensitive components; 3. nanosize droplets with low energy requirements. Membrane characteristics can have a marked influence on emulsification performance. The morphology of the membrane largely determines the disperse phase flux; wetting properties, pore size, porosity and probably pore shape mainly determine the obtained average droplet size and the droplet size distribution. When designing or choosing a membrane, the pore size should be chosen such that the required droplet sizes are obtained; the necessary membrane area to obtain the required disperse phase flux may depend on the choice of either minimizing the membrane area, minimizing the droplet standard deviation or enabling a stable process operation. For industrial-scale production of culinary cream a microsieve with a low porosity is the best suitable membrane in all cases.

Nomenclature

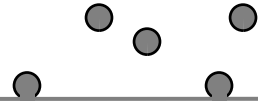
A_m	membrane area	(m^2)
a	slope	(-)
b	slope	(-)
C	constant	(-)
d_{dr}	droplet diameter	(m)
d_m	membrane thickness	(m)
d_p	pore diameter	(m)
K	membrane permeability	(m^2)
l_p	pore length	(m)
N	number of pores	(-)
N_{tot}	total number of pores	(-)
n	fraction of active pores	(-)
p_{crit}	critical pressure	(Pa)

p_{trm}	transmembrane pressure	(Pa)
R_m	membrane resistance	(m^{-1})
R_{up}	total resistance of the unconnected pore layer against flow	(m^{-3})
R_{up}'	total resistance of the unconnected pore layer against flow	(m^{-1})
R_s	sublayer resistance against flow	(m^{-3})
R_s'	sublayer resistance against flow	(m^{-1})
r_p	pore radius	(m)
S_m	pore surface area over solids volume	(m^{-1})
x	ratio of droplet diameter over pore diameter	(-)
α	wall contact angle	($^{\circ}$)
ε	membrane surface porosity	(-)
γ	interfacial tension	(N/m)
ϕ_s	total flux of disperse phase through the system	(m^3/s)
η	viscosity	(Pa s)
κ	product of fraction of active pores and porosity	(-)

Reference list

- 1 S.M. Joscelyne and G. Trägårdh, Membrane Emulsification - a Literature Review, J. Membrane Sci., 169 (2000) 107.
- 2 T. Nakashima, Porous Glass Material and its Recent Application, Review 1989, in Proceedings of the 38th SPG Forum, International: Membrane and Particle Science and Technology in Food and Medical Care, (2002) 108.
- 3 N. Yamazaki, H. Yuyama, M. Nagai, G.H. Ma and S. Omi, A Comparison of Membrane Emulsification Obtained Using SPG (Shirasu Porous Glass) and PTFE [Poly(Tetrafluoroethylene)] Membranes, J. Dispersion Sci. Technol., 23 (2002) 279.
- 4 J.O. You, S.B. Park, H.Y. Park, S. Haam, C.H. Chung and W.S. Kim, Preparation of Regular Sized Ca-Alginate Microspheres Using Membrane Emulsification Method, J. Microencapsulation, 18 (2001) 521.
- 5 N.C. Christov, D.N. Ganchev, N.D. Vassileva, N.D. Denkov, K.D. Danov and P.A. Kralchevsky, Capillary Mechanisms in Membrane Emulsification: Oil-in-Water Emulsions Stabilized by Tween 20 and Milk Proteins, Coll. Surfaces A: Physicochemical Eng. Aspects, 209 (2002) 83.
- 6 R. Katoh, Y. Asano, A. Furuya, K. Sotoyama and M. Tomita, Preparation of Food Emulsions Using a Membrane Emulsification System, J. Membrane Sci., 113 (1996) 131.
- 7 T. Nakashima, M. Shimizu and M. Kukizaki, Particle Control of Emulsion by Membrane Emulsification and Its Applications, Adv. Drug Delivery Rev., 45 (2000) 47.
- 8 A. Supsakulchai, G.H. Ma, M. Nagai and S. Omi, Uniform Titanium Dioxide (TiO₂) Microcapsules Prepared by Glass Membrane Emulsification With Subsequent Solvent Evaporation, J. Microencapsulation, 19 (2002) 425.
- 9 H. Yuyama, T. Watanabe, G.H. Ma, M. Nagai and S. Omi, Preparation and Analysis of Uniform Emulsion Droplets Using SPG Membrane Emulsification Technique, Coll. Surfaces A: Physicochemical Eng. Aspects, 168 (2000) 159.
- 10 T. Fuchigami, M. Toki and K. Nakanishi, Membrane Emulsification Using Sol-Gel Derived Macroporous Silica Glass, J. Sol-Gel Sci. Tech., 19 (2000) 337.

- 11 G.T. Vladislavjevic and H. Schubert, Preparation and Analysis of Oil-in-Water Emulsions With a Narrow Droplet Size Distribution Using Shirasu-Porous-Glass (SPG) Membranes, *Desalination*, 144 (2002) 167.
- 12 V. Schröder, Herstellen von Öl-in-Wasser-Emulsionen mit Mikroporösen Membranen, PhD thesis, Technische Hochschule Karlsruhe, 1999.
- 13 S.M. Joscelyne and G. Trägårdh, Food Emulsions Using Membrane Emulsification: Conditions for Producing Small Droplets, *J. Food Eng.*, 39 (1999) 59.
- 14 R.A. Williams, S.J. Peng, D.A. Wheeler, N.C. Morley, D. Taylor, M. Whalley and D.W. Houldsworth, Controlled Production of Emulsions Using a Crossflow Membrane. Part II: Industrial Scale Manufacture, *Trans. Inst. Chem. Eng.*, 76 (1998) 902.
- 15 Chapter 3, published as: A.J. Abrahamse, R. van Lierop, R.G.M. van der Sman, A. van der Padt and R.M. Boom, Analysis of Droplet Formation and Interactions During Cross-Flow Membrane Emulsification, *J. Membrane Sci.*, 204 (2002) 125.
- 16 C.J.M. van Rijn and M.C. Elwenspoek, Micro Filtration Membrane Sieve With Silicon Micro Machining for Industrial and Biomedical Applications, *Proc. IEEE*, 83 (1995) 83.
- 17 I. Kobayashi, M. Nakajima, K. Chun, Y. Kikuchi and H. Fujita, Silicon Array of Elongated Through-Holes for Monodisperse Emulsion Droplets, *AIChE Journal*, 48 (2002) 1639.
- 18 T. Kawakatsu, Y. Kikuchi and M. Nakajima, Regular-Sized Cell Creation in Microchannel Emulsification by Visual Microprocessing Method, *J. Am. Oil Chem. Soc.*, 74 (1997) 317.
- 19 T. Kawakatsu, G. Trägårdh, Y. Kikuchi, M. Nakajima, H. Komori and T. Yonemoto, Effect of Microchannel Structure on Droplet Size During Crossflow Microchannel Emulsification, *J. Surf. Det.*, 3 (2000) 295.
- 20 T. Kawakatsu, G. Trägårdh, Ch. Trägårdh, M. Nakajima, N. Oda and T. Yonemoto, The Effect of the Hydrophobicity of Microchannels and Components in Water and Oil Phases on Droplet Formation in Microchannel Water-in-Oil Emulsification, *Coll. Surfaces A: Physicochemical Eng. Aspects*, 179 (2001) 29.
- 21 I. Kobayashi, M. Nakajima, J. Tong, T. Kawakatsu, H. Nabetani, Y. Kikuchi, A. Shono and K. Satoh, Production and Characterization of Monodispersed Oil-in-Water Microspheres Using Microchannels, *Food Sci. Technol. Res.*, 5 (1999) 350.
- 22 T. Kawakatsu, H. Komori, M. Nakajima, Y. Kikuchi and T. Yonemoto, Production of Monodispersed Oil-in-Water Emulsion Using Crossflow-Type Silicon Microchannel Plate, *J. Chem. Eng. Jpn.*, 32 (1999) 241.
- 23 J. Tong, M. Nakajima and H. Nabetani, Preparation of Phospholipid Oil-in-Water Microspheres by Microchannel Emulsification Technique, *Eur. J. Lipid Sci. Technol.*, 104 (2002) 216.
- 24 S. Sugiura, M. Nakajima and M. Seki, Prediction of Droplet Diameter for Microchannel Emulsification, *Langmuir*, 18 (2002) 3854.
- 25 S. Sugiura, M. Nakajima, N. Kumazawa, S. Iwamoto and M. Seki, Characterization of Spontaneous Transformation-Based Droplet Formation During Microchannel Emulsification, *J. Physical Chem. B*, 106 (2002) 9405.
- 26 S. Sugiura, M. Nakajima and M. Seki, Preparation of Monodispersed Polymeric Microspheres Over 50 μm Employing Microchannel Emulsification, *Ind. Eng. Chem. Res.*, 41 (2002) 4043.
- 27 K. Suzuki, I. Fujiki and Y. Hagura, Preparation of Corn Oil/Water and Water/Corn Oil Emulsions Using PTFE Membranes, *Food Sci. Technol. Int. Tokyo*, 4 (1998) 164.
- 28 I. Kobayashi, M. Yasuno, S. Iwamoto, A. Shono, K. Satoh and M. Nakajima, Microscopic Observation of Emulsion Droplet Formation From a Polycarbonate Membrane, *Coll. Surfaces A: Physicochemical Eng. Aspects*, 207 (2002) 185.
- 29 Millipore catalogue: www.millipore.com/catalogue.nsf/home, (2002).
- 30 Chapter 2, published as: A.J. Abrahamse, A. van der Padt, R.M. Boom and W.B.C. de Heij, Process Fundamentals of Membrane Emulsification: Simulation with CFD, *AIChE Journal*, 47 (2001) 1285.



- 31 V. Schröder, M. Stang and H. Schubert, Emulgieren mit Mikroporösen Membranen, Lebensmittel- und Verpackungstechnik, 43 (1998) 80.
- 32 S.J. Peng and R.A. Williams, Controlled Production of Emulsions Using a Crossflow Membrane. Part I: Droplet Formation From a Single Pore, Trans. Inst. Chem. Eng., 76 (1998) 894.
- 33 A.W. Adamson and A.P. Gast, Physical Chemistry of Surfaces, John Wiley & Sons, Inc., Toronto, 1997.
- 34 J. Tong, M. Nakajima, H. Nabetani and Y. Kikuchi, Surfactant Effect on Production of Monodispersed Microspheres by Microchannel Emulsification Method, J. Surf. Det., 3 (2000) 285.
- 35 Chapter 4, A.J. Gijsbertsen-Abrahamse, A. van der Padt and R.M. Boom, Influence of Membrane Morphology on Pore Activation in Membrane Emulsification, J. Membrane Sci., in press.
- 36 Chapter 5, submitted as: A.J. Gijsbertsen-Abrahamse, A. van der Padt and R.M. Boom, Why Liquid Displacement Methods Are Often Wrong in Estimation the Pore Size Distribution.
- 37 S. Sugiura, M. Nakajima, J. Tong, H. Nabetani and M. Seki, Preparation of Monodispersed Solid Lipid Microspheres Using a Microchannel Emulsification Technique, J. Colloid Interface Sci., 227 (2000) 95.
- 38 C.J.M. van Rijn, M. van der Wekken, W. Nijdam and M. Elwenspoek, Deflection and Maximum Load of Microfiltration Membrane Sieves Made with Silicon Micromachining, J. Microelectromech. Syst., 6 (1997) 48.
- 39 W.S.W. Ho and K.K. Sirkar, Membrane Handbook, Van Nostrand Reinhold, New York, 1992.



Summary

Emulsions are widely used in foods, pharmaceuticals, cosmetics, paints, agents for crop protection and bitumen. They are produced on a large scale with rotor-stator systems, colloid mills and high-pressure homogenizers. Cross-flow membrane emulsification, relatively recently invented, may be a supplement to these processes. Under specific conditions monodisperse emulsions can be obtained and less energy is required which implies that less shear stress is exerted on the ingredients. In cross-flow membrane emulsification the to-be-dispersed phase is pressed through the membrane pores and droplets are formed at the pore openings in the membrane surface. A second liquid flows across the membrane surface, may enhance droplet detachment and carries the droplets away. Several applications are already studied, e.g. a low-fat spread and a drug-delivery system with an anti-cancer drug encapsulated. Many studies on cross-flow membrane emulsification focussed on obtaining monodisperse emulsions. Only in some cases the droplet formation process itself was analyzed. Besides, generally low disperse phase fluxes were found. Therefore, the objective of this thesis was to gain fundamental understanding of the mechanism of droplet formation during cross-flow membrane emulsification and of the disperse phase flux through the membrane as a function of the transmembrane pressure and the membrane characteristics. The obtained insights are useful for further development of membranes for emulsification.

Droplet formation was studied at a microscopic level with computational fluid dynamics simulations (CFD) and by microscopy experiments. A cylindrical pore with a diameter and a length of 5 μm and a rectangular cross-flow channel were modeled in CFX 4.2. The cross-flowing water (average velocity 0.5 m/s) deformed the droplet and a neck was formed. With a transmembrane pressure of $0.3 \cdot 10^5$ Pa, a droplet with a diameter of 33 μm detached after 1.06 ms; a small oil volume remained attached at the pore, forming a new droplet. Due to the droplet deformation, the pressure drop over the pore changed in time. As a consequence the velocity in the pore sharply decreased from about 1 m/s to 0.5 m/s during necking of the droplet. From the simulated droplet shape, the maximum membrane porosity to prevent hindrance of droplets growing simultaneously, was estimated to be 1.5%, which is much lower than the porosity of conventional membranes.

In the microscopy experiments a microsieve[®] was used, having uniform circular pores with a diameter of 7 μm . The membrane was only 1 μm thick and had a porosity of 15%. With transmembrane pressures ranging from $(0.05\text{--}0.09) \cdot 10^5$ Pa and cross-flow velocities of the 1%-Tween solution between 0.011 and 0.039 m/s, large hexadecane droplets were formed (52–255 μm) in 0.1 to over 2 s. Sometimes there was a time lag between the detachment of a droplet and the formation of a new droplet at the same pore. Although the membrane pores were uniform in size, the obtained emulsions were polydisperse. Observations showed this to be due to steric hindrance of droplets forming simultaneously and to collisions of detached

droplets with droplets at pores downstream. Consequently, droplet detachment frequencies were almost identical at some pores close together (0.86 and 0.88 s^{-1}). This was confirmed by the cross-correlation value of the detachment signals (around 0.8). A higher transmembrane pressure led to an increased number of pores at which droplets were formed (so-called active pores). Hence, steric hindrance increased and the average droplet size decreased.

The transmembrane pressure required to activate multiple pores was much larger than the critical pressure of each individual pore. The critical pressure is the pressure difference over a pore, just enough to form a droplet at that pore. Because the pores were equally sized, the critical pressures of the pores, calculated with the Laplace equation, were identical. Thus, the gradual activation of pores could not be explained by a difference in pore sizes. Further, possible variation in surface properties could not explain this effect. By taking the whole system into account, it was concluded to be due to the resistances against flow within the membrane structure. To describe flow in a microsieve, it was modeled as having two distinct layers, the pore layer and the substructure, each with a hydrodynamic resistance. This two-layer model predicts a linear increase of the number of active pores with increasing transmembrane pressure, which was validated by a larger-scale physical analogon. The resistance of the microsieve substructure, estimated from the experiments described above, was found to be 4 times lower than the resistance of a single pore. Nevertheless, it has a major impact on the pore activation.

Another model describes the disperse phase flux through an isotropic membrane with interconnected pores (isotropic membrane model). If the membrane thickness is 10 times the pore radius or larger, the isotropic membrane model approximates the two-layer model, and the latter can be used. This model was extended to describe the flow through a membrane with a pore size distribution. It shows that, depending on the membrane thickness or the sublayer resistance, the transmembrane pressure needs to be much larger than the critical pressure of the pores, in order to activate all the pores. This finding was also applied to a related field: it is demonstrated that when using liquid displacement methods to estimate a membrane pore size distribution, the pore sizes are underestimated, hence the number of pores is overestimated. To obtain correct results, the sublayer resistance should be estimated. It is suggested either to count the number of (active) pores or to perform the experiment several times, each time covering a different fraction of the membrane surface.

Finally, the surface areas of membranes with different characteristics (SPG, $\alpha\text{-Al}_2\text{O}_3$ and microsieve), required for industrial-scale culinary cream production, were estimated with the models described above. The differences in morphology lead to contrasting performance, e.g. a totally different fraction of active pores. In the culinary cream case (droplet size: $1\text{--}2 \mu\text{m}$; production volume: $20 \text{ m}^3/\text{h}$ with 30% disperse phase) the best suitable membrane was a microsieve with a low porosity, with an surface area of around 1 m^2 , either to minimize the membrane area, to minimize the droplet standard deviation or to enable a stable process operation. Depending on the strategy chosen, membranes may be optimized by decreasing the total membrane resistance or by changing the ratio of pore layer and sublayer resistances.

Samenvatting

Veel producten als levensmiddelen, farmaceutische en cosmetische producten, verf, gewasbeschermingsmiddelen en asfalt zijn emulsies. Ze worden op grote schaal geproduceerd met rotor/stator systemen, colloïdmolens en hoge-drukhomogenisatoren. Langsstrom-membraan-emulgeren, dat in de jaren 80 is uitgevonden, kan een aanvulling zijn op deze processen. Onder bepaalde omstandigheden kunnen monodisperse emulsies verkregen worden. Bovendien vergt het proces minder energie, waardoor ook de procesomstandigheden milder zijn. Bij langsstrom-membraanemulgeren wordt de te dispergeren fase door de poriën van het membraan gedrukt en worden druppels gevormd aan de porieopeningen op het membraanoppervlak. Een tweede vloeistof stroomt langs het membraanoppervlak, beïnvloedt het loskomen van de druppels van het oppervlak en voert de druppels af. Verschillende toepassingen van dit proces zijn ontwikkeld, zoals de productie van een spread met een laag vetgehalte en de vorming van een emulsie waarin een medicijn tegen kanker was geëncapsuleerd. De meeste studies over membraanemulgeren zijn gericht op de productie van monodisperse emulsies. Het druppelvormingsmechanisme is slechts in geringe mate bestudeerd en ook aan het vergroten van de doorzet van de te dispergeren fase door de membranen is weinig aandacht besteed. Het doel van dit promotieonderzoek was daarom: inzicht krijgen in het druppelvormingsmechanisme bij langsstrom-membraanemulgeren en in de stroming van de te dispergeren fase door het membraan als functie van de transmembraandruk en de membraaneigenschappen. Het verkregen begrip kan ingezet worden om membranen verder te ontwikkelen voor deze toepassing.

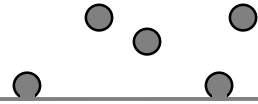
Het druppelvormingsproces werd op microscopische schaal onderzocht met computersimulaties van de vloeistofdynamica (computational fluid dynamics) en met experimenten m.b.v. lichtmicroscopie. Druppelvorming vanuit een cilindervormige porie met een diameter en een lengte van 5 μm in een langsstromkanaal werd gemodelleerd m.b.v. CFX 4.2. Het langsstromende water (gemiddelde snelheid 0,5 m/s) vervormde de druppel en er werd een nek gevormd. Bij een transmembraandruk van $0,3 \cdot 10^5$ Pa brak een druppel met een diameter van 33 μm na 1,06 ms af. Een kleine hoeveelheid olie bleef achter op de porie, die het begin vormde van een nieuwe druppel. Door de vervorming van de druppel nam de drukval over de porie af, waardoor de snelheid van de olie in de porie sterk afnam tijdens de vorming van een nek, van ongeveer 1 m/s naar 0,5 m/s. De porositeit die het membraan maximaal mag hebben om te voorkomen dat gelijktijdig vormende druppels elkaar belemmeren werd geschat m.b.v. de berekende druppelvorm en is ca. 1,5%. Deze porositeit is veel lager dan die van gangbare membranen.

Bij de microscopische experimenten werd een microzeef[®] gebruikt met ronde poriën, alle met een diameter van 7 μm . Het membraan was slechts 1 μm dik en had een porositeit van 15%.

Bij transmembraandrukken tussen $0,05 \cdot 10^5$ en $0,09 \cdot 10^5$ Pa en langsstroomsnelheden van de 1%-Tween oplossing tussen 0,011 en 0,039 m/s werden grote hexadecaandruppels gevormd (52–255 μm). Druppelvormingstijden varieerden van 0,1 s tot meer dan 2 s. Soms werd na het afbreken van een druppel niet direct een nieuwe druppel gevormd. Hoewel alle poriën gelijke afmetingen hadden, lieten de verkregen emulsies een brede druppelgrootteverdeling zien. Dit bleek te komen doordat de druppels die gelijktijdig groeiden, elkaar wegduwden en doordat druppels die al afgebroken waren botsten met druppels die aan verdergelegen poriën gevormd werden. Hierdoor waren de druppelvormingsfrequenties van een aantal dicht bij elkaar gelegen poriën vrijwel gelijk (0,86 and $0,88 \text{ s}^{-1}$). Dit werd bevestigd door de waarde van de kruiscorrelatie van de druppelafbreeksignalen (ca. 0,8). Het aantal poriën, waaraan druppels gevormd werden (zgn. actieve poriën) nam toe bij toenemende transmembraandruk. Het gevolg was dat de druppels elkaar bij hogere druk meer hinderden, waardoor de gemiddelde druppeldiameter afnam.

De transmembraandruk die nodig was om meer poriën te activeren, was veel hoger dan de kritieke druk van de afzonderlijke poriën. De kritieke druk is die drukval over de porie die juist groot genoeg is om een druppel te laten groeien. Omdat alle poriën van gelijke grootte waren, hebben ze dezelfde kritieke druk volgens de Laplace vergelijking. De geleidelijke activering van poriën bij een toenemende transmembraandruk kan dus niet verklaard worden door een verschil in poriegroottes. Evenmin kon dit verklaard worden door eventuele verschillen in bevochtiging van het membraan. De conclusie is dat de geleidelijke activering veroorzaakt werd door de morfologie van het membraan. De stroming van de te dispergeren fase door het membraan werd gemodelleerd door aan te nemen dat de microzeef uit twee verschillende lagen bestaat: de toplaag met poriën en een onderlaag (twee-lagen model). Het model voorspelt een lineaire toename van het aantal actieve poriën bij een toenemende transmembraandruk, hetgeen gevalideerd kon worden m.b.v. een fysisch analoog systeem op grotere schaal. De weerstand van de onderlaag werd geschat uit de hierboven beschreven experimenten met de microzeef. De weerstand van de onderlaag was 4 keer zo laag als de weerstand van een enkele porie. Toch heeft de weerstand van de onderlaag een grote invloed op de activering van poriën.

Om de stroming van de te dispergeren fase door een isotroop membraan met onderling verbonden poriën te beschrijven, is een ander model ontwikkeld (isotroop membraan model). Als de dikte van het membraan minstens 10 keer zo groot is als de poriestraal, dan geven beide modellen nagenoeg dezelfde voorspellingen en kan het twee-lagen model worden gebruikt. Het twee-lagen model werd zodanig uitgebreid, dat het de doorzet door een membraan met een poriegrootteverdeling beschrijft. Dit model geeft aan dat, afhankelijk van de dikte van het membraan, de transmembraandruk om alle poriën te activeren, veel hoger moet zijn dan de kritieke druk van de poriën. Dit inzicht werd toegepast in een gerelateerd onderzoeksgebied: de schatting van de poriegrootteverdeling in een membraan m.b.v. vloeistofverdringingsmethoden. Het uitgebreide twee-lagen model laat zien dat de porie-



groottes onderschat worden en dat dus het aantal poriën in een membraan wordt overschat met deze methoden. De resultaten van de methode kunnen gecorrigeerd worden door de weerstand van de onderlaag van het membraan te schatten. Dit kan gedaan worden door ofwel het aantal (actieve) poriën te tellen of door de metingen een aantal keren uit te voeren, waarbij steeds een andere fractie van het membraan afgedekt wordt.

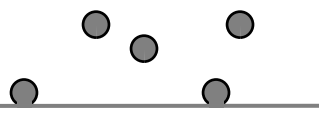
Ten slotte werd het membraanoppervlak van membranen met verschillende eigenschappen (SPG, α -Al₂O₃ en microzeef), benodigd voor koksroomproductie op industriële schaal, geschat m.b.v. de hierboven beschreven modellen. Omdat de membraanmorfologiën behoorlijk verschillen, verloopt de emulgering anders, wat bijvoorbeeld tot uitdrukking komt in een uiteenlopend aantal actieve poriën. Het meest geschikte membraan om koksroom met druppels van 1–2 μm met een productievolume van 20 m³/h met 30% disperse fase te maken, is een microzeef met een lage porositeit, waarvan ongeveer 1 m² nodig is. Het maakt daarbij niet uit of er gekozen wordt het oppervlak te minimaliseren, te proberen een zo smal mogelijke druppelgrootteverdeling te krijgen of de procesvoering zo stabiel mogelijk te maken. Afhankelijk van de gekozen strategie, kunnen in de toekomst membranen geoptimaliseerd worden door de totale membraanweerstand te verlagen of door de verhouding van de weerstanden van de twee lagen te veranderen.

Nawoord

Op één van Remko's eerste werkdagen bij proceskunde kreeg hij mij enthousiast om als AIO onderzoek te gaan doen aan het onderwerp membraanemulsificatie. Het lijkt op het eerste gezicht een eenvoudig proces, dus ik dacht met een systematische aanpak het effect van de verschillende proces- en membraanparameters op de druppelgrootte en de flux te kunnen bepalen. Beoordeel zelf maar na het lezen van dit proefschrift in hoeverre ik daarin geslaagd ben. Echter zonder de steun van een groot aantal mensen was ik zeker niet zo ver gekomen. Daarom, voor alle grote en kleine bijdragen, bedankt! Een aantal mensen wil ik hier met name noemen, te beginnen bij m'n begeleider:

Albert, de term "begeleider" is je op het lijf geschreven. Ik citeer: "de professional: heeft altijd tijd voor je, leest stukken snel, voorziet ze van adequaat commentaar, motiveert je, en combineert de rollen van coach en beoordelaar op bewonderenswaardige wijze" [1]. Niet alleen heb ik veel aan de inhoudelijke besprekingen gehad, je hebt me ook gestimuleerd naar m'n sterke en zwakke punten te kijken en er wat mee te doen! Ik denk dat het aantal beren op de weg daardoor drastisch is verminderd en ik toch bijna iedere dag (hoewel niet fluitend) de berg op ben gefietst. Ik ben blij dat je me ook na je vertrek naar FCDF wilde blijven begeleiden. Remko, het is verbazend hoe je met een paar uurtjes praten per maand toch steeds helemaal in m'n onderzoek zat. Je enthousiasme voor het onderwerp en je ideeën erover waren (en zijn) erg motiverend. Bovendien gaf je me de ruimte om het onderzoek op mijn eigen manier aan te pakken en heb ik de mogelijkheid gekregen verschillende "hoeken" van de aarde te zien.

Op het lab hielp Jos me met het vergaren van de benodigde spullen, Boudewijn bij het opzetten van het videosysteem en het doen van experimenten, André en Hans en anderen van de werkplaats bij het ontwerpen en het maken van de zoveelste module (vind maar eens een lijm die zowel tegen olie als tegen water kan). Voor de experimenten heb ik een aantal microzeven (soms inclusief modules) gekregen van Cees van Rijn en Wietze Nijdam van Aquamarijn, en van Stein Kuiper, die zijn overgebleven modules aan mij doneerde. Jullie en Jo Janssen (Unilever) wil ik bedanken voor discussies over uiteenlopende onderwerpen. Bij ATO heeft Wouter de Heij me een geweldige start gegeven bij het simuleren van de vorming van een druppel met CFX. Na een tijdje kwam mijn eerste "rekenbeest", zodat ik in elk geval niet meer op jouw pc hoefde te werken en nog iets later kwam de eerste gesimuleerde druppel uit een porie. Goed voor een artikel! Jammer dat je niet langer bij mijn project betrokken kon zijn. Omdat het heen en weer fietsen naar ATO toch wat onhandig werd, verhuisde m'n pc naar het biotechnion. Gelukkig hielp Gerrit bij het onderhouden van en het oplossen van problemen met m'n computers. Daarnaast dank aan alle ondersteunende medewerkers:



secretariaat, bibliotheek en medewerkers bij de leerstoelgroep levensmiddelen natuurkunde, die voor de nodige assistentie zorgden.

Graag wil ik alle studenten vermelden die een afstudeervak bij mij gedaan hebben: Deva, you did a lot of intriguing starting experiments. Renée, Sandra, Judith en José, er was heel wat doorzettingsvermogen voor nodig om experimenteel ook fatsoenlijke druppels te vormen! Hoewel niet alle resultaten voor artikelen zijn gebruikt, hebben jullie resultaten het inzicht in het proces behoorlijk vergroot. Ik ben blij dat jullie er met de andere studenten op het tweede bordes ook een gezellige tijd van maakten.

Een groot deel van het werk heb ik aan mijn bureau uitgevoerd. Gelukkig droegen al mijn kamergenoten bij aan een goede werksfeer: Esther, die me in het begin wegwijst maakte, Floor en Pieter en daarna werd zo'n twee jaar lang met Mark, René en Ed een prima kamergevoel opgebouwd. De etentjes en vooral de uitjes zal ik niet snel vergeten. Ed, door jou was er altijd een prima balans op de kamer tussen echt werken, gezelligheid én serieuze gesprekken met onderwerpen uiteenlopend van onzekerheid in het onderzoek tot samenwonen. René, ondanks dat het bij beiden wel eens tegenzat, zijn we toch allebei blij dat ik dit onderwerp had gekozen en dat jij nu met zetmeel werkt. Mark, het is fijn een collega te hebben die oprecht informeert hoe het met je gaat en ik ben blij dat je mijn paranimf wil zijn. Sandra, het is leuk dat je na een afstudeervak bij mij gedaan te hebben, nu als collega op hetzelfde onderwerp zit. Veel andere (voormalige) collega's bij proceskunde hebben inhoudelijk bijgedragen, d.m.v. discussies en suggesties, of eraan bijgedragen dat ik me thuisvoelde bij proceskunde.

Als laatste wil ik (schoon)familie en vrienden noemen; papa en mama zullen vaker dan anderen het idee gehad hebben dat het allemaal niet zo goed ging met m'n onderzoek omdat ik bij echte dieptepunten jullie bijna altijd kon bereiken. Bedankt dat jullie nooit keuzes voor me maken, maar wel altijd achter me staan. Rachel, het was altijd saai als jij vakantie had, want juist dan had ik behoefte om een e-mail te krijgen (>350 kreeg ik er van je). Tijdens m'n AIO-tijd heb ik Arjan leren kennen. Regelmatig informeerde je aan wat voor modelletje ik bezig was en gaf je jouw ideeën over hoe ik het aan kon pakken, met wie ik moest gaan praten, of hielp je me met Matlab. Hopelijk kunnen we nog lang praten over de dingen die ons bezighouden.

Referenties

- 1 H. Lelieveldt, Promoveren, wegwijzer voor de beginnend wetenschapper, Aksant, Amsterdam, 2001.

Curriculum vitae

Anna Jakoba Abrahamse werd op 30 augustus 1976 geboren te Serooskerke (w). In 1994 behaalde zij haar VWO diploma met lof aan de Roncalli Scholengemeenschap te Bergen op Zoom. In datzelfde jaar begon ze aan de studie levensmiddelentechnologie aan de Landbouwniversiteit te Wageningen (thans Wageningen Universiteit). Afstudeervakken werden afgelegd in de richtingen Meet-, regel- en systeemtechniek, uitgevoerd bij ATO, en Proceskunde. Stage liep ze bij RHM Technology in High Wycombe, UK. Evenals het propaedeutisch examen in 1995, legde zij het doctoraalexamen in november 1998 met lof af. Sinds januari 1999 is zij als AIO werkzaam bij de sectie Proceskunde van Wageningen Universiteit, waar het onderzoek, beschreven in dit proefschrift, werd uitgevoerd. Vanaf oktober 2001 is ze halftijds werkzaam als post-doc, eveneens bij de sectie Proceskunde van Wageningen Universiteit.